Targeted expression of *bgl23-D* a dominant-negative allele of *ATCSLD5* and expression analysis of plant intracellular Ras-group related leucine-rich repeat (LRR) proteins (PIRLs) in *Arabidopsis thaliana*

（シロイヌナズナにおける *ATCSLD5* のドミナントネガティブアレル *bgl23-D* の標的発現と植物細胞内 Ras グループ関連ロイシンリッチリピート (LRR) タンパク質 (PIRLs) の発現解析）

FIROSE HOSSAIN MD

フィロズ　ホセイン　エムディ

2023

Contents

Abbreviations

A. thaliana	: *Arabidopsis thaliana*
A. tumefaciens	: *Agrobacterium tumefaciens*
ATCSLD5	: *Arabidopsis thaliana* cellulose synthase-like D5
bgl23-D	: *bagel23-D*
Cm^r	: Chloramphenicol resistance
DAPI	: 4',6-diamidino-2-phenylindole
EMS	: ethyl methanesulfonate
GC	: guard cells
GMC	: guard mother cells
GFP	: green fluorescent protein
GUS	: β-glucuronidase
Km^r	: kanamycin resistance
mRFP	: monomeric red fluorescent protein
mRNA	: messenger ribonucleic acid
MS	: Murashige and Skoog
PCR	: polymerase chain reaction
PMI	: pollen mitosis I
PMII	: pollen mitosis II
P_{35S}	: cauliflower mosaic virus 35S promoter
Pnos	: nopaline synthase promoter
QC	: quiescent center
SEM	: scanning electron microscopy
sGFP	: synthetic green fluorescent protein
SGC	: single guard cell
WT	: wild type

Chapter 1

Introduction

Arabidopsis thaliana

Arabidopsis thaliana is a small plant in the mustard family that has become the model system of choice for research in plant biology. *A. thaliana* is native to Europe, Asia, and northwestern Africa, also appears to be native in tropical afroalpine ecosystems (Hedberg 1957). *A. thaliana* is a 20-25 cm tall annual or rarely biannual plant. The base leaves of *A. thaliana* are green to slightly purplish with a serrated border; the stem leaves are smaller, unstalked, and covered with trichomes. The flowers are grouped in a corymb, which is typical Brassicaceae structure. The fruit is a siliqua with 20-30 seeds (Padole and Ingle 2017). *A. thaliana* may be grown in the lab under fluorescent lights and ambient conditions in Petri plates or in a greenhouse using pots or hydroponics (Meinke et al. 1998).

However, *A. thaliana* has minimal agro-economic value; it possesses various characteristics that make it an excellent model for studying the genetic, cellular, and molecular biology of flowering plants (Padole and Ingle 2017). The present importance of *Arabidopsi*s study reflects the growing understanding among biologists that this simple angiosperm may serve as a useful model for tackling fundamental issues of biological structure and function common to all eukaryotes as well as for plant biology (Meinke et al. 1998). *A. thaliana* has a large number of accessions and ecotypes that have been obtained from wild populations growing across several ecological and geographic zones, while Landsberg erecta (Ler), Columbia (Col-0) and Wassilewskija (Ws) are mostly used (Alonso-Blanco and Koornneef 2000; Hoffmann 2002; Al-Shehbaz and O'Kane 2002).

A. thaliana provides a vast number of advantages for using it as a model plant over the previously used model plants such as maize (*Zea mays*), tomato (*Solanum lycopersicum),* and barley (*Hordeum vulgare*). *A. thaliana* is helpful for genetic mapping and sequencing due to its diploid and small genome size of around 135 mbps and five chromosomes (Bennett et al. 2003). *A. thaliana* was the first plant genome to be sequenced in 2000, and the most recent version is maintained by The Arabidopsis Information Resource (TAIR). Until now, 27,000 genes that encode 35,000 proteins have been functionally assigned. However, its small size, rapid lifecycle, self-pollinating nature, which assists genetic experiments, and ability to produce thousands of seeds make *A. thaliana* a valued genetic model plant (Padole and Ingle 2017). Introducing *A. thaliana* to *Agrobacterium tumefaciens* provides an efficient transformation vector, making *A. thaliana* a flexible model organism for use in the biology laboratory. *A. thaliana* is extensively used in plant science, genetics, and evolution, and it has contributed to our understanding of germination and other features of plant growth that are vital in commercial crops (Saeidfirozeh et al. 2018; Hasegawa et al. 2016).

Forward and reverse genetics

Forward genetics is the method of identifying the genetic basis of a certain phenotype by screening a population for random genomic changes that influence gene function (Ali Khan et al. 2021). The process of forward genetic screening begins with measurement or observation of a phenotype followed by mapping of the causative loci or genes (Aklilu 2021). Forward genetics offers an unbiased approach since it places a strong emphasis on finding the genes or genetic components that contribute to a given phenotypic or feature of interest (Moresco et al. 2013). Forward genetics is now extensively used in plant biology to identify the responsible gene of mutant phenotype. In contrast, reverse genetics examines the phenotype of an organism after the disruption of a known gene.

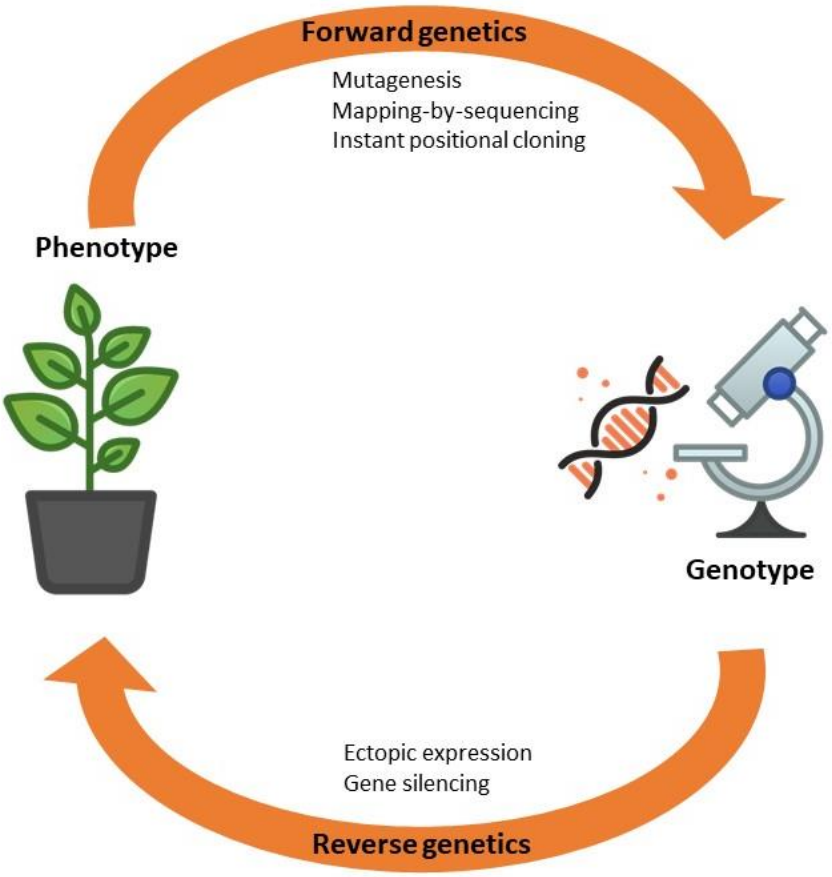

Fig. 1-1. Schematic illustration of forward and reverse genetics. Forward genetics (e.g mapping-by-sequencing) involves identifying the underlying genetic basis of phenotype, while reverse genetics (e.g gene silencing) involves alternation of genetic structure and study of the resulting phenotype. This figure is modified from Ali Khan et al. (2021).

EMS mutagenesis

Mutagenesis is the process of producing heritable changes in an organism's genome (Maple and Møller 2007). Producing mutants with altered phenotypic and physiological responses is a valuable technique for determining the biological functions of genes in an organism. Many mutagenesis techniques, including chemical, irradiation, and insertional procedures, have been developed; each has benefits and drawbacks for the investigation of gene function (Kim et al. 2006). EMS mutagenesis is the most extensively used approach for mutagenesis because of its convenience of use, high rate of mutagenicity with low mortality rates, random non-biased distribution of mutation in the genome, and potential to generate novel mutant phenotypes (Kim et al. 2006; Maple and Møller 2007). To produce point mutations, ethylmethanesulfate (EMS) is regarded as an effective and widely employed chemical mutagen (Till et al. 2004).

EMS alkylates guanine bases (adds a methyl group), resulting in base mispairing: an alkylated guanine pairs with thymine bases rather than cytosine bases, resulting in G/C to A/T transitions (Maple and Møller 2007). In an EMS mutagenesis procedure, usually the seeds from the parental genotype are treated with the EMS mutagen. The resultant plants from these seeds are of the M1 generation and will be heterozygous due to induced mutations. The M1 generations are then self-fertilized and produce the M2 generation. M2 is the first generation after mutagenesis in which homozygous recessive mutants can be identified and these M2 generations are most usually used for phenotypic screening purpose (Maple and Møller 2007).

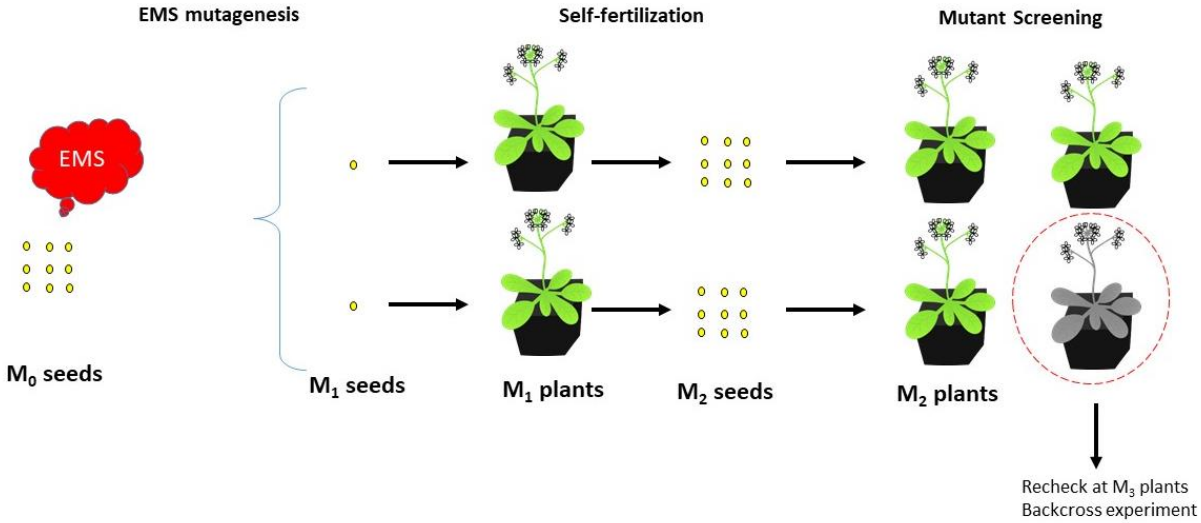

Fig.1-2. Schematic illustration of EMS mutagenesis. This figure is modified from Mizuno et al. (2014).

Structure of stomata

Stomata are small pores in the leaf epidermis that exchange gas and vapor between plants and the environment, regulating two key physiological processes such as photosynthesis and transpiration. Stomata are found in all land plants in species-specific patterns, and they perform an important function in facilitating atmospheric carbon dioxide consumption while decreasing plant water loss and promoting plant development and survival (Chowdhury et al. 2021).

Stomatal morphological features can influence plant growth and development as well as functions. Stomatal density and stomatal index are two terms that are frequently used to describe leaf development and plant growth (Kusumi 2013). A stoma is made up of two guard cells that enclose a pore. Guard cells in *Arabidopsis* are kidney-shaped and capable of rapidly adjusting internal turgor to change their shape and pore aperture (Pillitteri and Dong 2013). When guard cells are turgid, stomatal apertures open, allowing mesophyll chloroplasts to access carbon dioxide for photosynthesis. Furthermore, the discharge of water vapor from open stomata enhances water and nutrient uptake through the roots via transpiration (Schroeder et al. 2001; Pillitteri and Torii 2012). A typical structure of stomata is shown in Fig. 1-3.

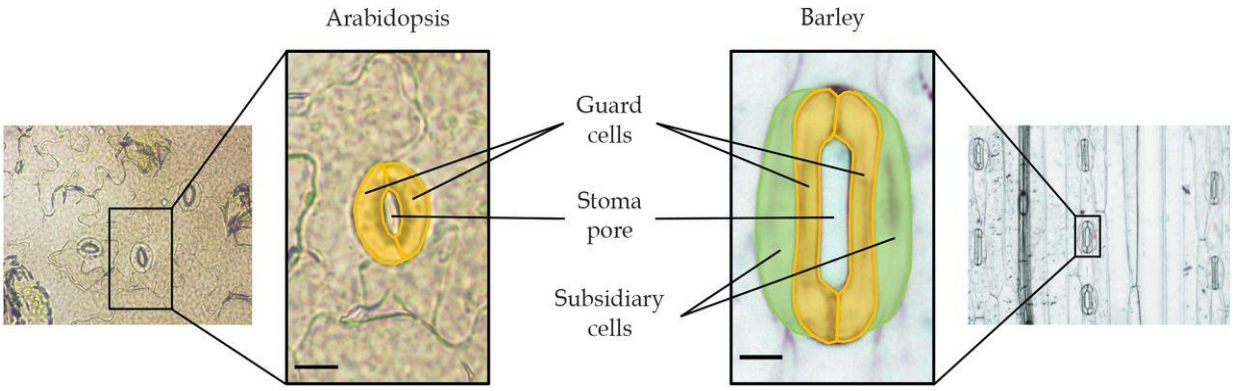

Fig. 1-3. The stomata of *A. thaliana* and barley (*Hordeum vulgare*). Different components of stomata in *Arabidopsis* and barley are labelled. This figure is cited from Sai et al. (2022).

Developmental pathway of stomata

Stomatal development is an excellent model for studying intra- and intercellular signaling networks, cell polarity, and cell-type differentiation (Pillitteri et al. 2008). In the model plant *A. thaliana*, a succession of cell divisions and subsequent cell-state transitions are necessary for the development of a mature stoma. Each transitional state is characterized by a drastic change in

morphology, transcript accumulation, and protein localization (Dong et al. 2009; Geisler et al. 2000; Zhao and Sack 1999).

The development of stomata begins with a subset of prodermal cells, which undergo a cellular transition and produce meristemoid mother cells (MMCs) (Fig. 1-4). After that, MMC generates a small, triangular-shaped cell called a meristemoid and a larger cell called a stomatal-lineage ground cell (SLGC) through entry division (Fig. 1-4). An SLGC can differentiate terminally into a lobed pavement cell, or it can undertake an asymmetric spacing division to form a satellite meristemoid that is always orientated away from an existing stomatal precursor. Different components of cell-cell signaling controlled the oriented division of SLGCs that ensure stomata develop at least one cell apart from one another through the one-cell spacing rule (Geisler et al. 2000; Hara et al. 2007; Hunt and Gray 2009). A meristemoid loses the ability to repeat an asymmetric division after a number of amplifying divisions. In contrary to the triangular meristemoid's asymmetric divisions, the round GMC divides once symmetrically to create two cells, which concurrently go through a final cell-state transition to form highly specialized GCs that work together to govern the size of the stomatal opening. Mature GCs are terminally differentiated and do not divide further (Pillitteri and Torii 2012).

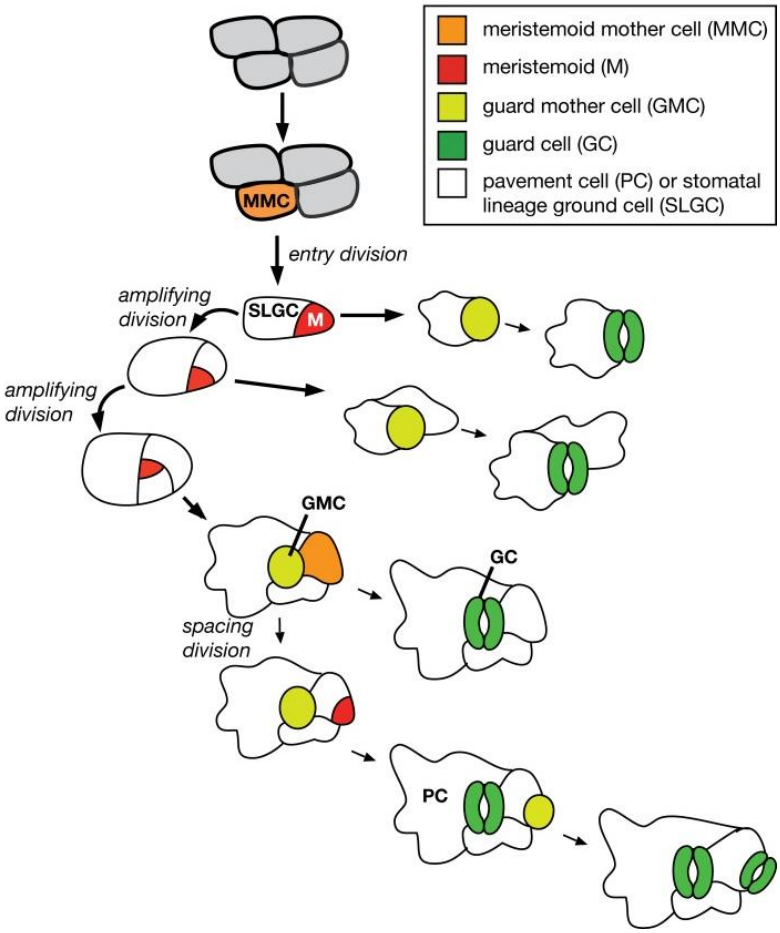

Fig. 1-4. Development of stomata in *A. thaliana*. The protodermal cells differentiate to a meristemoid mother cells (MMC) or pavement cells. MMCs further divide asymmetrically and generate meristemoid cell and stomatal-lineage ground cells (SLGC). Guard mother cell is formed by the asymmetric amplifying divisions of the meristemoid cells. The GMC divides once symmetrically to two identical guard cells (GCs). This figure is cited from Pillitteri and Dong (2013).

Pollen development in *A. thaliana*

Pollen development is an important step in plant development that is required for effective breeding and seed formation (Gómez et al. 2015). Anther and pollen development have been extensively studied in *A. thaliana* (Wilson and Zhang 2009); however, it is a complicated and essential procedure that results in the discharge of viable pollen and fertilization of plants. Pollen development begins in the young anther locules and is divided into two key stages: microsporogenesis and microgametogenesis. The diploid microsporocytes or meiocytes are produced by the primary sporogenous layer (Fig. 1-5). After that, meiotic division occurs, which generates four haploid microspores called tetrads. Microspores are released, after the degradation of the callose by the enzymatic activity of callase contributed by the tapetum (Fig. 1-5). Later on, microspore growth and development occur in a continuous cycle of vacuole biogenesis, fusion, and fission events (Owen and Makaroff 1995; Yamamoto et al. 2003). The microspore nucleus is forced to move to the cell's periphery by this vacuole. Subsequently, Pollen mitosis I (PMI) gives rise to two daughter cells with radically different shapes and cell fates (Twell et al. 1998) (Fig. 1-5).

Following pollen mitosis I, the generative cell migrates inward, forming a 'cell within a cell' arrangement that allows gamete movement within the pollen tube. The degradation of the callose wall that separates the vegetative and generative cells leads to generative cell migration. Then the small generative cell undergoes a second mitotic division at pollen mitosis II (PMII) to complete the final stage of pollen development and generate two sperm cells (Fig. 1-5) (Honys et al. 2006). Upon successful pollination, the two sperm cells move towards the ovule in the female gametophyte to form the diploid zygote.

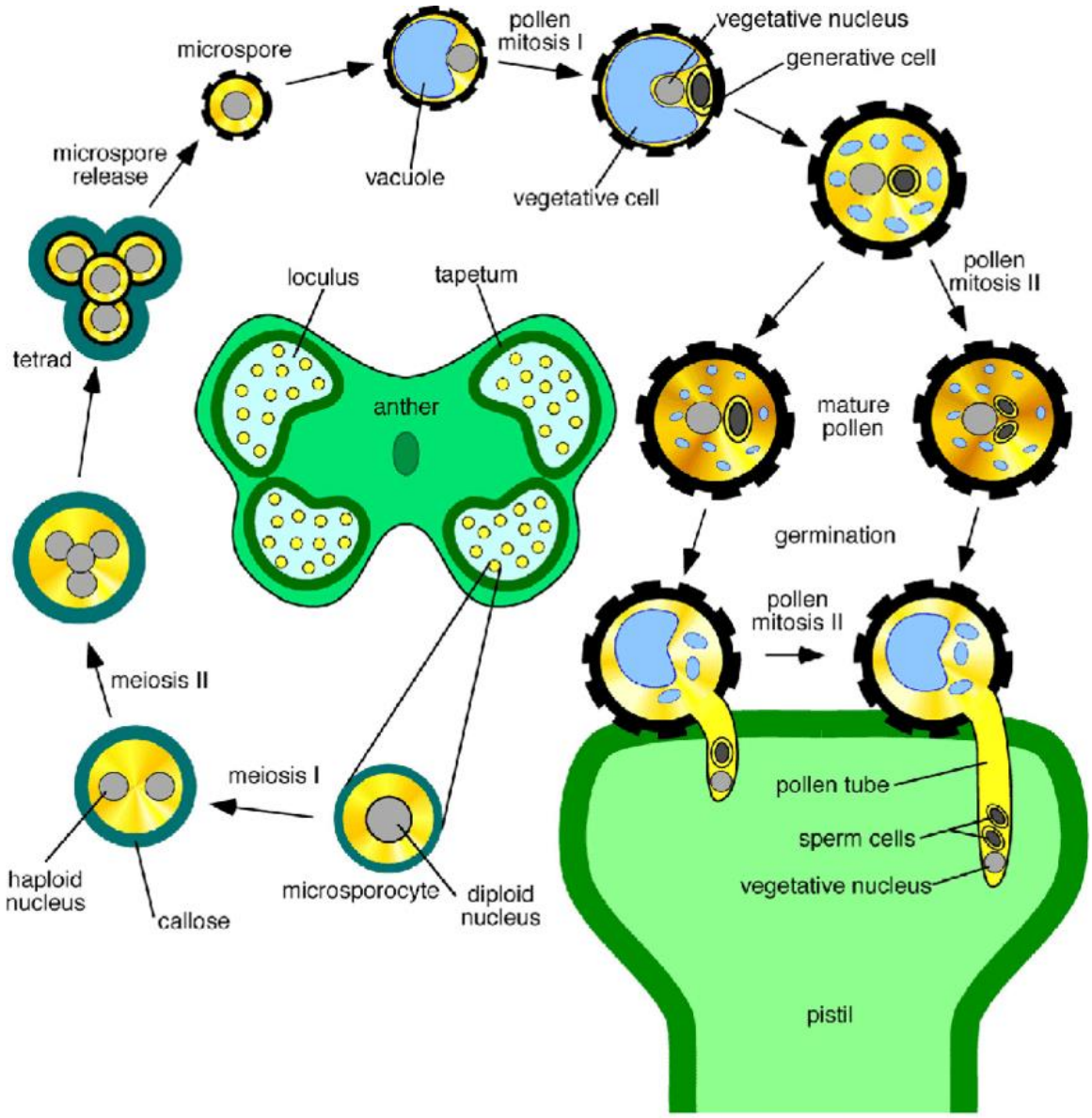

Fig. 1-5. Schematic illustration of the main events of pollen development. The meiocytes undergo meiotic division to produce four identical microspores. Through two round mitotic divisions, the microspores produce mature pollen grains containing two sperm cells and one vegetative cell. This figure is cited from Honys et al. (2006).

Structure of pollen grains and tapetum

A flower's pollen grains are tiny structures that contain androecium, the male reproductive organ of the flower. The majority of pollen grains are made up of three separate parts. The central cytoplasmic part serves as source of the nuclei responsible for the fertilization process. The other parts constituting the wall of the grain are an inner layer, the intine and an outer layer, the exine. Normal exine structure is presumably crucial for protecting male gametes from physical trauma,

chemical penetration, and bacterial infection during pollination in pollen grains (Suzuki et al. 2008).

The tapetum is a specialized tissue that lines the sporangium locule and serves as a barrier between the sporogenous tissue and the sporangial wall (Fig. 1-6). The tapetum is crucial for exine synthesis and offers a favorable environment for the growth of microspores (Xie et al. 2020). Tapetum cells serve as nurse cells for microspores, aid in the development of pollen outer walls, and provide an important nutritional supply for proper pollen growth (Gu et al. 2014; Xu et al. 2014). The tapetum, the innermost layer of the anther wall, appears in stage 4 and entirely degenerates at stage 12, during which time the microsporocytes undertake meiosis and mitosis to make mature pollen (Sanders et al. 1999). The tapetum secretes enzymes that catalyze the release of microspores from the tetrad and give nutrients for pollen exine production before degenerating. Tapetal remnants are released to aid pollen maturation when the tapetum undergoes programmed cell death (PCD) (Qian et al. 2021).

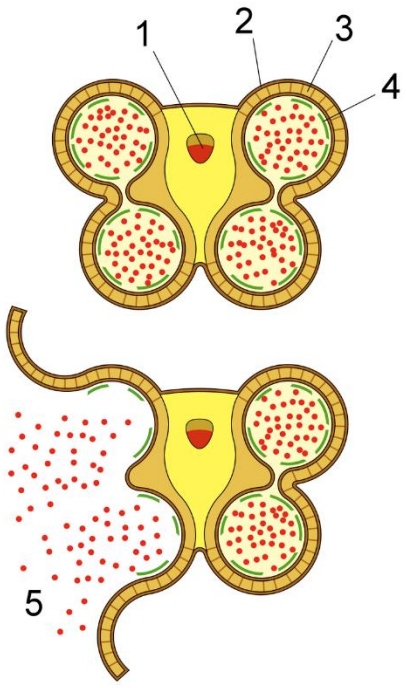

Fig. 1-6. Section of anther, showing tapetum and release of pollen grains. The numerical numbers in the figure represent: (1) the vascular bundle; (2) the epidermis; (3) the fibrous layer; (4) the tapetum; and (5) the pollen grains. Image is taken from the internet source (https://en.wikipedia.org/wiki/Tapetum_%28botany%29).

Gateway® recombinational cloning

The Gateway® cloning method establishes a new trend in molecular biology by resolving the drawbacks of the classic cloning approaches in terms of adaptability, effectiveness, and compatibility (Katzen 2007). The Gateway technology is based on site-specific recombination reactions that mediate the incorporation and excision of bacteriophages (Hartley et al. 2000). The Gateway cloning technology utilizes two distinct enzyme combinations, each of which conducts a unique recombination reaction. The BP clonase enzyme mix recombines *att*B and *att*P sites to produce *att*L and *att*R sites, whereas the LR clonase enzyme mix catalyzes the opposite reaction (Fig. 1-7). Each recombination event is accurate, with no nucleotides added or removed. Because *att* site recognition is extremely specific (BP clonase enzymes never use *att*L or *att*R sites), each recombination reaction yields only one set of derivatives (Reece-Hoyes and Walhout 2018).

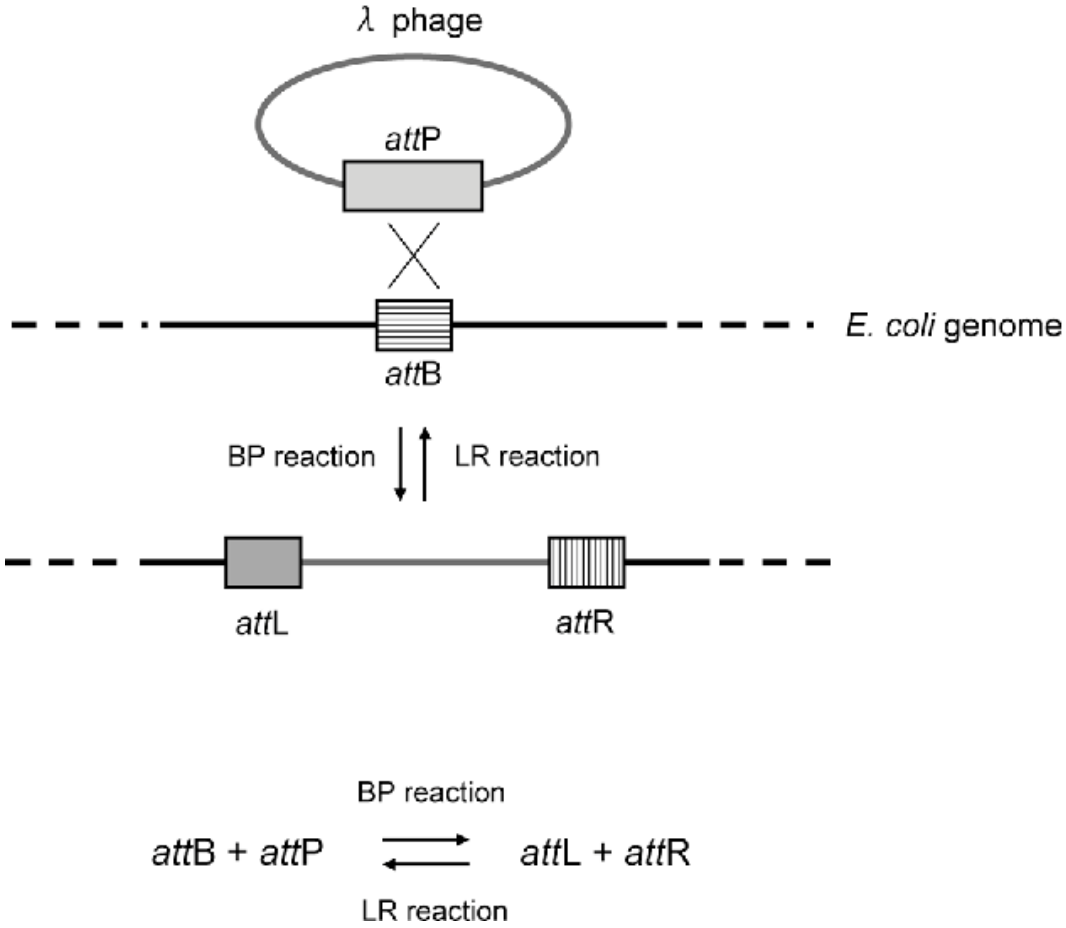

Fig. 1-7. Outline of Gateway cloning representing site-specific recombination by the BP and LR reactions. This figure is cited from Nakagawa et al. (2009).

The Gateway system is advantageous over classic cloning since it has high throughput and a large collection of open reading frames. A large group of scientists had produced their own Gateway-

compatible vector sets and tested them for high-throughput cloning and expression of genes in plants, bacteria, and mammalian cell line (Busso et al. 2005; Curtis and Grossniklaus 2003).

Leucine-rich repeats (LRRs) and Leucine-rich repeat (LRR) proteins

A leucine-rich repeat (LRR) is a kind of protein structural motif that forms an α/β horseshoe fold (Kobe and Deisenhofer 1994). It is made up of repetitive sequences of 20-30 amino acids that are exceptionally high in the hydrophobic amino acid leucine. These tandem repetitions are frequently folded together to form a solenoid protein domain known as the leucine-rich repeat domain (Kobe and Kajava 2001; Gay et al. 1991). LRR proteins are a broad and diverse protein superfamily found in mammals, yeast, protists, bacteria, and plants (Kobe and Deisenhofer 1994; Kajava 1998). A characteristic of these proteins is an LRR domain made up of tandemly repeated leucine-rich motifs ranging in length from 18 to 29 amino acids.

LRR proteins are involved in many different aspects of signal transduction in plants (Vernon 2002). For instance, LRR-receptor-like kinases (RLKs) and related receptor-like proteins (RLPs) together make a large family of plasma membrane proteins having extracellular N-terminal LRR domains. They play important role in numerous developmental, environmental and defense-related pathways (Shiu and Bleecker 2001; Morris and Walker 2003). Other classes of proteins have been identified that are involved in various cellular and physiological processes, such as pollen tube growth, root development, Ran GTPase activation, transcription regulation and meristem cell organization (Rose and Meier 2001; Stratford et al. 2001; Baumberger et al. 2001). Thus, LRR proteins play important roles in the growth and development of plants.

Plant intracellular Ras-group related leucine-rich repeat proteins (PIRLs)

Plant intracellular Ras-group LRR proteins is a small group of proteins that are structurally related to Ras-group LRRs (Forsthoefel et al. 2005; You et al. 2010). They are defined by their conserved Leu-rich domain consisted of unit motifs that are similar to those fungal and animal Ras-group proteins (Forsthoefel et al. 2005). A deviating hydrophilic N- and C-terminal domains of PIRL outside of Leu-rich domain make them a unique plant-specific class of proteins (Forsthoefel et al. 2018). PIRLs are different from other larger, well-studied classes of plant LRR protein such as NBS-LRR pathogen response proteins (McHale et al. 2006).

The *A. thaliana* genome has a total of nine *PIRL* genes which are categorized into three subfamilies based on their evolutionary relationship. Four members of *PIRL* genes, *PIRL1, PIRL2, PIRL3*, and *PIRL9* constitute the largest group subfamily I, while *PIRL6*, *PIRL7,* and *PIRL8*, represent subfamily II, and *PIRL4* and *PIRL5* form the subfamily III, respectively (Forsthoefel et

al. 2005). Among all of the nine *PIRL* genes *PIRL6* and *PIRL7* showed highest 78%, *PIRL1* and *PIRL9* showed 77%, *PIRL4* and *PIRL5* showed 68% and *PIRL2* and *PIRL3* showed 67% similarity in their amino acid sequences, respectively (Forsthoefel et al. 2005). The comprehensible structural relationship between Ras-group LRRs and PIRLs propose a significant function for the *PIRLs* in the growth and development of plants (Forsthoefel et al. 2010). Up to now, functions of five PIRLs have been revealed, *PIRL6* was essential for male and female gametogenesis (Forsthoefel et al. 2018), *PIRL1* and *PIRL9* redundantly worked for the differentiation of microspores into pollen (Forsthoefel et al. 2010), *PIRL2* and *PIRL3* were involved in pollen morphogenesis (Forsthoefel et al. 2013). To elucidate the physiological functions of remaining *PIRL* genes it is requisite to know their precise expression pattern.

Objectives of the study

In the fields of molecular biology, plant biology, and functional genomics, it is often required to alter the normal structure of specific tissues or cells for multiple purposes, such as the study of the functions of the gene. Furthermore, knowing the gene's tissue-specific expression analysis can be crucial for understanding the function of particular genes. Therefore, the objectives of the present study are as follows:

- Identification of *bgl23-D*, a novel dominant-negative allele of *ATCSLD5* and use of *bgl23-D* as a genetic tool to inhibit ATCSLD5 functions in target tissues or cells (**Chapter 2**)
- Elucidation of the tissue specific expression analysis of plant intracellular Ras-group related leucine-rich repeat proteins (PIRLs) (**Chapter 3**)

Chapter 2

Targeted expression of *bgl23-D*, a dominant-negative allele of *ATCSLD5*, affects cytokinesis of guard mother cells and exine formation of pollen in *Arabidopsis thaliana*

Introduction

In plant cells, cellulose is synthesized at the plasma membrane by cellulose synthases commonly known as CESA proteins (Cosgrove 2005), while pectin and hemicellulose are synthesized in the Golgi apparatus (Sandhu et al. 2009; Harholt et al. 2010; Liepman et al. 2010). In *Arabidopsis thaliana*, about 10 cellulose synthase genes, *ATCESA1–ATCESA10* have been identified (Richmond and Somerville 2000). Among these, ATCESA4, ATCESA7, and ATCESA8 were thought to be responsible for secondary cell wall formation, while other ATCESAs had a role in primary cell wall synthesis (Somerville 2006). Plants possess *CSL* (*Cellulose Synthase Like*) genes, which show a higher degree of sequence similarity with *CESA* genes (Richmond and Somerville 2001). They have been classified into six independent groups, *CSLA* (*ATCSLA*), *CSLB* (*ATCSLB*), *CSLC* (*ATCSLC*), *CSLD* (*ATCSLD*), *CSLE* (*ATCSLE*), and *CSLG* (*ATCSLG*) subfamilies *in A. thaliana* (Yin et al. 2011). Having variations in sequence, each CSL was found to participate in the biosynthesis of various polysaccharides, for instance, xylan, xyloglucan, mannan, and most likely cellulose (Richmond and Somerville 2000; Doblin et al. 2002). *CSLDs* are more related to *CESAs* than any members of *CSL* subfamilies, with a sequence similarity ranging from 6% to 42% (Zhu et al. 2010). Up to now, several mutants of *ATCSLD* genes have been reported. For instance, mutations in *ATCSLD1* and *ATCSLD4* caused impairment in the germination of pollen and growth of pollen tubes (Bernal et al. 2008). The *atcsld2* and *atcsld3* mutant plants showed root hair phenotypes (Favery et al. 2001; Wang et al. 2001; Bernal et al. 2008). Mutation in *ATCSLD5* caused reduced growth, a relatively lower level of xylan, and homogalacturonan synthase activity with altered xylan occurrence (Bernal et al. 2007). Gu et al. (2016) reported that *ATCSLD5* was a direct target of SPEECHLESS and was involved in cell plate formation, including stomata lineage cells. In addition, analysis of the *sos6* mutant, an allele of *ATCSLD5,* revealed that *ATCSLD5* was vital for osmotic stress tolerance in *A. thaliana* (Zhu et al. 2010). *CSLD* genes also play important roles in other plants. In rice, abnormalities in the formation of root hair and growth were found for the mutations in *OsCSLD4* and *OsCSLD1,* where *OsCSLD4* was an ortholog of *ATCSLD5,* and *OsCSLD1* was highly similar to *ATCSLD2* and *ATCSLD3* (Kim et al. 2007; Li et al. 2009; Hu et al. 2010; Wu et al. 2010). A maize *csld1* mutant showed a defect in cell division and expansion (Hunter et al. 2012).

In this study, the author uncovered a new dominant-negative mutation of *ATCSLD5* termed *bgl23-D* due to its mutant phenotype of bagel-shaped guard cells. The author expressed cDNA of *bgl23-D* in *A. thaliana* WT by cell- or tissue-specific promoters to inhibit *ATCSLD5* and possibly other *ATCSLDs* for functional analysis of *ATCSLDs* in specific cells and tissues. In addition to the cytokinesis defect of guard mother cells (GMCs) originally observed in the *bgl23-D* mutant, new phenotypes of exine patterning and pollen structure were observed by expressing *bgl23-D* cDNA

in anther or tapetum. These results suggest that one or more *ATCSLDs* are involved in exine formation and that *bgl23-D* could be a useful tool for investigating the unknown function of *ATCSLDs* in plants.

Materials and methods

Screening of *bgl23-D* mutant

M2 seeds from ethylmethanesulfonate (EMS) mutagenized seeds of *A. thaliana* L*er* were purchased from Lehle Seeds (Round Rock, Texas, USA). The surface sterilized seeds were sowed on Murashige and Skoog (MS) medium and grown at 22 °C under continuous light. The abaxial epidermis of cotyledons from 14-day-old seedlings was observed by bright field microscopy for stomata phenotype.

Mapping and investigation of *bgl23-D* mutation

The *bgl23-D* mutant was crossed with *A. thaliana* (Col-0 accession). F2 plants indicating bagel-shaped stomata phenotype were grown and F3 seeds were harvested. The author selected F2 lines where all F3 seedlings showed the mutant phenotype. Fifty of these homozygous (*bgl23-D/bgl23-D*) F2 lines were combined and DNA was extracted with the DNeasy Plant Mini Kit (Qiagen) according to the manufacturer's instructions. The bulk population genomic DNA was subjected to whole-genome sequencing and analyzed by Mitsucal for mapping and identification of a mutation as described previously (Suzuki et al. 2018). The *bgl23-D* mutant of the Columbia background was established by three backcrosses with *A. thaliana* (Col-0) and was used for further experiments.

Genetic, protein domain structure of BGL23 (ATCSLD5) gene and multiple sequence alignment

The domain structure of the protein was drawn using the MyDomains-Image Creator (https://prosite.expasy.org/mydomains/). Amino acid sequence derived from the *bgl23-D* mutation was predicted by the Softberry online tool (http://www.softberry.com/). The BGL23 protein was retrieved from the Uniprot database (https://www.uniprot.org/). Multiple sequence alignments between protein sequences were performed by Clustal Omega (https://www.ebi.ac.uk/Tools/msa/clustalo/) and the result is shown with ESPript3.0 (http://espript.ibcp.fr/ESPript/ESPript/).

Preparation of entry clones and binary constructs

The cDNA clone pda17615 (RAFL09-06-N09) corresponding to AT1G02730 (*BGL23*/*ATCSLD5*) was obtained from the Experimental Plant Division, RIKEN Bio Resource Center (Tsukuba, Japan). Because the RAFL09-06-N09 contained a one-nucleotide deletion at two sites (T192 and T3137) within the coding sequence, the author repaired the sequence of the cDNA by two-round inverse PCR with primers listed in Table 2-1 and used it for further experiments as the *BGL23* cDNA clone. The coding sequence was amplified from the *BGL23* cDNA clone by adaptor PCR, first with *att*B1-BGL23-F and *att*B2-BGL23-R primers, and second with *att*B1-adaptor and *att*B2-adaptor primers as described previously (Nakagawa et al. 2007a). The amplified fragment was incorporated into pDONR201 to make an entry clone pDONR201-*BGL23* (*att*L1-*BGL23*-*att*L2) by BP reaction according to the manufacturer's instruction (Life Technology). The entry clone pDONR201-*bgl23-D* (*att*L1-*bgl23-D*-*att*L2) was prepared by introducing the mutation (C2989T) in pDONR201-*BGL23* using inverse PCR with primers listed in Table 2-1. Promoter entry clones were prepared as follows: The 5'-upstream sequences of SDD1 (AT1G04110), FAMA (AT3G24140), ATSP146 (AT5G57080), and BGL23 (AT1G02730) were amplified from the genomic DNA of *A. thaliana* (Col-0) with the primers listed in Table 2-1. The 5'-upstream sequence of FKP1 (AT4G11820) was amplified from the genomic clone (Ishiguro et al. 2010) with the primers FLK-3355-B1 and FLK-23-B1 (Table 2-1). The BP reaction was performed using the amplified fragment and pDONR-P4P1R (Invitrogen) to make the pDONR-L4-*ProSDD1*-R1, pDONR-L4-*ProFAMA*-R1, pDONR-L4-*ProATSP146*-R1, pDONR-L4-*ProBGL23*-R1, and pDONR-L4-*ProFKP1*-R1 entry clones (Table 2-1) according to the manufacturer's instructions (Invitrogen). The 5'-upstream sequence of FIL (AT2G45190) was amplified from the genomic clone with the primers FIL-3836F+att4 and FIL-1R+att1Long (Table 2-1). A linearized vector fragment of pDONR-P4P1R was prepared by PCR from an existing entry clone with primers DONR-attR1-LongF and DONR-attL4-R (Table 2-1). The two PCR products were joined by the SLiCE method (Motohashi 2017) to make a pDONR-L4-*ProFIL*-R1 entry clone. The entry clones pDONR-L4-*ProMUTE*-R1 were identical to *att*L4-P_{MUTE}-*att*R1 in Aboulela et al. (2017), pDONR-L4-*ProFBP1*-R1 was identical to pDONR-FBP1p in Suzuki et al. (2013), and pDONR-L4-*ProSP11*-R1was identical to pDONR-SPp in Ishiguro et al. (2010). The entry clones of pDONR-L4-*Pro*-R1, the pDONR201-*bgl23-D,* and binary vector R4pGWB401 were used for tripartite LR reaction as described previously (Nakagawa et al. 2008). The resultant binary constructs were designated as R4pGWB401-*ProX:bgl23-D*. Binary vector pGWB402 (Nakagawa et al. 2007b) was used to make the pGWB402-*Pro35S:bgl23-D* construct. For subcellular localization analysis, N-terminal fusion constructs of BGL23 and bgl23-D with synthetic green fluorescent protein (sGFP) and monomeric red fluorescent protein (mRFP) were prepared as follows: The entry clones pDONR201-*BGL23* and pDONR201-*bgl23-D* were subjected to LR reaction with pGWB406 and

pGWB455 (Nakagawa et al. 2007b) to make pGWB406-*Pro35S:sGFP-BGL23*, pGWB406-*Pro35S:sGFP-bgl23-D*, pGWB455-*Pro35S:mRFP-BGL23*, and pGWB455-*Pro35S:mRFP-bgl23-D*, respectively. A plasmid harboring mRFP-tagged sialyltransferase (ST) for Golgi marker (pH7RGW2-*Pro35S:ST-mRFP*) was gifted from Tomohiro Uemura (Uemura et al. 2012).

Generation of transgenic plants and growth conditions of *A. thaliana*

Transformation of *Agrobacterium tumefaciens* C58C1 (pMP90) was done using the freeze–thaw method as described previously (Weigel and Glazebrook 2002). The floral inoculating method was used to transform *A. thaliana* (Col-0) as per Narusaka et al. (2010). T0 seeds were surface sterilized and selected on MS medium supplemented with MS salts, 1% (w/v) sucrose, 0.01 % (w/v) myo-inositol, and 0.8% (w/v) agar with kanamycin (30 mg/L) and cefotaxime (100 mg/L). T1 plants were transplanted onto Jiffy-7 plant pot (Jiffy Products International BV, Zwijndrecht, Belgium) and grown at 22 ºC under a 16/8 h light/dark cycle. Homozygous T3 lines of a single transgene locus were prepared and used for further experiments. These transgenic lines were designated as *ProX:bgl23-D* (X indicates gene name) in this study.

Transient expression in *Nicotiana benthamiana* leaves for localization analysis

Transient expression of binary constructs in *N. benthamiana* leaves was performed according to the modified agroinfiltration method described in Aboulela et al. (2018) and fluorescence signal was observed by confocal microscopy.

PI staining and DAPI staining

Propidium iodide (PI) staining was done as described before (Nakamura et al. 2012). To observe the quiescent center (QC), primary roots from 3- to 5-day-old vertically grown seedlings were immersed in PI staining solution (SIGMA, P4170) at a concentration of 10 μg/mL. The roots were examined using a confocal microscope after being washed with deionized water. For nuclear staining, cotyledons were fixed in 90% ethanol and 10% acetic acid at -20 °C for 1 h. Fixed cotyledons were rinsed in 200 mM NaPi buffer (pH 7.0), then stained in 100 mM NaPi buffer containing 1 mM EDTA, 0.1% Triton X-100 and 0.4 μg/mL 4’6-diamidino-2-phenylindole (DAPI) under vacuum (0.05 Mpa) for 5 min. The stained samples were observed with a TCS SP5 confocal laser scanning microscope.

Analysis of stomata and pollen phenotype

For analysis of stomata phenotypes, the abaxial epidermis of fully expanded rosette leaves or cotyledons was peeled off as described by Svozil et al. (2016) and examined under a BZ-X710 All-in-One fluorescence microscope (KEYENCE, Osaka, Japan). The pollen phenotype of 60-day-old plants was examined by an S-4800 field emission SEM (Hitachi High-Tech, Tokyo, Japan) or TM3000 miniscope (Hitachi High-Tech) as described previously (Tanaka et al. 2013). Pollen grains from 60-day-old plant were stained in DAPI solution as described in Tanaka (et al. 2013) and observed by a BZ-X710 All-in-One fluorescence microscope (KEYENCE). Semi-thin sectioning of floral buds at various developmental stages was carried out according to Aboulela et al. (2018) The RX-860 rotary microtome (Yamato Kohki Industrial, Saitama, Japan) was used to prepare sections ranging in size from 3 to 5 μm. The sections were stained with toluidine blue solution as described previously (Aboulela et al. 2018) and observed by the BZ-X710 All-in-One fluorescence microscope (KEYENCE).

Stress treatment and germination assay

The salt and osmotic tolerance abilities of transgenic *A. thaliana* were determined by seed germination assay in different concentrations of NaCl, KCl, and mannitol. After incubation at 4 °C in the dark for 48 h, plates were transferred to a growth chamber (22 °C, continuous light), and germinated seeds were counted every 12 h. The seed germination rate was calculated according to Billah et al. (2020) using the following formula:

$$\text{Germination rate (\%)} = (\text{Number of seeds germinated / total number of seeds}) \times 100\ \%$$

Water loss from transgenic and WT plants were determined as described previously (Zhao et al. 2017).

Chlorophyll fluorescence measurements

A Closed FluorCam 800MF (Photon system instruments, Czech Republic) was used to measure chlorophyll fluorescence in *A. thaliana* leaves. After 30 minutes of incubation in the dark, plants were used for chlorophyll fluorescence measurements. The chlorophyll fluorescence parameters such as F_v/F_m, øPSII, and non-photochemical quenching (NPQ), were calculated using chlorophyll fluorescence parameters as follows (Baker 2008): $F_v/F_m = (F_m - F_o)/F_m$, øPSII = $(F_m' - F)/F_m'$, and NPQ = $(F_m - F_m')/F_m'$. øPSII and NPQ were measured with an actinic light intensity of 100 μmol photons m^{-2} sec^{-1}.

Confocal microscopy

Plant samples were viewed with a TCS SP5 confocal laser scanning microscope (Leica Microsystems, Wetzlar, Germany) using an HCX IRAPO L 25.0x0.95 water immersion objective lens. The sGFP was excited with an argon laser line (488 nm) and the fluorescence signal was detected at 500–530 nm. The mRFP and PI were excited with a helium-neon laser line (543 nm) and the fluorescence signals were detected at 555–615 nm. DAPI was excited with a diode laser line (405 nm) and fluorescence was observed at 420–470 nm.

RNA extraction, cDNA synthesis, and reverse transcription PCR (RT-PCR)

Total RNAs were extracted from the various tissues (leaf, flower, and flower bud) using the RNeasy Mini Kit (Qiagen). cDNA was synthesized from 0.5 μg of RNA using the ReverTraAce™ qPCR RT Master MIX with gDNA Remover (FSQ-301, TOYOBO, Osaka, Japan) as per the manufacturer's protocol. The resulting cDNAs were diluted five times with nuclease-free water and 2 μL aliquots were used as templates for RT-PCR. PCR amplifications were performed with a final volume of 20 μL by using 2x Quick Taq™ HS DyeMix (TOYOBO) for 30 cycles (94 °C for 2 min, 94 °C for 30 s, 58 °C for 30 s, and 68 °C for 1 min) using a T100 thermal cycler (Bio-Rad, CA, USA). The primers for an endogenous *BGL23* (RT-BGL23(bgl23-D)-F and RT-BGL23-R), a *bgl23-D* transgene (RT-BGL23(bgl23-D)-F and RT-bgl23-D-R), and *ACTIN2* (RT-ACT2-F and RT-ACT2-R for internal control) are listed in Table 2-1. Amplified fragments were separated using 1% agarose gel electrophoresis and visualized with HydraGreen Safe DNA Dye (ACTGene, NJ, USA).

Statistical analysis

The data in all figures are presented as mean ± SE from three independent biological replicates. The ordinary one-way ANOVA (Dunnet's test) and Tukey's multiple comparison test were done to assess the significant differences among multiple groups, while the unpaired two-tailed Welch's *t*-test was performed for the mean comparison between two groups. GraphPad Prism Software version 8.0 (GraphPad Software, San Diego, CA, USA) was used to create all of the graphical diagrams and the statistical analysis in this study.

Table 2-1. Oligonucleotides used in this study

Oligonucleotides	Sequence
Inverse-PCR-BGL23-F1-repair-deltaT192*	TCGGAGATCtAACGGTGAT
Inverse-PCR-BGL23-R1-repair-deltaT192	TTCCCGCTGCTAATGGAAGT
Inverse-PCR-BGL23-F2-repair-deltaT3137**	CTTCAGGGTCTTCtTAAGGTAATTG
Inverse-PCR-BGL23-R2-repair-deltaT3137	AACAGCTGCAGGGTGTGC
attB1-BGL23-F	AAAAAGCAGGCTCCGACACTATGGTGAAATCAGCAGCTTC
attB2-BGL23-R	AGAAAGCTGGGTAGACACTTCAAGGGAATTGAAACTGCATA
Inverse-PCR-for-bgl23-D-F-C2989T***	TCTTGATCTATtTCCTCTCGATAACA
Inverse-PCR-for-bgl23-D-R-C2989T	ACGTTATGTCGAGTGATTGGA
ProSDD1-attB4	5'-GGGGACAACTTTGTATAGAAAAGTTGGCTGAGACACTCACCATGGGGTGAGCTGTGTG-3'
ProSDD1-attB1	5'-GGGGACTGCTTTTTTGTACAAACTTGTGACACTTGGAGAGAGTTAAAAAAAGGAGTT-3'
ProFAMA-attB4	5'-GGGGACAACTTTGTATAGAAAAGTTGGCTGAGACACTGAAGCTTCCAAACTTCATG- 3'
ProFAMA-attB1	5'-GGGGACTGCTTTTTTGTACAAACTTGTGACACTTGCTATTCGTGGTAGTTGAAT- 3'
ProATSP146-attB4	5'-GGGGACAACTTTGTATAGAAAAGTTGGCTGAGACACTCCACCGGCAACACCACCAC-3'
ProATSP146-attB1	5'-GGGGACTGCTTTTTTGTACAAACTTGTGACACTCTTTGGCTCTGCTTTTTGACTG-3'
ProBGL23-attB4	5'-GGGGACAACTTTGTATAGAAAAGTTGGCTGAGACACTTAGGAAATTGTGCCTAATGACGTG-3'
ProBGL23-attB1	5'-GGGGACTGCTTTTTTGTACAAACTTGTGACACTCTTTGGTTCACAATTAGCAGTG-3'
ProFIL-3836F+att4	5'-TGTATAGAAAAGTTGGAAGTGTACTGCCATGTAACACGGT-3'
ProFIL-1R+att1Long	5'-TTTACGTTTCTCGTTCAACTTTTTTGTACAAACTTGCTTTTTTGTAAGAAGGGGAAAAATATTGGAAGCTGATCTTTTTTTGGGAGTG-3'
FLK-3355-B4	5'-GGGGACAACTTTGTATAGAAAAGTTGTCTAGAGTCTGATGCCACATGTACACAGTGGCGGAT-3'
FLK-23-B1	5'-GGGGACTGCTTTTTTGTACAAACTTGCTCTGAAGAGACTGAAATCGAAAGGT-3'
RT-BGL23-WT-F	5'-AAACGAGCAGTTCTGGGTCA-3'

*Small letter is T192 deleted in RAFL09-06-N09

**Small letter is T3137 deleted in RAFL09-06-N09

***Small letter is T of C2989T in *bgl23-D*

Results

Isolation and characterization of *bgl23-D* mutant

The author isolated a mutant showing a stomata phenotype that looks bagel-shaped by screening EMS mutagenized *A. thaliana* (L*er*). The mutation was dominant, as all F1 resulting from 10 different backcrosses (n = 10, number of backcrosses) exhibited the bagel-shaped stomata. From these results, the author named this mutant *bagel23-D* (*bgl23-D*). The *bgl23-D* mutant showed a variety of incompletely divided single guard cells (SGCs), SGC with a pore at one side along the division plane of GMC (Fig. 2-1aii), and SGC with two pores at both sides along the division plane of GMC (Fig. 2-1aiii), and oval SGC with a narrow pore at one side along the division plane of GMC (Fig. 2-1aiv). Incompletely divided SGCs had two nuclei (Fig. 2-1b), meaning the various degrees of cytokinesis defect during GMC division.

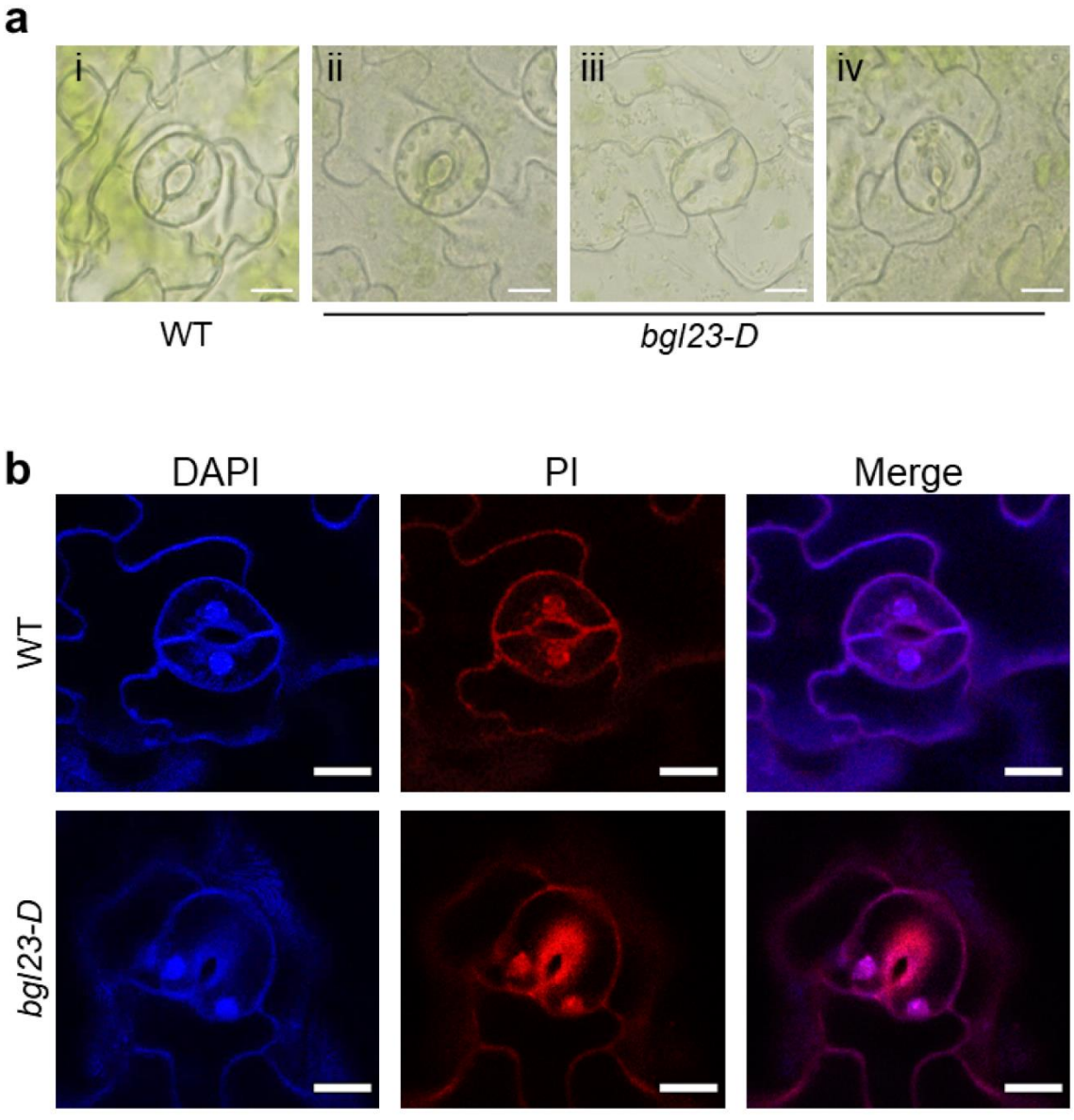

Fig. 2-1. Phenotype of *bgl23-D* mutant. **a** Bagel-shaped single guard cells (SGCs) in *bgl23-D* mutant. **ai** WT. **aii** SGCs with pore at one side along division plane of guard mother cell (GMC). **aiii** SGC with two pores at both sides along division plane of GMC. **aiv** Oval SGC with a narrow pore at one side along division plane of GMC. **b** Bagel-shaped SGCs with two nuclei in *bgl23-D* mutant. Scale bars = 10 μm (**a**, **b**).

Identification of *a bgl23-D* mutation

Whole-genome sequencing of homozygous F2 lines and analysis by Mitsucal revealed that the ratio of SNPs linked to *bgl23-D* mutation was maximum around 0.5 Mb of chromosome 1 (Fig. 2-2a). The author searched base substitutions typically caused by EMS that were expected to affect protein function in the 0–5 Mb region of chromosome 1 using Mitsucal. As a result, the author found a C to T substitution at the position of 3,220 bp in the AT1G02730 encoding cellulose synthase-like D5 (ATCSLD5) (Fig 2-2b). The author introduced a construct of own promoter-driven *ATCSLD5* cDNA containing C3220T (C2989T in the cDNA) substitution (*ProBGL23:bgl23-D* construct) into WT-Col and found that the transgenic plants showed bagel-shaped stomata phenotype (Fig. 2-3), as seen in the *bgl23-D* mutant. From these results, the author concluded that *ATCSLD5* with C3220T mutation was the responsible gene for the *bgl23-D* mutant. The *bgl23-D* mutation occurred in the third exon (Fig. 2-4a) and resulted in an L997F amino acid substitution in the 4th transmembrane domain of the ATCSLD5 (Fig. 2-4b and Fig. 2-5). The disruptant of *ATCSLD5* (SAIL_724_G04) also showed cytokinesis defects, including GMC (Gu et al. 2016), meaning that *bgl23-D* mutation exerted a dominant-negative effect on cell plate formation during cytokinesis.

Because a salt overlay sensitive 6 (*sos6*) mutant, an allele of *ATCSLD5,* was sensitive to salt and osmotic stresses (Zhu et al. 2010), the author performed a seed germination assay under various conditions to test the stress sensitivity of the *bgl23-D* mutant. The germination rate of *bgl23-D* mutant was decreased by the treatment with NaCl, KCl, and mannitol, while WT showed no decrease in germination rate under these stress conditions (Fig. 2-6a-c). These results indicated that *bgl23-D* mutant was sensitive to salt and osmotic stress like *sos6* mutant.

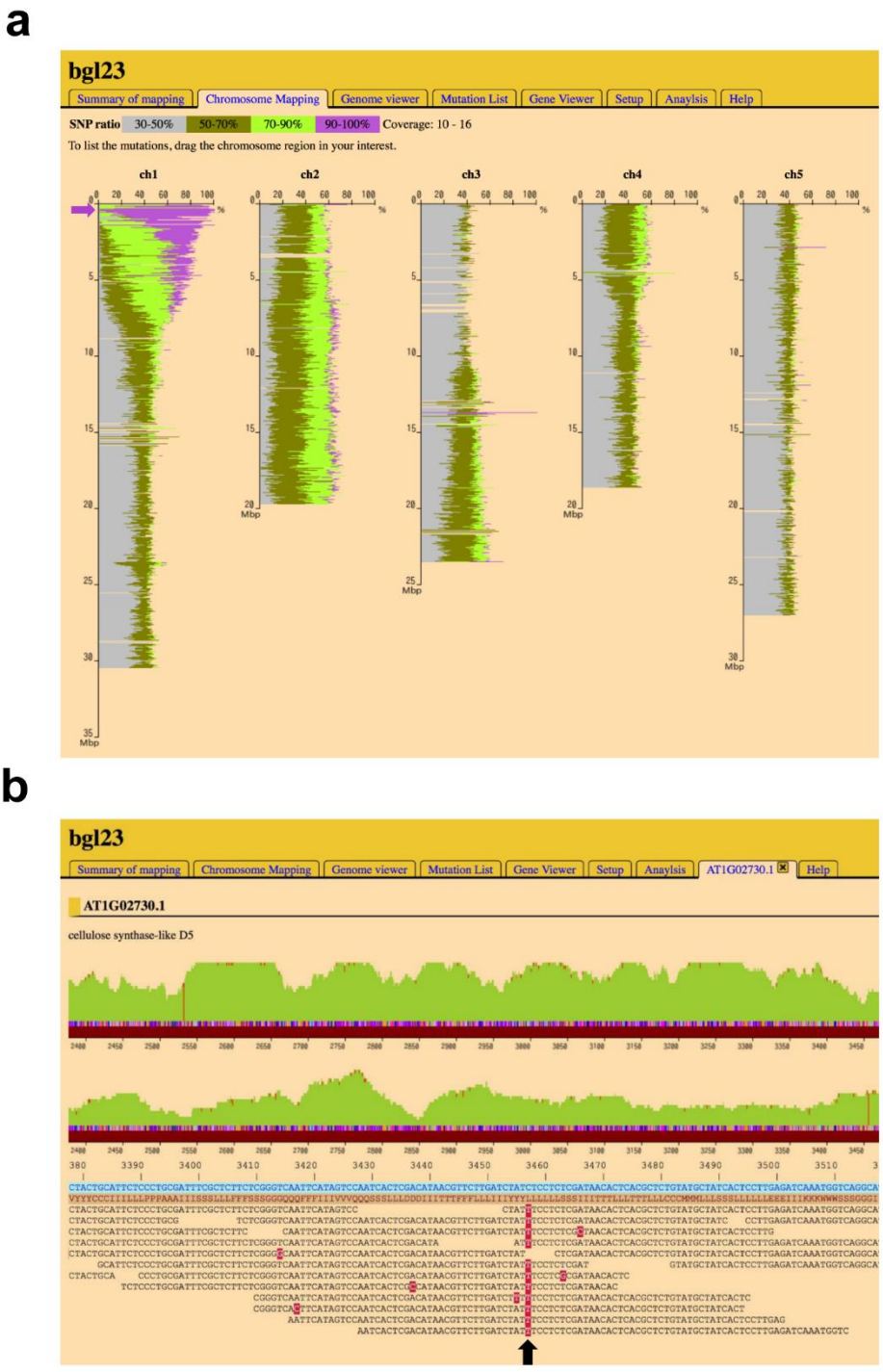

Fig. 2-2. Mapping of *bgl23-D* mutation by Mitsucal computer system. **a** Chromosome mapping for *bgl23-D.* The Arabidopsis chromosomes were depicted, ranging from ch1 to ch5. The ratio of substitutions are represented by horizontal axes in percentage, while vertical axes indicate the coordinate of chromosome in Mb. The purple arrow indicates the peak region showing the maximum ratio of SNPs linked to *bgl23-D* mutation. **b** Gene viewer of ATCSLD5 (AT1G02730),

corresponding gene for *bgl23-D* mutation. The lower part of the figure represents the alignment of the reads. The reference sequences (sky blue background) and amino acid sequence (brown background) for AT1G02730 were shown by the top two lines. The single nucleotide substitution in reads was denoted by the white character in the red box and indicated by the black arrow.

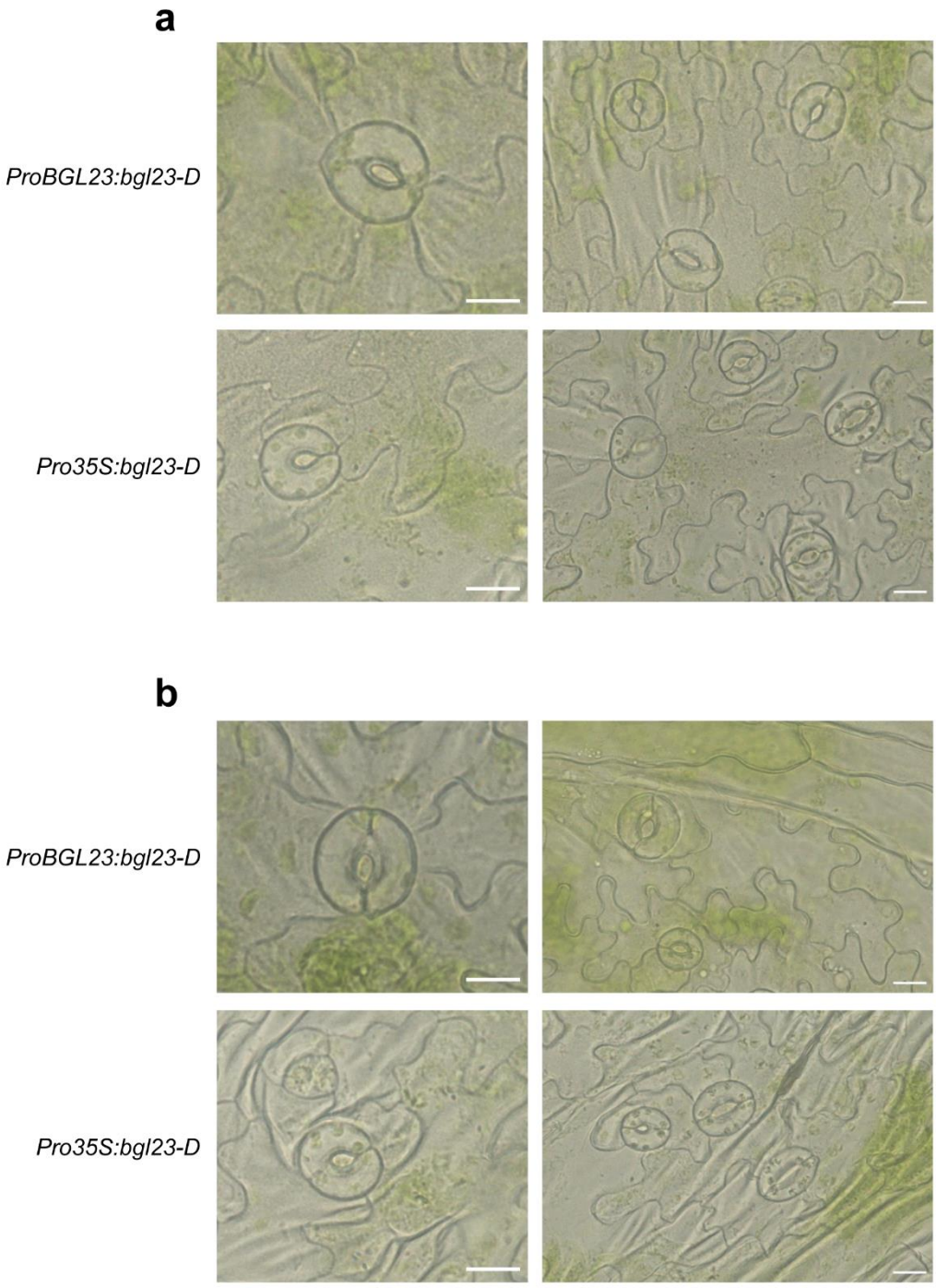

Fig. 2-3. Bagel-shaped stomata in *ProBGL23:bgl23-D* and *Pro35S:bgl23-D*. a Bagel-shaped stomata in T1 of *ProBGL23:bgl23*-D (upper) and *Pro35S:bgl23*-D (lower). **b** Bagel-shaped stomata in T3 of *ProBGL23:bgl23-D* (upper) and *Pro35S:bgl23-D* (lower). Scale bars = 10 μm.

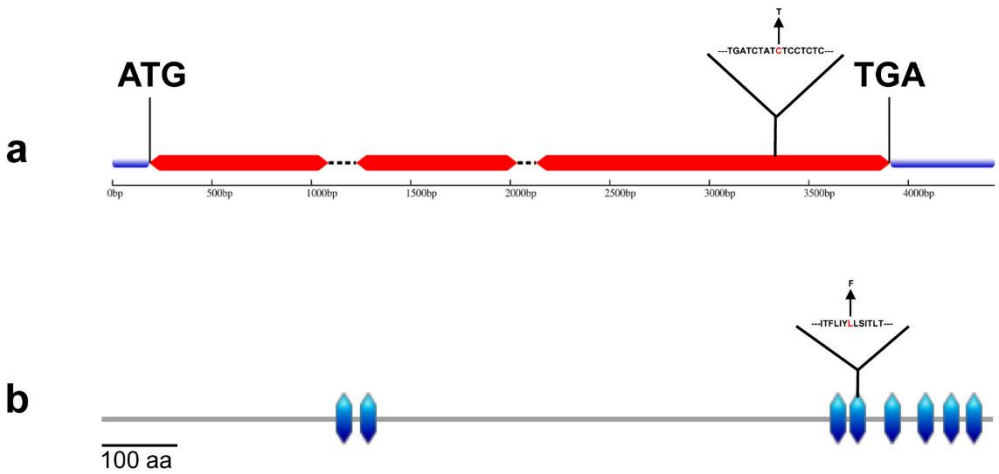

Fig. 2-4. The *bgl23-D* mutation in *ATCSLD5*. **a** Exon/Intron structure of *ATCSLD5* and position of *bgl23-D* mutation. Red boxes, black dashed lines, and blue boxes indicate exons, introns, and untranslated regions, respectively. **b** Domain structure of ATCSLD5 and position of *bgl23-D* mutation. Hexagonal blue boxes indicate the transmembrane domain.

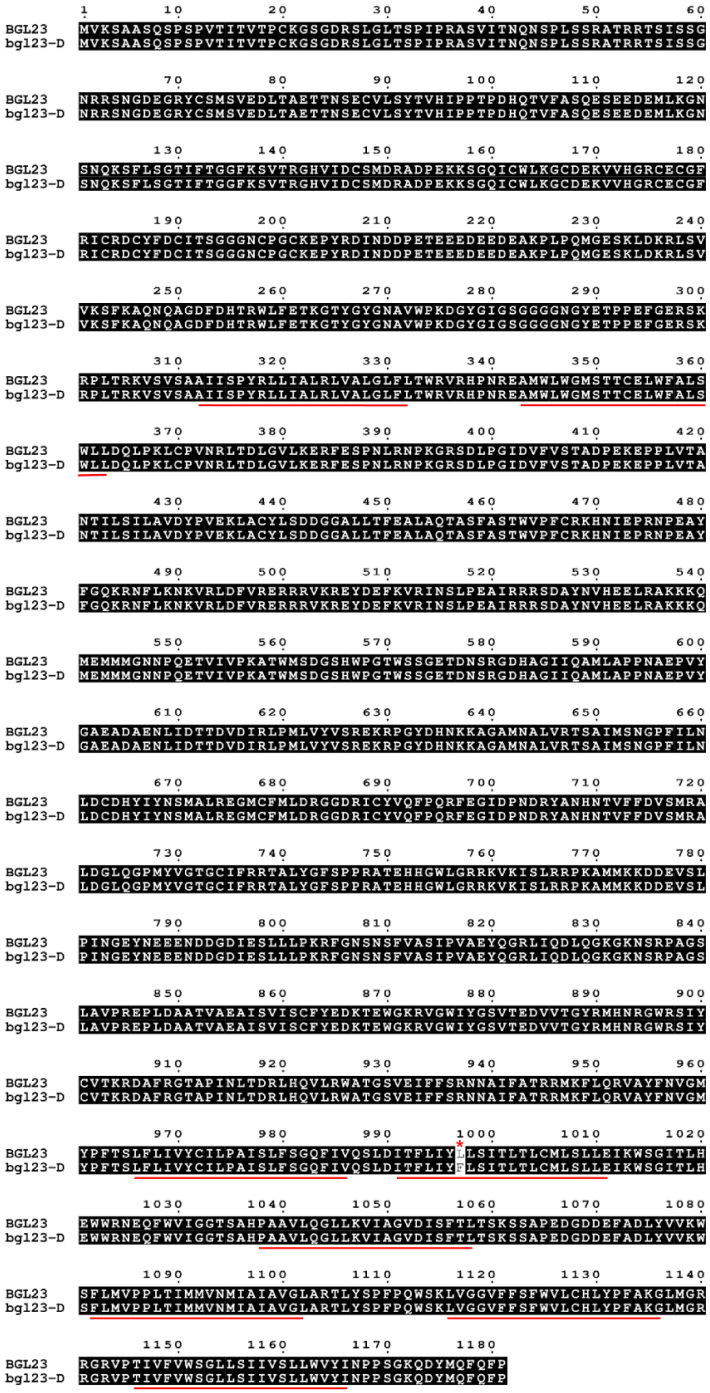

Fig. 2-5. Amino acid sequence alignment of BGL23 and bgl23-D protein. Amino acid sequence alignment of BGL23 (WT) protein and bgl23-D (mutant) protein. The red underlines indicate the position of the transmembrane domain. TMD1 (312aa-332aa); TMD2 (343aa-363aa); TMD3 (966aa-986aa); TMD4 (991aa-1011aa); TMD5 (1038aa-1058aa); TMD6 (1082aa-1102aa); TMD7 (1116aa-1136aa); and TMD8 (1146aa-1166aa). TMD, transmembrane domain. The red asterisk indicates the substitution of amino acid by *bgl23-D* mutation.

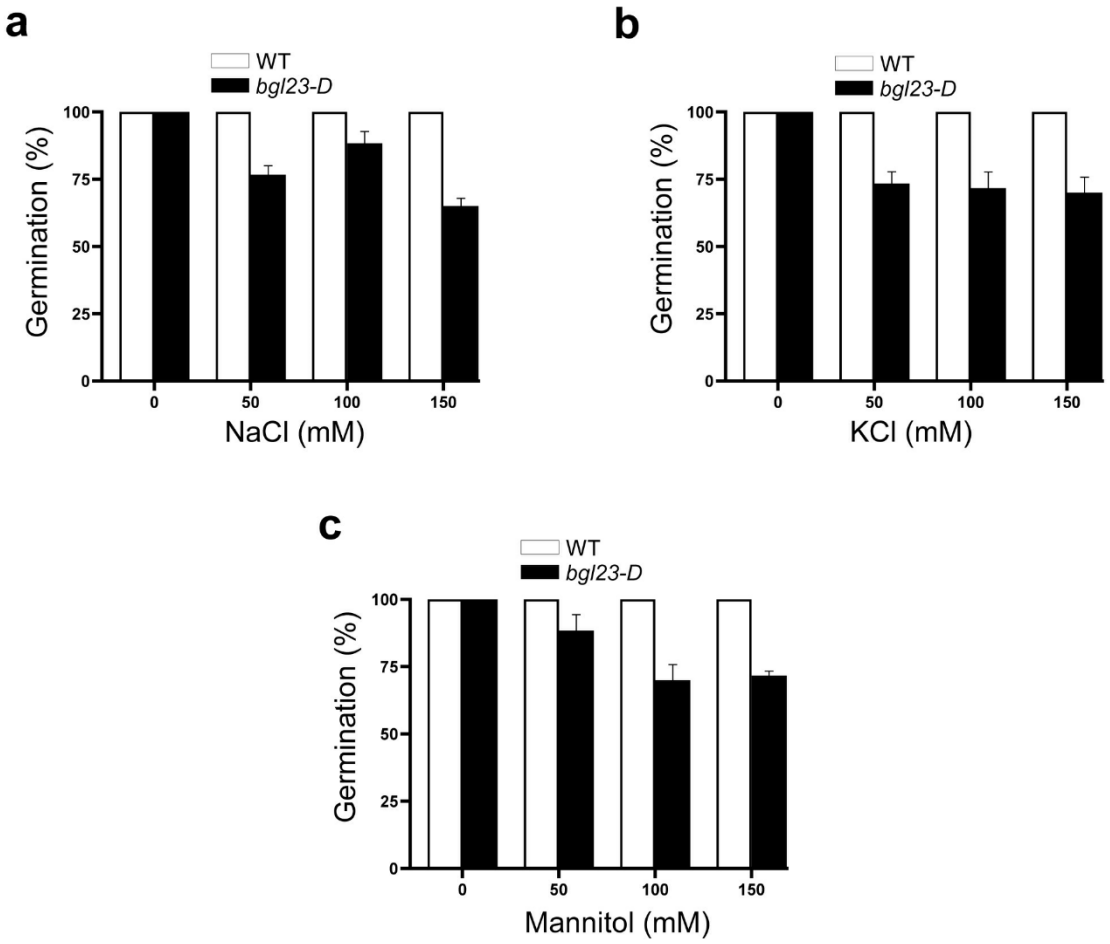

Fig. 2-6. Salt and osmotic stress responses of *bgl23-D* mutant. Seed germination of WT and *bgl23-D* mutant on different concentrations of NaCl (**a**), KCl (**b**), and Mannitol (**c**). 20 seeds from each plant line were used for the germination assay. Germination of seeds was analyzed at 84 h. The data are presented as mean ± SE from three independent biological replicates (n = 3).

The *bgl23-D* mutation did not affect subcellular localization of the protein

To analyze the effect of *bgl23-D* mutation on the subcellular localization of the protein, the author transiently expressed sGFP-BGL23 and sGFP-bgl23-D with Golgi marker ST-mRFP (Uemura et al. 2012) in *N. benthamiana* leaves. Both sGFP-BGL23 and sGFP-bgl23-D exhibited co-localization with ST-mRFP as dot-like structures (Fig. 2-7a and Fig. 2-7b), which is consistent with previous report (Bernal et al. 2007) that indicated co-localization of YFP-ATCSLD5 and STtmd-GFP. Furthermore, the author co-expressed sGFP-BGL23 with mRFP-bgl23-D, or sGFP-bgl23-D with mRFP-BGL23, and found overlap of GFP and RFP signals in both combinations (Fig. 2-7c and Fig. 2-7d). These results indicated that the bgl23-D protein was normally localized, and the *bgl23-D* mutation did not affect subcellular localization of the protein.

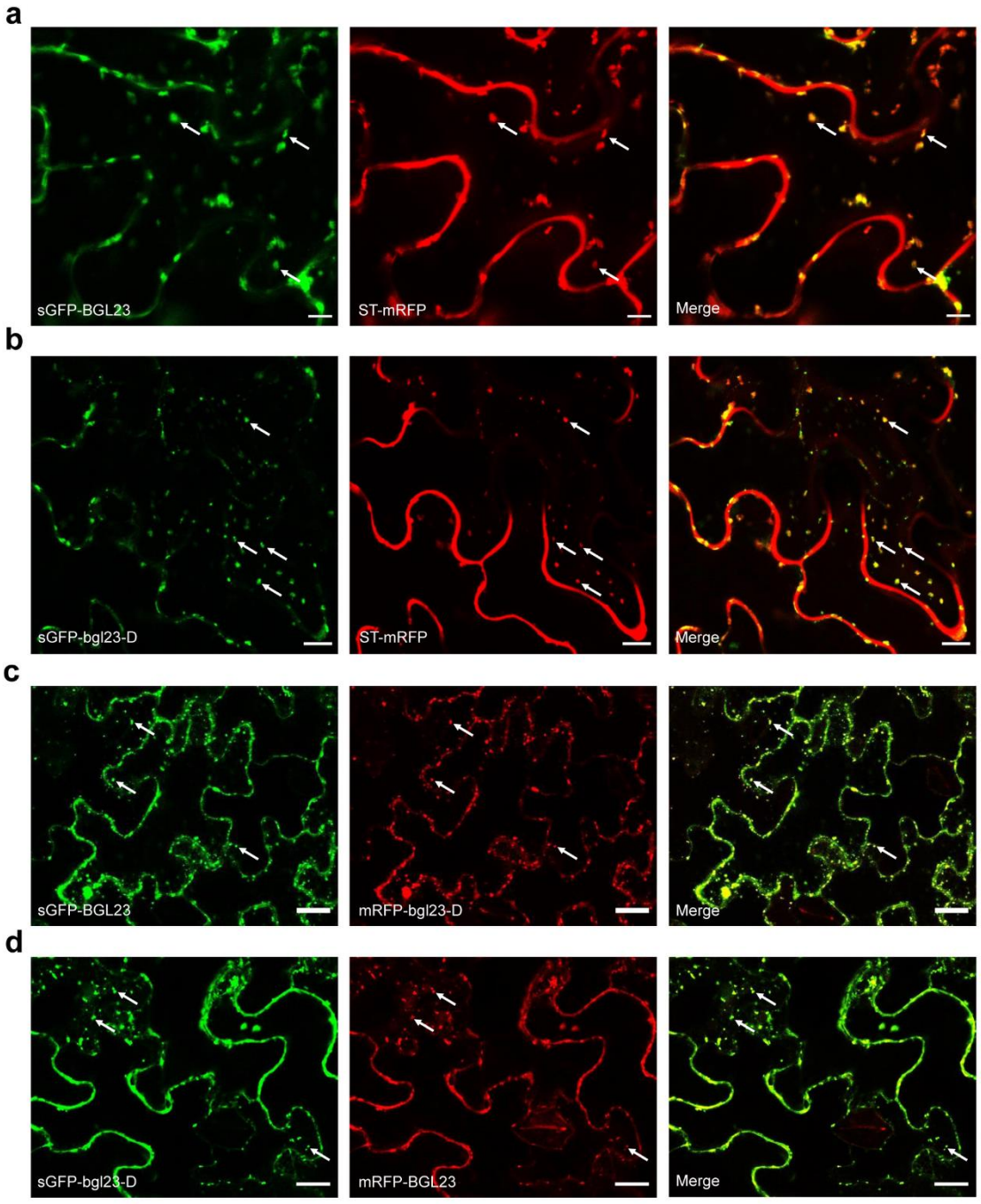

Fig. 2-7. Subcellular localization and co-localization of BGL23 and bgl23-D in *N. benthamiana* leaf epidermal cells. **a**, **b** Co-localization of sGFP-BGL23 and sGFP-bgl23-D with Golgi marker ST-mRFP**.** Arrows indicate Golgi apparatus (**a**, **b**). **c** Co-localization of sGFP-BGL23 and mRFP-bgl23-D. Arrows indicate punctate dot-like structures labeled with sGFP and mRFP. **d** Co-localization of sGFP-bgl23-D and mRFP-BGL23. Arrows indicate punctate dot-like structures labeled with sGFP and mRFP. Scale bars = 20 μm (**a-d**).

Expression of *bgl23-D* cDNA with specific promoters to suppress the function of ATCSLD5 in target cells and tissues

Because *bgl23-D* is a dominant-negative allele, the author planned to use it as a genetic tool to suppress the function of ATCSLD5 in target cells and tissues by expressing *bgl23-D* cDNA with a specific promoter. The author selected two kinds of targets, (1) stomata: the region showing phenotype in the *bgl23-D* mutant, and (2) pollen and root: the regions not showing phenotype in the *bgl23-D* mutant. Promoters of stomata lineage-specific genes such as promoter of *SDD1* (*ProSDD1*) (Berger and Altmann 2000), promoter of *MUTE* (*ProMUTE*) (Pillitteri et al. 2007), and promoter of *FAMA* (*ProFAMA*) (Shirakawa et al. 2014) were used to target stomata. The author also use the promoter of *FIL* (*ProFIL*) (Siegfried et al. 1999; Sarojam et al. 2010) to target stomata on the abaxial side of a leaf. For pollen, the author used the promoter of tapetum-specific genes *SP11* (*ProSP11*) (Takayama et al. 2000), *FKP1* (*ProFKP1*) (Ishiguro et al. 2010) and *FBP1* (*ProFBP1*) (Suzuki et al. 2013). The author also used the promoter of the *ATSP146* gene (*ProATSP146*) (Nakamura et al. 2012) specifically expressed in anther and QC to target pollen and root. In addition to these specific promoters, own promoter (*ProBGL23*) and constitutive promoter *Pro35S* were also employed in this study. The schematic illustration of each construct is shown in Fig. 2-8. The author examined the expression of introduced *bgl23-D* as well as endogenous *BGL23* in established *Pro:bgl23-D* T3 transgenic lines by RT-PCR (Fig. 2-9c). The expression of *bgl23-D* was detected in the leaf of *ProSDD1:bgl23-D*, *ProMUTE:bgl23-D*, *ProFAMA:bgl23-D*, *ProFIL:bgl23-D*, *ProBGL23:bgl23-D*, and *Pro35S:bgl23-D* (Fig. 2-9a), and in the flowers of *ProSP11:bgl23-D*, *ProFKP1:bgl23-D*, *ProFBP1:bgl23-D*, and *ProATSP146:bgl23-D* (Fig. 2-9b). These T3 transgenic lines were used in this study except for experiments analyzing T1.

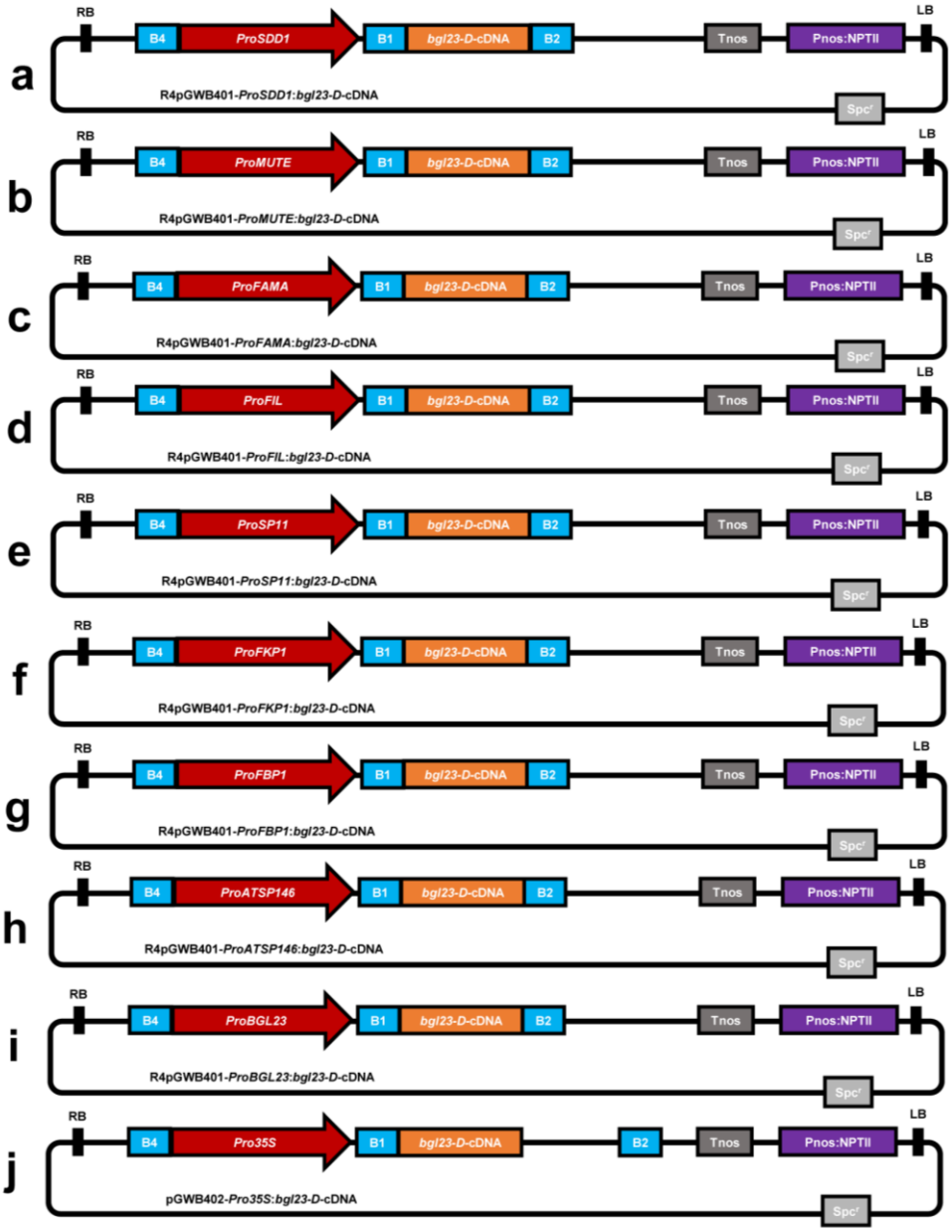

Fig. 2-8. Schematic illustration of vector constructs for expression of *bgl23*-D cDNA by specific promoters. **a** R4pGWB401-*ProSDD1:bgl23-D*-cDNA. **b** R4pGWB401-*ProMUTE:bgl23-D*-cDNA. **c** R4pGWB401-*ProFAMA:bgl23*-D-cDNA. **d** R4pGWB401-*ProFIL:bgl23-D*-cDNA. **e** R4pGWB401-*ProSP11:bgl23-D*-cDNA. **f** R4pGWB401-*ProFKP1:bgl23-D*-cDNA. **g** R4pGWB401-*ProFBP1:bgl23-D*-cDNA. **h** R4pGWB401-*ProATSP146:bgl23-D*-cDNA. **i** R4pGWB401-*BGL23:bgl23-D*-cDNA. **j** pGWB402-*Pro35S:bgl23-D*-cDNA. The region mentioned in the figures; B1, *attB*1; B2, *attB2*; B4, *attB4*; LB, left border; RB, right border; Tnos, nopaline synthase terminator; the gene for spectinomycin resistance (Spc^r) in bacteria. No scale was followed to draw the figures.

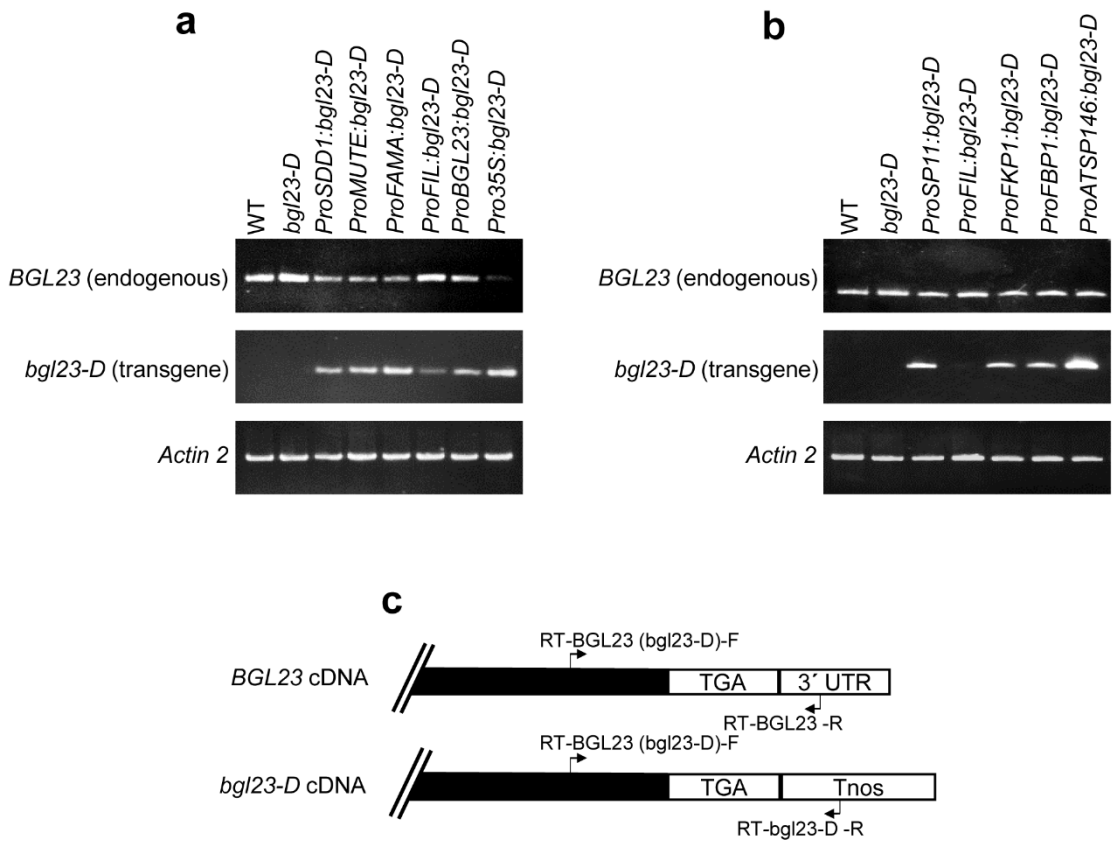

Fig. 2-9. Expression analysis of *BGL23* (endogenous) and *bgl23-D* (transgene) by RT-PCR. **a** Expression of *BGL23* (endogenous) and *bgl23-D* (transgene) in leaf. RNA was isolated from the leaf of 14-day-old WT and transgenic plants grown in MS plate. **b** Expression of *BGL23* (endogenous) and *bgl23-D* (transgene) in floral organs. RNA was extracted from flower buds and open flowers from 60-day-old WT and transgenic plants. *ACTIN2* was used as an internal control. **c** Position of primers in *BGL23* cDNA and *bgl23-D* cDNA for RT-PCR. Black arrows indicate the position of forward and reverse primers. The figures are not drawn to any scale.

Expression of *bgl23-D* cDNA by stomata lineage–specific promoters caused incompletely divided GCs

First, the author analyzed the effect of *bgl23-D* expression by stomata lineage-specific promoters. T1 plants of *ProSDD1:bgl23-D*, *ProMUTE:bgl23-D*, and *ProFAMA:bgl23-D* exhibited bagel-shaped incompletely divided GCs like *bgl23-D* mutant as expected from the dominant nature of *bgl23-D* for stomata phenotype (Fig. 2-10a). T1 plants of *ProBGL23:bgl23-D* and *Pro35S:bgl23-D* also showed bagel-shaped stomata phenotype (Fig. 2-3a). The homozygous T3 of each transgenic line exhibited a more clear stomata phenotype (Fig. 2-10b and Fig. 2-3b) and two nuclei were observed in bagel-shaped SGCs by DAPI staining (Fig. 2-10c). The frequency of bagel-shaped stomata was 18.93 ± 2.47%, 29.33 ± 1.35%, 23.07 ± 2.31% and 33.6 ± 0.23% in the *bgl23-D* mutant, *ProSDD1:bgl23-D*, *ProMUTE:bgl23-D*, and *ProFAMA:bgl23-D*, respectively (Fig. 2-10d). Among the three stomata lineage-specific promoter constructs, *ProFAMA:bgl23-D* showed the most efficient (33.6%) and significant abnormalities in stomata structure. *ProSDD1:bgl23-D* and *ProFAMA:bgl23-D* showed statistically significant differences in terms of the frequency of bagel-shaped stomata compared to *bgl23-D* mutant (Fig. 2-10d). Although the frequency of bagel-shaped stomata between *ProSDD1:bgl23-D* and *ProMUTE:bgl23-D,* and *ProSDD1:bgl23-D* and *ProFAMA:bgl23-D* was not statistically significant (Fig. 2-10d), *ProFAMA:bgl23-D* exhibited a statistically significant difference in frequency of bagel-shaped stomata compared to that of *ProMUTE:bgl23-D* (Fig. 2-10d). In addition to bagel-shaped SGC with a small pore (Fig. 2-11a-d) commonly generated in constructs of the stomata lineage-specific promoter**,** SGC with two small pores (Fig. 2-11e), donut-shaped SGC having a single pore at the middle of the cell (Fig. 2-11f and Fig. 2-11g), and the most severely affected spherical SGC without a pore (Fig. 2-11h) were observed in *ProFAMA:bgl23-D*.

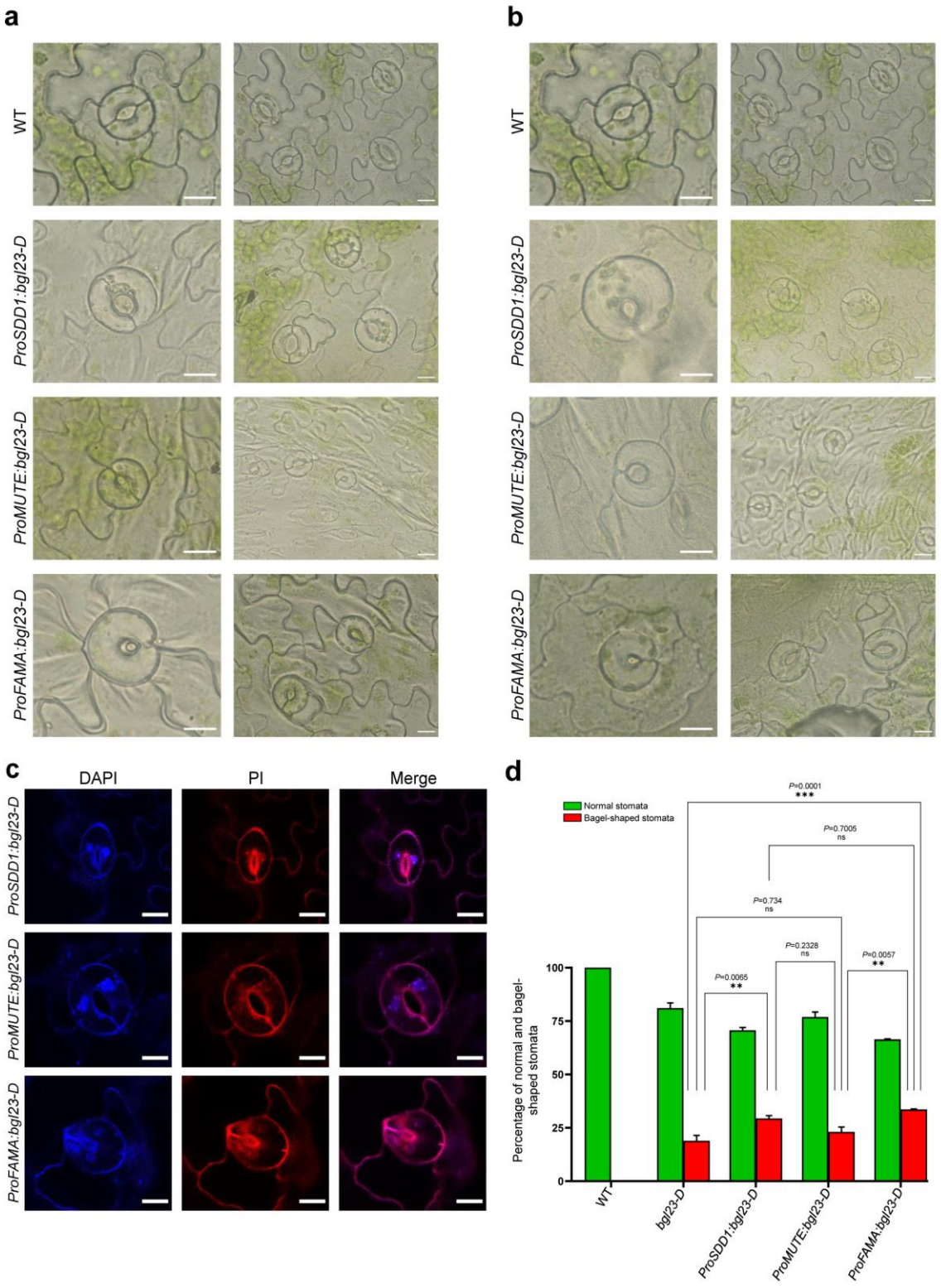

Fig. 2-10. Bagel-shaped stomata in transgenic plants expressing *bgl23-D* cDNA by promoters of stomata lineage genes. **a** Bagel-shaped stomata in T1 of *ProSDD1:bgl23-D*, *ProMUTE:bgl23-D,* and *ProFAMA:bgl23-D*. **b** Bagel-shaped stomata in T3 of *ProSDD1:bgl23-D*, *ProMUTE:bgl23-D,* and *ProFAMA:bgl23-D.* **c** Observation of nuclei in SGCs of *ProSDD1:bgl23-D*, *ProMUTE:bgl23-D,* and *ProFAMA:bgl23-D*. Image of abaxial epidermis of cotyledon stained

with DAPI and PI. **d** Frequency of normal and bagel-shaped stomata in transgenic plants. Abaxial epidermis of leaves was peeled from 14-day-old T3 plants. Fifty stomata were counted from a single plant, while a total of 250 stomata were counted from five individual plants. Single biological replicates consist of 250 stomata. Three independent biological replicates were performed. The data are presented as mean ± SE (n = 3). Asterisks indicate significant differences (*P < 0.05; **P < 0.01; ***P < 0.001; and ns = not significant) at a significance level of P < 0.05 (Tukey's multiple comparison test). Scale bars = 10 μm (**a-c**).

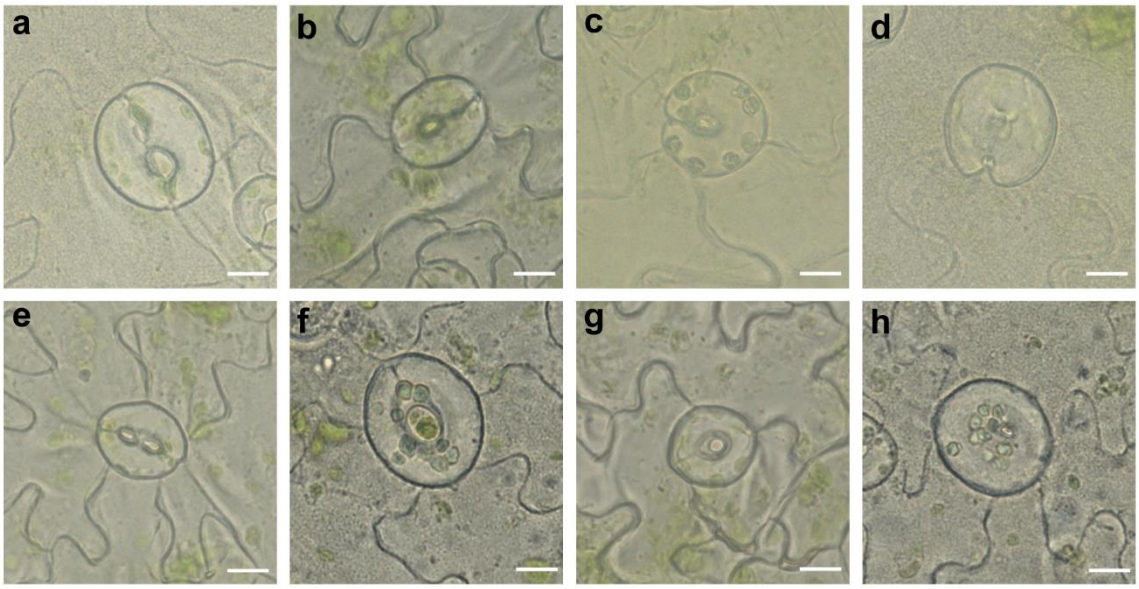

Fig. 2-11. Severely affected bagel-shaped stomata in *ProFAMA*:*bgl23-D*. **a-h** Various bagel-shaped phenotypes of stomata in T3 of *ProFAMA:bgl23-D*. Scale bars = 10 μm.

Expression of *bgl23-D* cDNA by *FIL* promoter generated incompletely divided GMC in both abaxial and adaxial epidermis of the leaf with different frequencies

The *FIL* gene is expressed in the abaxial side of developing leaf and floral organs (Siegfried et al. 1999; Sarojam et al. 2010). In the *ProFIL:bgl23-D* transgenic plants, the author found bagel-shaped stomata similar to those caused by stomata lineage promoter constructs in the epidermis of both the abaxial and adaxial side of leaves (Fig. 2-12a). Next, the author examined and compared the frequency of bagel-shaped stomata on the abaxial and adaxial surfaces. Despite no statistically significant difference, the abaxial surface had a higher rate of bagel-shaped stomata at about 21.3%, whereas the adaxial surface had a lower rate of abnormal stomata at 16.3% (Fig. 2-12b). In contrast, the almost same frequency of bagel-shaped stomata was observed on the abaxial and adaxial surfaces in the *bgl23-D* mutant (abaxial 22.4%, adaxial 23.3%) (Fig. 2-12c) and *Pro:FAMA-bgl23-D* (abaxial 30.4%, adaxial 31.6%) (Fig. 2-12d). Taken together, these results indicated that the difference in frequency of bagel-shaped stomata between abaxial and adaxial

surfaces observed in *ProFIL:bgl23-D* is due to the abaxial preferred expression of *bgl23-D* by FIL promoter.

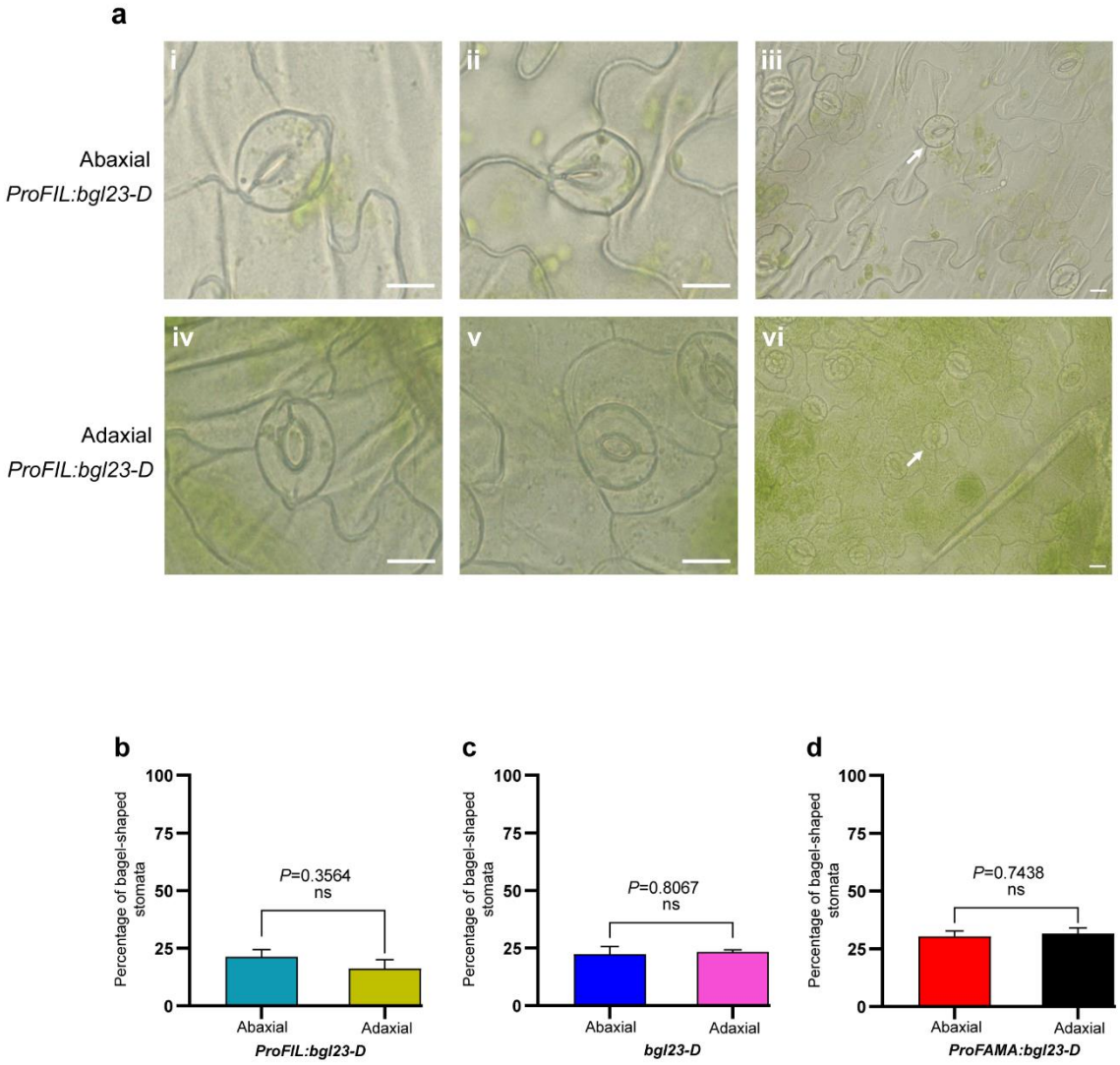

Fig. 2-12. Bagel-shaped stomata on the abaxial and adaxial sides of the leaf in *ProFIL:bgl23-D*, *bgl23-D* mutant and, *ProFAMA:bgl23-D*. **a** Bagel-shaped stomata on the abaxial (**i-iii**) and adaxial (**iv-vi**) surface of the leaf in *ProFIL:bgl23-D*. White arrows in **iii** and **vi** indicate bagel-shaped stomata. Scale bars = 10 µm. **b** Frequency of bagel-shaped and normal stomata on the abaxial and adaxial surface of the leaf of *ProFIL:bgl23-D*. **c** Frequency of bagel-shaped and normal stomata on the abaxial and adaxial surface of the leaf of *bgl23-D*. **d** Frequency of bagel-shaped and normal stomata on the abaxial and adaxial surface of the leaf of *ProFAMA:bgl23-D*. **b-d** Abaxial and adaxial epidermis of leaf was peeled from the same plant (14-day-old) and stomata were counted from five individual plants of *ProFIL:bgl23-D, bgl23-D* mutant and *ProFAMA:bgl23-D*. Fifty stomata were counted from a single plant, while a total of 250 stomata were counted from five individual plants. Single biological replicates consist of 250 stomata. Three independent biological replicates were performed. The data are presented as mean ± SE (*n* =

3). Statistical significant was determined (ns= not significant) at a significance level of $P < 0.05$ (unpaired two-tailed Welch's *t*-test).

Expression of *bgl23-D* by tapetum- or anther-specific promoters disrupted pollen shape and exine formation

The pollen wall is an important structure to protect pollen from the adverse environment and facilitate pollination for successful reproduction. The exine is an outer structure of the pollen wall and constitutes a characteristic reticular pattern in *A. thaliana* (Suzuki et al. 2018). Exine formation largely depends on the innermost anther layer, tapetum, which supplies pollen with structural components necessary for the construction of exine (Pacini et al. 1985; Blackmore et al. 2007). The author analyzed pollen phenotype caused by the expression of *bgl23-D* with tapetum- or anther-specific promoters in T1 transgenic plants. Compared with pollen grains in WT and *bgl23-D* mutant exhibiting regular shape and normal reticular exine (Fig. 2-13a, Fig. 2-13e and Fig. 2-13b, Fig. 2-13f), about 94.95% of pollen grains generated in T1 plants of *ProSP11:bgl23-D* were slightly shrunken with partial loss of the characteristic reticular structure of exine (Fig. 2-13c, Fig. 2-13g, and Fig. 2-14a). In the case of *ProATSP146:bgl23-D*, about 50% of pollen grains from T1 plants were slightly shrunken and about 50% of those were severely shrunken, both with partial loss of the reticular structure of exine (Fig. 2-13d, Fig. 2-13h, and Fig. 2-14b). T3 homozygous line of *ProSP11:bgl23-D* exhibited the same pollen phenotype as T1, while exine pattern of pollen grains in T3 homozygous line of *ProATSP146-bgl23-D* were more severely affected than T1 (Fig. 2-15). Normal-shaped pollen grains with typical exine structure were observed in *ProFKP1:bgl23-D* and *ProFBP1:bgl23-D* (Fig. 2-16).

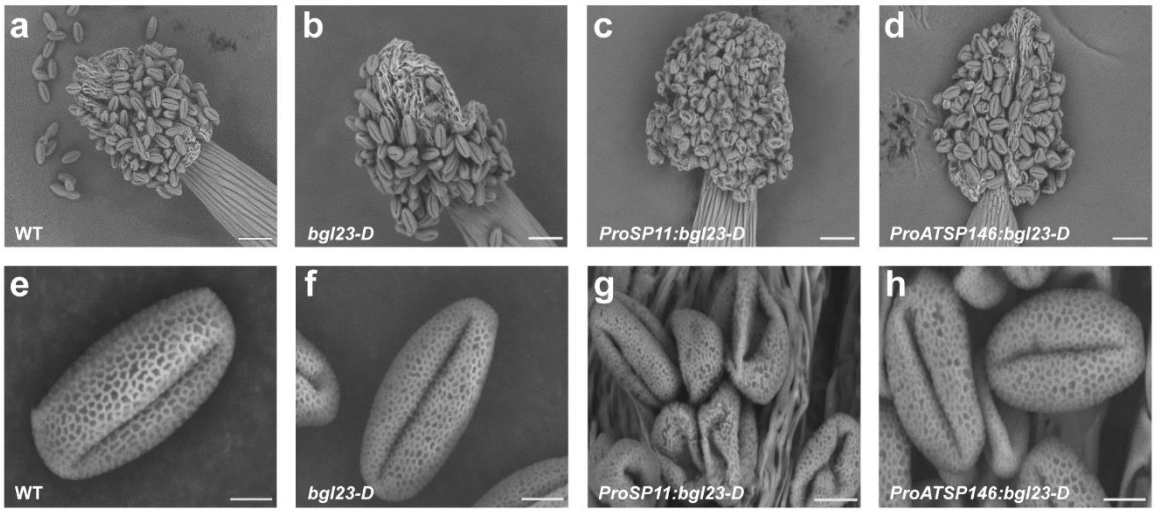

Fig. 2-13. SEM analysis of anther pollen surface structure in *bgl23-D* mutant, *ProSP11:bgl23-D*, and *ProATSP146:bgl23-D*. Anthers were obtained from T1 plants of WT, *bgl23-D* mutant, *ProSP11:bgl23-D,* and *ProATSP146:bgl23-D,* respectively (60-day-old). **a**, **e**

WT. **b**, **f** *bgl23-D* mutant. **c**, **g** *ProSP11:bgl23-D*. **d**, **h** *ProATSP146:bgl23-D*. Scale bars = 50 μm (**a-d**), 5 μm (**e-h**).

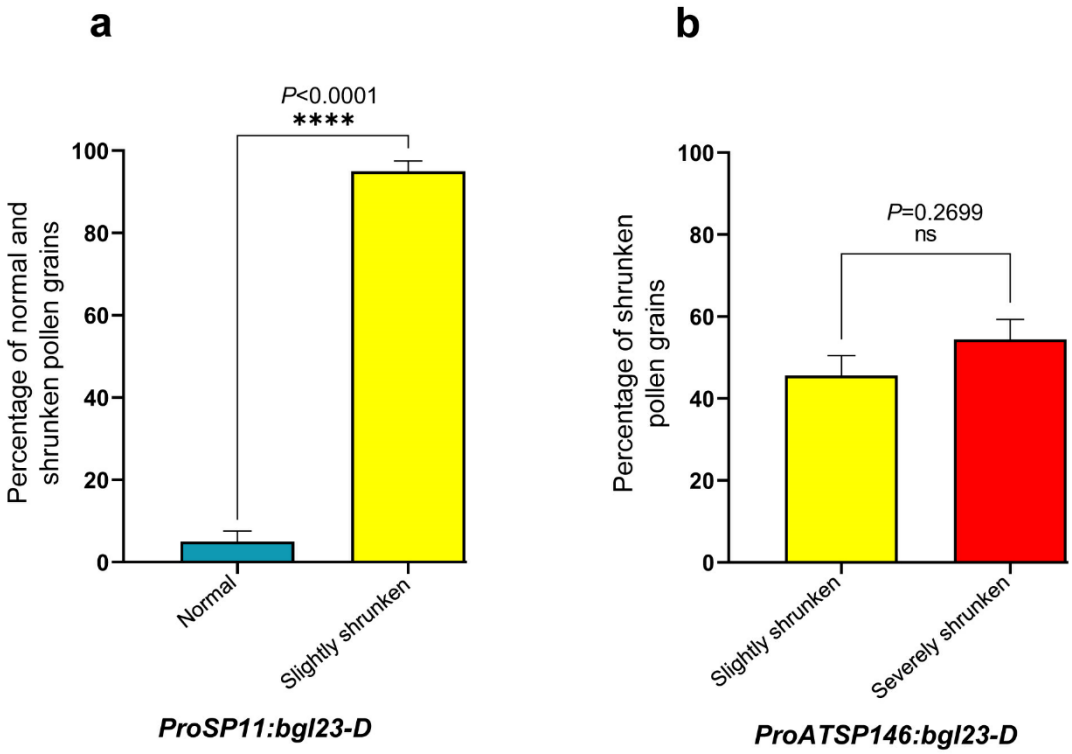

Fig. 2-14. Analysis of shrunken pollen grains produced in T1 plants of *ProSP11:bgl23-D* and *ProATSP146:bgl23-D*. **a** Percentage of normal and shrunken pollen grains in T1 plants of *ProSP11:bgl23-D*. **b** Percentage of shrunken pollen grains in T1 plants of *ProATSP146:bgl23-D*. Anthers were analyzed from 60-day-old three independent T1 plants of *ProSP11:bgl23-D* and *ProATSP146:bgl23-D*, respectively. Pollen grains were counted by the ImageJ software. Data were pooled from one large experiment, where total number of pollen grains was 357 from three anthers (171, 110, and 76 pollen grains were found in anther one, two, and three, respectively) of *ProSP11:bgl23-D*, and 288 from three anthers (104, 102, and 82 pollen grains were found in anther one, two, and three respectively) of *ProATSP146:bgl23-D*. Asterisks indicate significant differences (****$P < 0.0001$ and ns = not significant) at a significance level of $P < 0.05$ (unpaired two-tailed Welch's *t*-test).

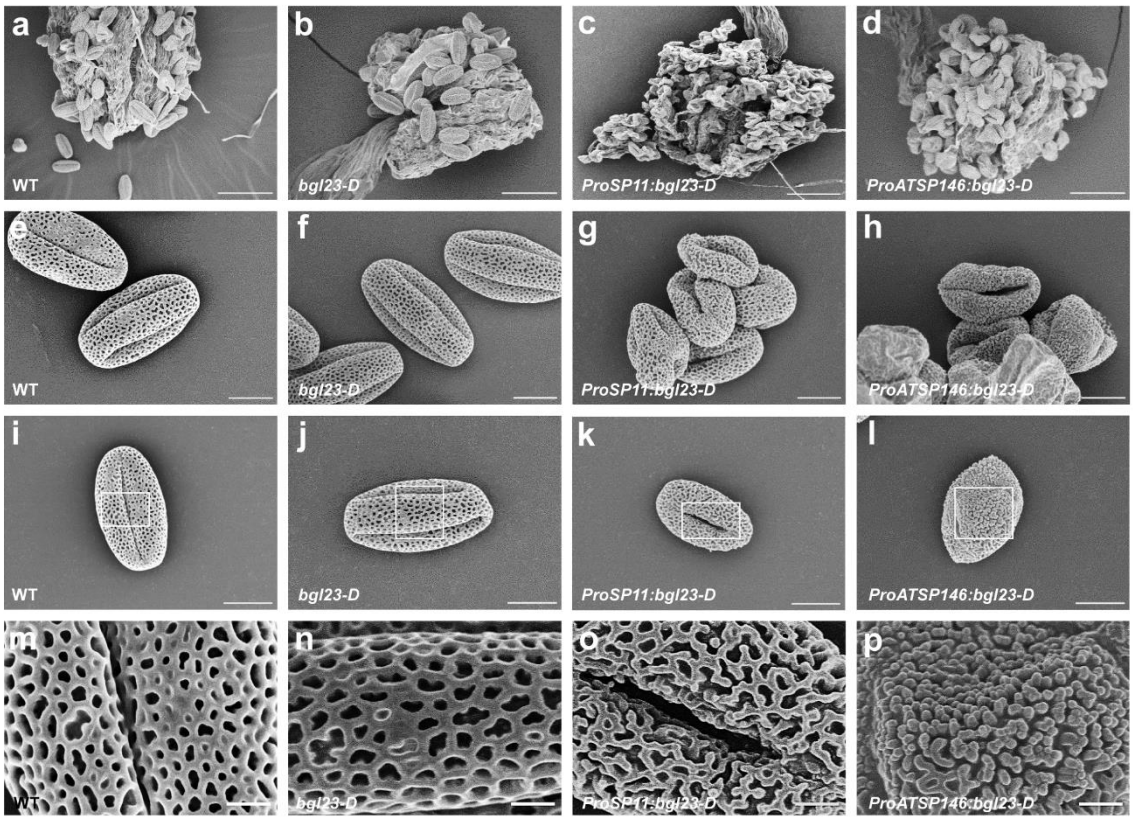

Fig. 2-15. SEM analysis of anther and pollen surface structures. Anthers were obtained from 60-day-old plants. **a**, **e**, **i**, and **m** WT. **b**, **f**, **j**, and **n** *bgl23-D* mutant. **c**, **g**, **k**, and **o** *ProSP11:bgl23-D*. **d**, **h**, **l**, and **p** *ProATSP146:bgl23-D*. Bottom panels indicate the magnified image of exine in white boxed portion of the upper panel. Scale bars = 50 μm (**a-d**), 10 μm (**e-l**), 2 μm (**m-p**).

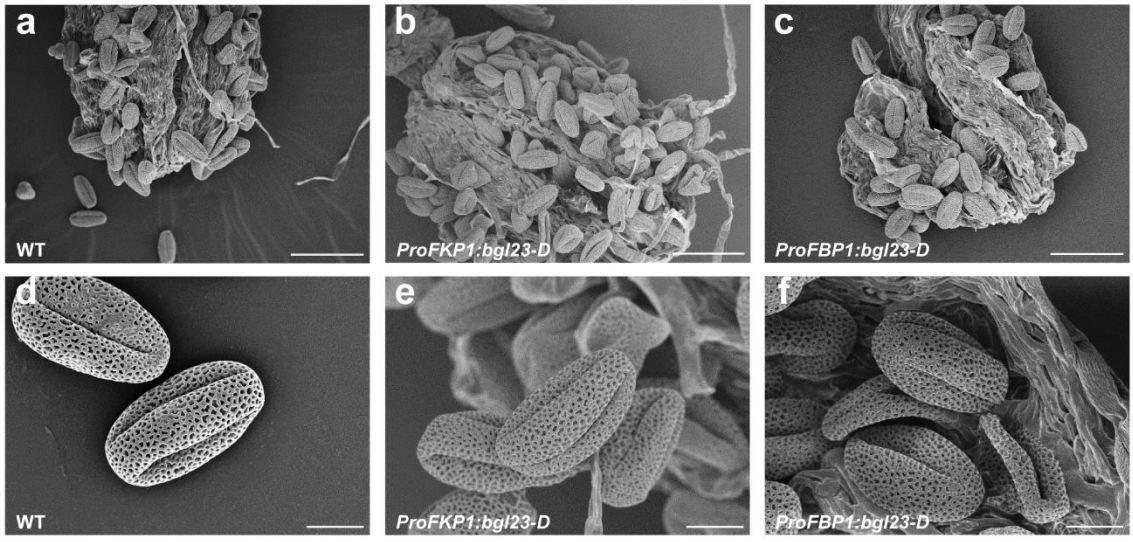

Fig. 2-16. SEM analysis of anther and pollen surface structure. Anthers were obtained from 60-day-old WT and T3 plants. **a**, **d** SEM images of WT. **b**, **e** *ProFKP1*:*bgl23-D*. **c**, **f** *ProFBP1:bgl23-D*. Scale bars = 50 μm (**a-c**), 10 μm (**d-f**).

The author further analyzed pollen phenotype of *ProSP11:bgl23-D* and *ProATSP146:bgl23-D* by DAPI staining and semi-thin sectioning. DAPI staining showed that *ProSP11:bgl23-D* produced pollen grains with two sperm nuclei and one vegetative nucleus, a normal pattern as found in WT and *bgl23-D* mutant (Fig. 2-17). In the case of *ProATSP146:bgl23-D*, a significant amount of severely shrunken pollen grains with no DAPI signal were generated in addition to pollen grains of normal three nuclei in DAPI staining (Fig. 2-17). Next, tapetal cells were observed by semi-thin sectioning of anthers at different developmental stages. WT, *bgl23-D* mutant, *ProSP11:bgl23-D,* and *ProATSP146:bgl23-D* exhibited normal microspore development in the tetrad stage (Fig. 2-18a-d). Furthermore, microspores were discharged normally from the tetrads in WT, *bgl23-D* mutant, *ProSP11:bgl23-D*, and *ProATSP146:bgl23-D* anthers, and no clear defects were observed during the early unicellular stage (Fig. 2-18e-h). An obvious defect in microspores started to appear in *ProATSP146:bgl23-D* at the late unicellular stage (Fig. 2-18l; arrowheads). The development of half of the *ProATSP146:bgl23-D* microspore was arrested at the late unicellular stage, resulting in severely shrunken microspores compared to WT, *bgl23-D* mutant, and *ProSP11:bgl23-D* (Fig. 2-18i-k), while the tapetum was normal (Fig. 2-18l). At the bicellular stage, microspores were normal and tapetum degeneration had started normally in WT, *bgl23-D* mutant, and *ProSP11:bgl23-D*, respectively (Fig. 2-18m-o). In contrast, microspores with no cellular content (Fig. 2-18p; arrows) and severely shrunken in shape (Fig. 2-18p; arrowheads) were observed in *ProATSP146:bgl23-D*. At the tricellular stage, the tapetum disappeared, showing numerous normal pollen grains in WT, *bgl23-D* mutant, and *ProSP11:bgl23-D* (Fig. 2-18q-s). Although the tapetum disappeared normally, severely shrunken pollen grains having no cellular content were generated in *ProATSP146:bgl23-D* (Fig. 2-18t; arrowheads), which is consistent with the result of DAPI staining.

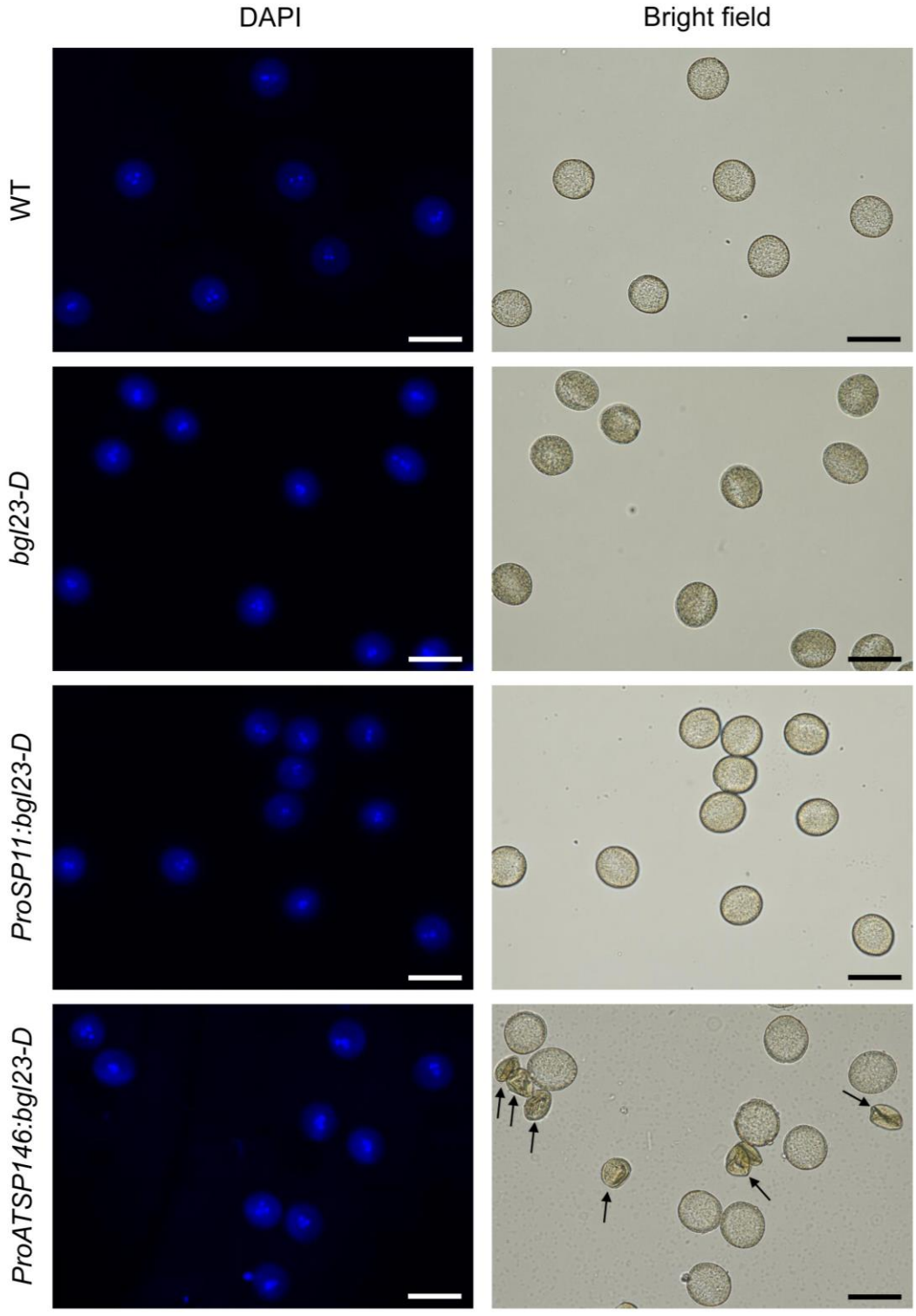

Fig. 2-17. DAPI staining of mature pollen grains in the WT, *bgl23-D* mutant, *ProSP11:bgl23-D*, and *ProATSP146:bgl23-D*. Arrows indicate severely shrunken pollen grains with no DAPI signal in DAPI channel. Scale bars = 30 μm.

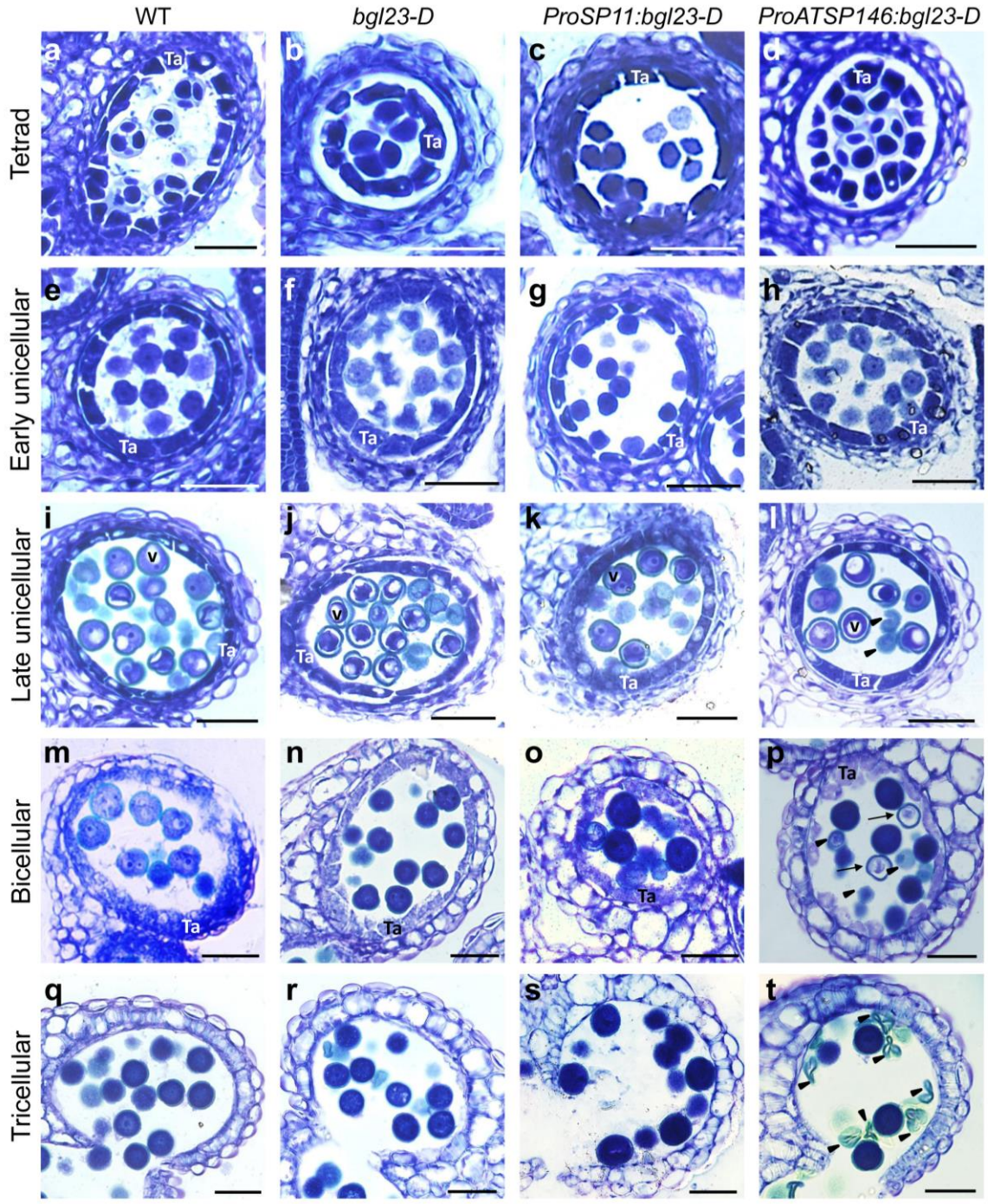

Fig. 2-18. Semi-thin sections of anthers at various developmental stages in the WT, *bgl23-D* mutant, *ProSP11:bgl23-D*, and *ProATSP146:bgl23-D*. Sections of anthers during tetrad (**a-d**), early unicellular (**e-h**), late unicellular (**i-l**), bicellular (**m-p**), and tricellular stages (**q-t**). Arrowheads and arrows indicate severely shrunken microspore and microspore having no cellular content. Ta, tapetum. V, vacuole. Scale bars = 30 μm.

Expression of *bgl23-D* in QC by *ATSP146* promoter did not affect the cellular organization in the root apical region

Since the promoter activity of *ATSP146* was found in both the anther and the QC (Nakamura et al. 2012), the author analyzed the QC and root phenotypes of *ProATSP146:bgl23-D*. As a result, *ProATSP146:bgl23-D* had a normal QC pattern and well-organized cell layer in the root apical region, as observed in WT (Fig. 2-19).

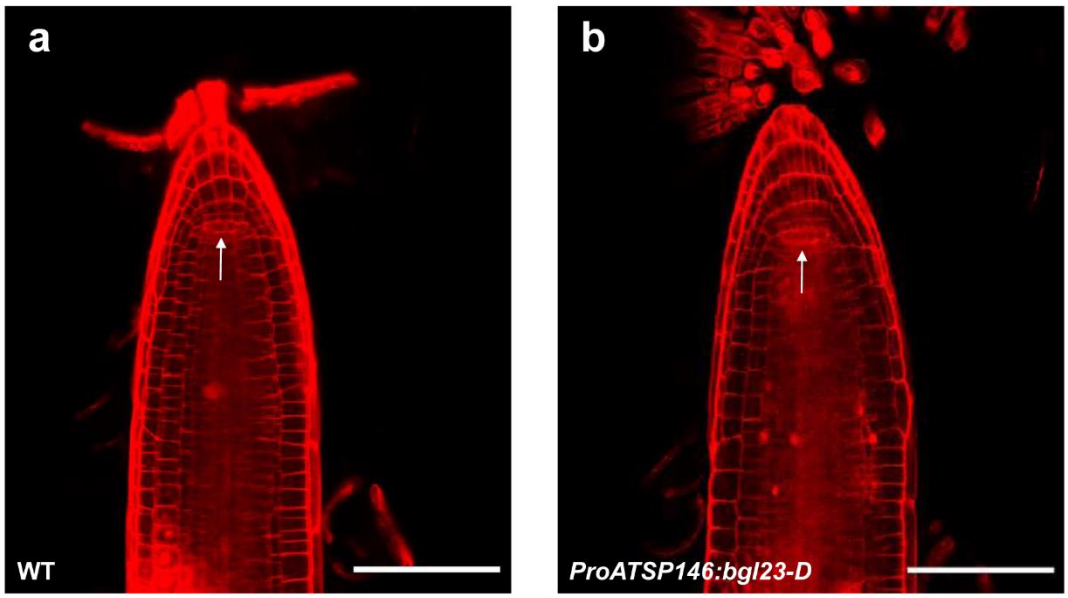

Fig. 2-19. Analysis of root apical region in WT and *ProATSP146:bgl23-D* plants. **a, b** Apical region of primary root (3- to 5-day-old) of WT and *ProATSP146:bgl23-D*, respectively. White arrows indicate quiescent center. Scale bars = 20 μm.

Leaf growth was enhanced in the *bgl23-D* mutant and transgenic plants expressing *bgl23-D* under control of stomatal lineage-specific promoter

Because stomata play important roles in photosynthesis and transpiration, the author analyzed shoot growth of transgenic plants showing bagel-shaped SGCs caused by the expression of *bgl23-D* with stomata lineage-specific promoters. The *ProSP11:bgl23-D* which did not show guard cell abnormalities (Fig. 2-20) and exhibited only pollen phenotype was used as a control in this experiment. The *bgl23-D* mutant, *ProSDD1:bgl23-D*, *ProMUTE:bgl23-D*, and *ProFAMA:bgl23-D* plants showed larger rosette diameter after 18 days of germination compared with WT and *ProSP11:bgl23-D* (Fig. 2-21a and Fig. 2-21b). In addition, the *bgl23-D* mutant, *ProSDD1:bgl23-D*, *ProMUTE:bgl23-D*, and *ProFAMA:bgl23-D* exhibited larger leaf size than the WT and *ProSP11:bgl23-D* (Fig. 2-21c). Next, the author measured the epidermal cell size of abaxial leaves from 6-week-old plants. The size of epidermal cells in *bgl23*-D mutant, *ProSDD1:bgl23-D*, *ProMUTE:bgl23-D*, and *ProFAMA:bgl23-D* was increased 2.5 to 3.5-fold, comparable to that of

WT and *ProSP11:bgl23-D (*Fig. 2-21d*).* To investigate mechanisms that increase cell size and growth, the author measured the chlorophyll fluorescence and water loss of plants since *bgl23-D* affected stomata, which are important for photosynthesis and transpiration. The maximum photochemical quantum yield of photosystem II (F_v/F_m) was almost similar within WT, *ProSP11:bgl23-D*, *bgl23-D*, *ProSDD1:bgl23-D*, *ProMUTE:bgl23-D*, and *ProFAMA:bgl23-D*, respectively (Fig. 2-22a). Under growth light intensity (100 photons µmol m^{-2} sec^{-1}), The effective quantum yield of photosystem II (øPSII) among the transgenic plants was found to be similar, while NPQ of *bgl23-D* mutant, *ProSDD1:bgl23-D*, *ProMUTE:bgl23-D*, and *ProFAMA:bgl23-D* was comparable to that of WT, meaning that photosynthetic activity was similar within WT and transgenic plants (Fig. 2-22b and Fig. 2-22c*).* In water loss assay using detached rosette leaves, *ProFAMA:bgl23-D* which had high percentage of abnormal stomata lost more water than WT, while *bgl23-D* mutant which had low percentage of abnormal stomata showed no statistically significant difference compared to WT (Fig. 2-21e), suggesting that the increased transpiration was not the main factor in the increased growth of *bgl23-D* mutant and *ProFAMA:bgl23-D.*

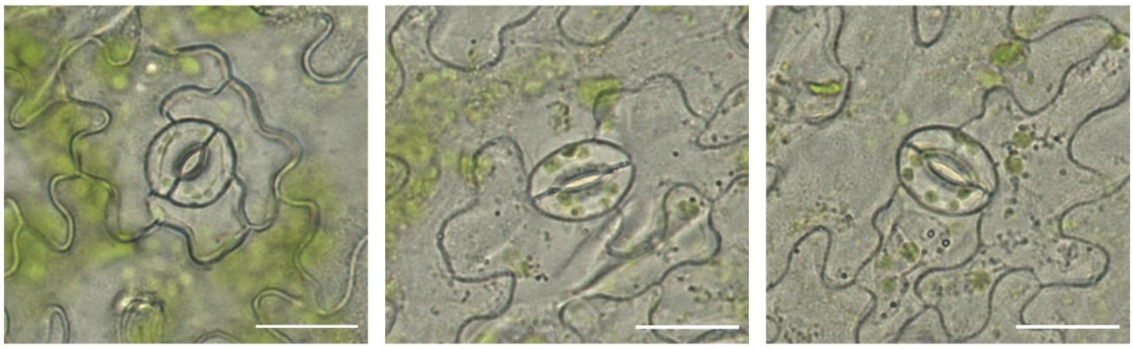

ProSP11:bgl23-D

Fig. 2-20. Stomata in *ProSP11:bgl23-D*. Abaxial epidermis of leaf was peeled from 14-day-old T3 plant and observed using BZ-X710 All-in-One microscope (KEYENCE). Scale bars = 20 µm.

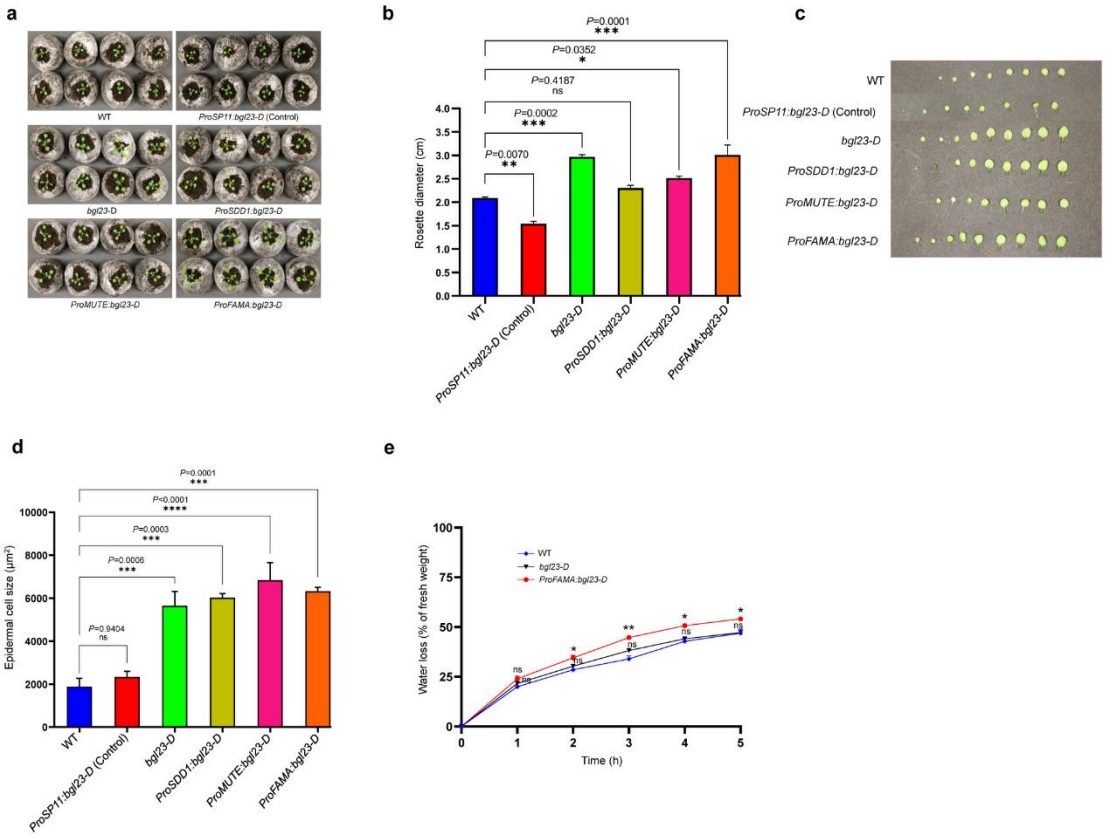

Fig. 2-21. Growth analysis of shoots. **a** Images showing rosette leaves of WT, *ProSP11:bgl23-D*, *bgl23-D* mutant, *ProSDD1:bgl23-D*, *ProMUTE:bgl23-D,* and *ProFAMA:bgl23-D*. **b** Rosette diameter was measured from 18-day-old plant. Single biological replicate consist of 10 plants. Three independent biological replicates were performed. The data are presented as mean ± SE (n = 3). The rosette diameter data was distributed normally according to the Shapiro-Wilk normality test. Asterisks indicate significant differences (*P < 0.05; **P < 0.01; ***P < 0.001; and ns = not significant) based on an ordinary one-way ANOVA at a significance level of P < 0.05 (Dunnett's multiple comparison test). **c** Leaves were taken from 18-day-old plant. **d** Determination of size leaf epidermal cells. Epidermal cell size was measured from the leaves of 6-week-old plants. An area of 30 cells from three individual plants per genotype was measured by the ImageJ software. Three independent biological replicates were performed (n = 3)**.** Asterisks indicate significant differences (*P < 0.05; **P < 0.01; ***P < 0.001; and ****P < 0.0001) based on an ordinary one-way ANOVA at a significance level of P < 0.05 (Dunnett's multiple comparison test). **e** Comparison of rates of water loss in WT, *bgl23-D* mutant, and *ProFAMA:bgl23-D.* Rosette leaves were detached from 4-week-old plants and weighted immediately by a precision balance (HR-202i; A&D, Tokyo, Japan) and then placed in a growth chamber (25 °C and 50–60% humidity), and weighted again at particular time intervals. The percentage of water loss was assessed based on the initial fresh weight of the plants. Five plants were tested per genotype. Three independent biological replicates

were performed (n = 3). Asterisks indicate significant differences (*P < 0.05; **P < 0.01; and ns = not significant) at a significance level of P < 0.05 (unpaired two-tailed Welch's t-test).

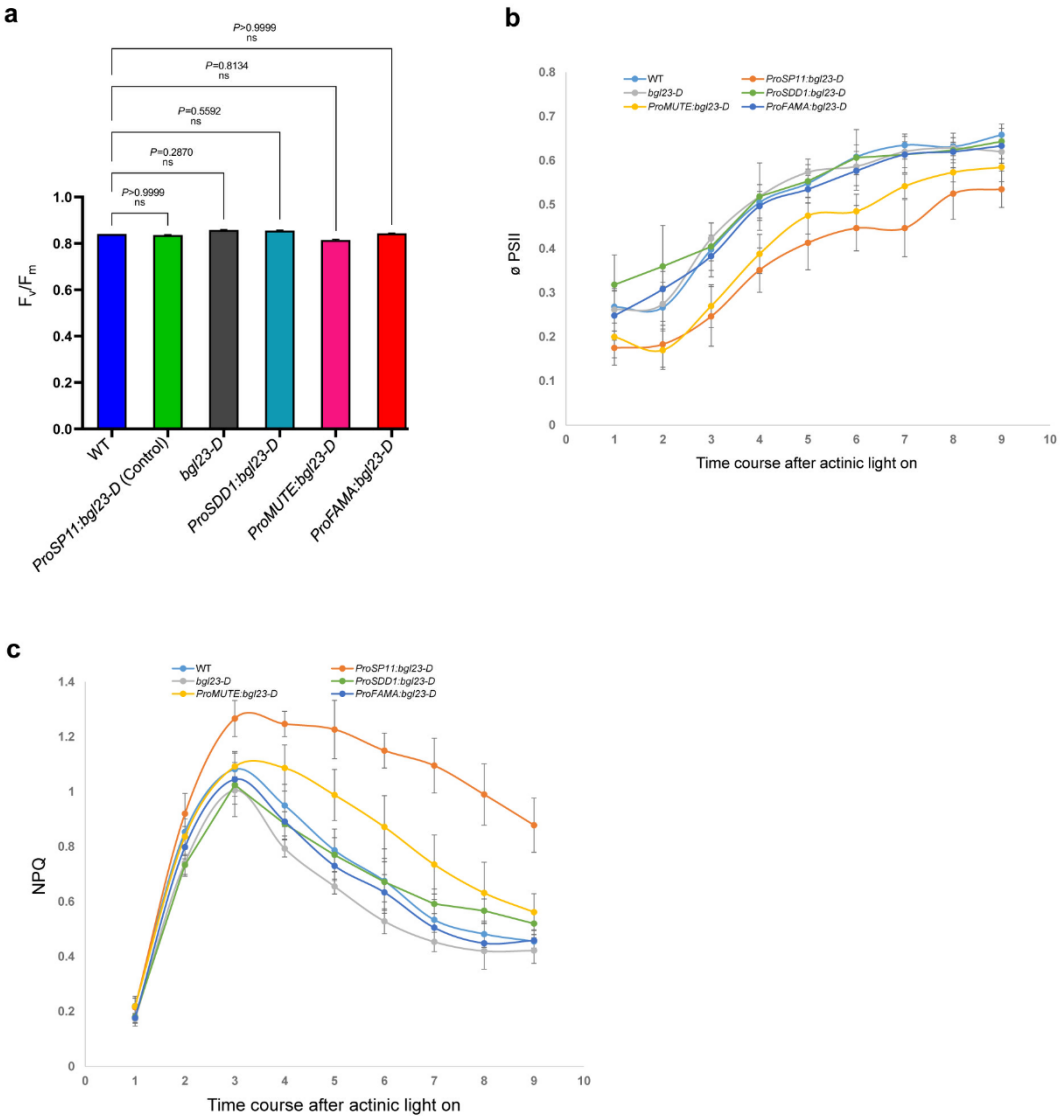

Fig. 2-22. Analysis of chlorophyll fluorescence. **a** Maximum light quantum efficiency (F_v/F_m). Chlorophyll fluorescence was measured from two plants per genotype (n = 6). Three independent biological replicates were performed. Non-parametric Kruskal-Wallis test was performed at a significance level of P < 0.05 followed by Dunn's multiple comparison test (ns = not significant). **b, c** Estimation of øPSII and non-photochemical quenching (NPQ) upon actinic light intensity at different time points. øPSII and NPQ were measured from the leaves of two plants per genotype (n = 6) using a flash of light at a 13 s time interval. The numerical numbers in the graph's horizontal axes (**b**, **c**) represent time intervals. A total of nine flashes of actinic light were performed at a consecutive interval of 13 s.

Discussion

The ATCSLD5 plays a key role in the growth and development of *A. thaliana* (Bernal et al. 2007). In the present study, the author identified a novel dominant-negative mutation in the *ATCSLD5* as the mutated gene responsible for the *bgl23-D* mutant phenotype using a forward genetic approach (Fig. 2-4a and Fig. 2-4b). *ATCSLD5* is a target of the transcription factor SPEECHLESS (SPCH) and highly expressed in the early stage of stomata lineage. The *csld5* mutant showed an increased number of clustered stomata and incompletely divided GMCs, meaning that the ATCSLD5 function was necessary both for asymmetric and symmetric division in stomata lineage cells (Gu et al. 2016). In contrast, the author observed only undivided GMCs and no cluster of stomata in the *bgl23-D* mutant (Fig. 2-1aii-aiv). The author speculated that symmetric division of GMC required higher activity of ATCSLD5 than preceding asymmetric division of stomata lineage cells, and *bgl23-D* mutation reduced ATCSLD5 activity to an extent insufficient for symmetric division of GMC. Leucine 997, the mutation site of *bgl23-D* is conserved in ATCSLD1 to ATCSLD6 (Wang et al. 2001) (Fig. 2-23), meaning that it is an important amino acid residue for the function of ATCSLDs. Although the molecular mechanism of negative dominancy by the *bgl23-D* mutation is unknown, if the ATCSLD5 forms a complex to synthesize polysaccharides like CESA complex, the ATCSLD5 carrying *bgl23-D* mutation may be incorporated into the complex and lower its activity. CSLD3 was reported to form a high-order complex (Yang et al. 2020) supporting the authors hypothesis.

All stomata lineage promoter constructs, *ProSDD1:bgl23-D*, *ProMUTE:bgl23-D*, and *ProFAMA:bgl23-D* generated abnormal bagel-shaped stomata (Fig. 2-10a, Fig. 2-10b, and Fig. 2-10c) but the frequency of abnormality was higher in *ProSDD1:bgl23-D* and highest in *ProFAMA:bgl23-D* (Fig. 2-10d). In addition, *ProFAMA*:*bgl23-D* showed severe phenotype with cytokinesis defect (Fig. 2-11) including a most severe oval-shaped GC with no pore (Fig. 2-11h). Among these stomata lineage genes, *SDD1* and *MUTE* were mainly expressed in meristemoid and GMC. According to the eFP browser of the TAIR database (Winter et al. 2007), the expression level of *SDD1* was higher than *MUTE* in GMC of cotyledons. On the other hand, *FAMA* was strongly expressed in GMC and young GC (Von Groll et al. 2002; Ohashi-Ito and Bergmann 2006; Pillitteri et al. 2008). The highest frequency of abnormal bagel-shaped stomata in *ProFAMA*:*bgl23-D* is due to the activity of the *FAMA* promoter that expresses *bgl23-D* cDNA in the timing of GMC cytokinesis.

The development pattern of generating leaves, flowers, and floral organs is influenced by the abaxial–adaxial axis. Although the expression of *FIL* was found only on the abaxial side of the leaf, cotyledon, and floral organs (Siegfried et al. 1999), the *ProFIL:bgl23-D* showed bagel-shaped

stomata on both the abaxial and adaxial sides of the leaf (Fig. 2-12a), where a higher frequency of bagel-shaped stomata was observed on the abaxial side (Fig. 2-12b). At present, it is unknown why bagel-shaped stomata were generated not only on abaxial but also on the adaxial side of leaves in *ProFIL:bgl23-D*. Further study is needed to reveal the mechanism causing the formation of bagel-shaped stomata on the adaxial side.

The tapetum supplies metabolites, enzymes, nutrients, and structural components of exine and plays important roles in pollen development (Ariizumi and Toriyama 2011). The *SP11* gene is expressed in tapetum at an early developmental stage and in pollen at a late developmental stage (Takayama et al. 2000; Shiba et al. 2001) The effect of *bgl23-D* on pollen phenotype was sporophytic, since 94.95% of pollen grains produced in T1 of *ProSP11:bgl23-D* were abnormal (Fig. 2-13 and Fig. 2-14). This result strongly suggests that tapetum expression of *bgl23-D* is responsible for pollen phenotype in *ProSP11:bgl23-D*. Aboulela et al. (2018) reported that disruption of tapetum expressing *AtSEC23A* or *AtSEC23D* gave rise to an incomplete exine network as observed in *ProSP11:bgl23-D*, also supporting the significance of *bgl23-D* expression in tapetum for pollen phenotype. Although the *ATSP146* was expressed throughout the anther (Nakamura et al. 2012), tapetum expression might be essential for phenotype of exine patterning in the *ProATSP146:bgl23-D* transgenic plant (Fig. 2-13 and Fig. 2-15). In addition, DAPI staining demonstrated that, severely shrunken pollen grains in *ProATSP146:bgl23-D* did not show any nuclei, meaning that there were abnormalities in cellular division (Fig. 2-17). Semi-thin sectioning further revealed the exact timing of cellular abnormalities. The microspore was released normally from the tetrad, however, severely shrunken pollen grains appeared before the onset of pollen mitosis I (PMI) at the late unicellular stage (Fig. 2-18l). Microspores with no cellular content further clarify the abnormalities in cellular division after pollen mitosis I (PMI) (Fig. 2-18p; arrows) at the bicellular stage. These results suggested that *bgl23-D* was expressed also in microspore and disturbed cell division to some extent in *ProATSP146:bgl23-D*. Risso-Pascotto et al. (2005) reported abnormal pollen grains found in *Brachiaria jubata* due to symmetric pollen mitosis I and suppression of pollen mitosis II (PMII), which is a similar observation of *ProATSP146:bgl23-D.* Because *bgl23-D* mutant did not show pollen phenotype (Fig. 2-15), it seems that *ATCSLD5* itself is not expressed in the tapetum and does not function in exine formation and pollen development. Therefore, it is quite interesting that *ProSP11:bgl23-D* and *ProATSP146:bgl23-D* showed the phenotype of exine and pollen formation. The author hypothesize that *bgl23-D* inhibited unknown ATCSLD(s), expressed in the tapetum, and played a role in exine and pollen formation. Among the six *ATCSLD* genes, *ATCSLD1* and *ATCSLD4* were necessary for tip growth of pollen tubes (Bernal et al. 2007; Wang et al. 2011). *ATCSLD2* and *ATCSLD3* were functional in tip growth of root hair (Favery et al. 2001; Wang et al. 2001; Bernal et al. 2007), and *ATCSLD5* was involved in cell plate formation, especially in stomata lineage cells

(Gu et al. 2016). The target of *bgl23-D* in tapetum might be a remaining *ATCSLD6* (AT1G32180), whose function has not been reported and is highly expressed in the anther of the young flower (Winter et al. 2007). It is an interesting issue to clarify whether *ATCSLD6* is engaged in the polysaccharide synthesis of the primary cell wall for exine formation.

In addition to transgenic *A. thaliana* expressing *bgl23-D* cDNA by the promoter of stomata lineage genes (*ProSDD1:bgl23-D*, *ProMUTE:bgl23-D*, and *ProFAMA:bgl23-D*), *bgl23-D* mutant exhibited increased rosette diameter, larger leaf size, and faster plant growth (Fig. 2-21) despite the loss of ATCSLD5 function, which resulted in reduced growth in *atcsld5-1* knockout plants (Bernal et al. 2007). We speculated that the difference in shoot growth between *atcsld5-1* knockout plant and *bgl23-D* mutant is based on the difference in allele. If the *bgl23-D* mutation only affects cell plate formation of GMC, growth parameters should be similar to *ProSDD1:bgl23-D*, *ProMUTE:bgl23-D*, *ProFAMA:bgl23-D*. Additionally, *ProFAMA:bgl23-D*, which generated a high frequency of bagel-shaped stomata (Fig. 2-10d), showed a higher growth tendency among transgenic *A. thaliana.* Enhanced rosette size and plant growth have been reported recently in *ALTERED MERISTEM PROGRAM 1* (*AMP1*) overexpression lines (*AMP1-GFP/OX7*), while AMP1 is required for stomata development and guard cell aperture (López-García et al. 2020). One possible explanation regarding the increased growth of transgenic *A. thaliana* is that due to the bagel-shaped guard cells, stomata are kept open for a relatively longer time. Therefore, prolonged stomatal opening enhances photosynthetic activity, which ultimately increases plant growth. Higher plant growth was reported in *ARABIDOPSIS* H^+*−ATPASE 2 (AHA2)* overexpression lines (*GC1::AHA2*) by Wang et al. (2014) which exhibited increased stomatal opening in response to light, while the constitutive open stomata phenotype did not affect plant growth. Moreover, multiple wheat genotypes were studied by Condon et al. (1987), who demonstrated that increased stomatal conductance, particularly abaxial stomatal conductance, may have a significant impact on crop biomass. Although obvious larger epidermal cell size was observed in case of *bgl23-D* mutant, *ProSDD1:bgl23-D*, *ProMUTE:bgl23-D*, and *ProFAMA:bgl23-D* (Fig. 2-21), photosynthetic activity (Fig. 2-22) and transpiration (Fig. 2-21e) may not be the main factors for increased growth. Our results suggested that cell size was increased by *bgl23-D* mutation through unknown mechanisms and resulted in increased rosette size in the *bgl23-D* mutant and transgenic plants expressing *bgl23-D* under control of stomata lineage-specific promoter. Future studies, such as transcriptome analysis, will elucidate the molecular mechanism of growth enhancement by *bgl23-D.*

Fig. 2-23. Transmembrane domain 4 of ATCSLD1-ATCSLD6. Asterisk indicate the position of *bgl23-D* mutation in ATCSLD5. Amino acids conserved in ATCSLD1-ATCSLD6 are shown in red.

In conclusion, the authors utilized the dominant effect of *bgl23-D* along with cell- or tissue-specific promoters to inhibit the function of ATCSLD5 in particular cells or tissues. The results of this study demonstrate that *bgl23-D* could arrest the cell division during GC development, which is consistent with the reported function of ATCSLD5 in cell plate formation of GMC. Furthermore, although the *bgl23-D* mutant did not show pollen and exine phenotype, its expression by promoters of tapetum- or anther-specific genes disrupted pollen structure and exine patterning, indicating that *bgl23-D* inhibited unknown ATCSLD(s) function for exine formation in the tapetum. Additionally, expression of *bgl23-D* in stomata lineage cells may play a positive role in the growth of plants. Therefore, the findings of this study will open the way to use *bgl23-D* as a tool for functional analysis of ATCSLDs in specific tissues and organs and manipulate plant growth**.**

Chapter 3

Expression analysis of plant intracellular Ras-group related leucine-rich repeat proteins (PIRLs) in *Arabidopsis thaliana*

Introduction

Leucine-rich repeat (LRR) proteins contain a characteristic LRR domain consisting of 18–29 amino acid repeats rich in leucine residues. These proteins are widespread in plants, animals, and bacteria (Kajava 1998; Kobe and Deisenhofer 1994). In animals and lower eukaryotes, an intracellular LRR protein subfamily known as Ras-group LRR proteins with a variably long LRR domain are functionally involved in signal transduction (Claudianos and Campbell 1995; Forsthoefel et al. 2005; Jeong et al. 2009; Lee et al. 2004; Li et al. 2000; Sieburth et al. 1998). Plants contain a small group of proteins that are structurally analogous to Ras-group LRRs, named plant intracellular Ras-group related LRR proteins (PIRLs) (Forsthoefel et al. 2005; You et al. 2010). The *A. thaliana* genome has nine *PIRL* genes that are categorized into three subfamilies based on their evolutionary relationship (Forsthoefel et al. 2005). To date, the functions of five PIRLs have been identified. *PIRL6* has been found to be essential for male and female gametogenesis (Forsthoefel et al. 2018), while *PIRL1* and *PIRL9* redundantly work during the differentiation of microspores into pollen (Forsthoefel et al. 2010). In addition, *PIRL2* and *PIRL3* have been found to be involved in pollen morphogenesis (Forsthoefel et al. 2013). However, to elucidate the physiological functions of the remaining *PIRL* genes, it is requisite to know their precise expression patterns. In this study, the author used a promoter:GUS assay to examine in detail the expression patterns of *PIRL* genes in *A. thaliana.* The author found that *PIRL* genes were expressed in the root, root hairs, shoot apex, leaves, anther, pollen, and pollen tube. The author also performed a phylogenetic analysis of *A. thaliana* PIRL proteins with homologous PIRL proteins from other plants and in silico analyses examining the co-expression of *PIRL* genes. The results of these experiments should improve the understanding of the function of *PIRL* genes during plant growth and development.

Materials and methods

Phylogenetic analysis of PIRLs protein

The amino acid sequences of all nine *A. thaliana* PIRLs were retrieved from The Arabidopsis Information Resource (TAIR) database version 10 (https://www.arabidopsis.org/). A NCBI (https://www.ncbi.nlm.nih. gov/) BLASTP was carried out using *A. thaliana* PIRL1 amino acid sequences as a query to identify PIRL homolog candidates in other plants. A total of 49 amino acid sequences (Table 3-1) were obtained, containing sequences from *Brassica rapa*, *Capsella rubella*, *Oryza sativa*, *Hibiscus syriacus*, *Zea mays*, and *Ricinus communis*. All amino acid sequences were verified by examining their entries in the appropriate databases, e.g., TAIR (https://www.arabidopsis.org/), the Rice Genome Annotation Project (RGAP)

(http://rice.plantbiology.msu.edu/), Phytozome v12.1 (https://phytozome.jgi.doe.gov/), and Uniprot (https ://www.uniprot.org/). ClustalW was used to perform multiple sequence alignment. A phylogenetic tree was constructed using the neighbor-joining (NJ) method (Saitou and Nei 1987) implemented in MEGA7 (Kumar et al. 2016) with 1, 000 bootstrap replicates. The domain structures of the nine *A. thaliana* PIRL proteins were predicted using Uniprot and were drawn using the MyDomains-Image Creator (https://prosite.expasy.org/mydomains/).

Plasmid construction

The promoter entry clones pDONR201-ProPIRL1 to pDONR201- ProPIRL9 were prepared with the primers listed in Table 3-2. The promoter:GUS binary constructs were prepared with pDD333 and pGWB3450 vectors according to the method described by Sultana et al. (2020).

Generation of transgenic *A. thaliana*

Transformation of *Agrobacterium tumefaciens* C58C1 (pMP90) was performed using the freeze-thaw method as per Weigel and Glazebrook (2002). Transformation of *A. thaliana* (Col-0 accession) was performed using the floral inoculation method (Narusaka et al. 2010). Harvested T0 seeds were kept at 4 ºC for 3 days, after which they were grown on Murashige and Skoog (MS) agar medium containing kanamycin (30 mg/L) and Cefotax (100 mg/L) (Chugai Pharmaceutical Co., Tokyo, Japan) at 22 ºC under continuous light. Fifteen-day-old selected plants (T1) were transferred to Jiffy-7 plant pots (Jiffy Products International BV, Zwijndrecht, Belgium) and were grown at 22 ºC under a 16-h light/8-h dark daily cycle.

Histochemical GUS staining

Plants were selected at different time points for histochemical staining, including 1-day-after-germination (DAG) seedlings, as well as plants at 4-DAG, 8-DAG, 16-DAG, and the flowers of 40-DAG plants. Staining was performed as described by Nakamura et al. (2012) and plants were observed using a stereo microscope (SZX16, Olympus, Tokyo, Japan) equipped with a Nikon digital camera (DXM1200F) as well as an All-in-One microscope (BZ-X710, KEYENCE, Osaka, Japan).

In silico expression and co-expression of *PIRL* genes

The expression value was obtained for each *PIRL* gene in several different tissues (cotyledon, hypocotyl, root, leaf, flower, sepal, petal, and pollen) using microarray data from the Arabidopsis eFP browser (Winter et al. 2007). Expression values were then normalized using the log2 transformation. Finally, a heat map was generated by TBtools software (Chen et al. 2020).

Microarray data showing visual expression during different developmental stages was also retrieved from the Arabidopsis eFP browser (Winter et al. 2007). The co-expression gene network of *PIRLs* and co-expressed genes were analyzed using the ATTED-II (https://atted.jp/) (Obayashi et al. 2018).

Table 3-1: **Amino acid sequences used for construction of phylogenetic tree**

Gene ID/Accession no.	Gene name	Amino acid sequences
At5g05850/ sp|Q9FFJ3	PIRL1	MATELNPKNFPVLSYVLDRLPSFTAKSSSSSDVEPPPSKSDPSSSSNHSIEIVTQMPHLAHPDVLASMTNATADVSQTRSVLRTLGPRPDHETVDRARARLREID ASLSESFEEIALSPNDIDVAEKEQKRREAVEQEKIWYKSILKLNELHESYEKLLKEAEERLVRIYESAEKNAAAVAEEEAAEVEVNEEVVSILQQAAENPLDRV DLSGRKLKLLPEAFGKIQGLLVLNLYNNQLQAIPDSIAGLHNLLELDVSTNFLETLPDSIGLLSKLKILNVSCNKLTTLPDSICHCGSLVVLDASYNNLTYLPTNI GFELVKLEKLLIHLNKIRSLPTSIGEMRSLRYLDAHFNELNGLPNSFGLLTNLEYLNLSSNFSDLQDLPASFGDLISLQELDLSNNQIHSLPDAFGTLVNLTKLNL DQNPLVVPPDEVVKQGVDAVKMYMGKRWVSMLEEEEKMANMKDEMDQTNTDWLTRTTSKLKTYVTEVSEYLGSNPPRDPYLDQQL
At3g26500/ sp|Q9LRV8	PIRL2	MDHDLDKFPLLSYVLHQHDSNLHAPPSMAAQETLLPSFPLLSNPEIMSMLTQSIPTTITQTLFVFNSLGSRPDPLAVSSARFKIAQIMDSLSPEEAAKESEIYAGV VRLDEVHDSYEKKLKDTEEELSRVYSTEVESMLRSGEEVNEKVLAVLKEAESGGTVERIDLSSQELKLIPEAFWKVVGLVYLNLSGNDLTFIPDAISKLKKLE ELDVSSNSLESLPDSIGMLLNLRILNVNANNLTALPESIAHCRSLVELDASYNNLTSLPTNIGYGLQNLERLSIQLNKLRYFPGSISEMYNLKYLDAHMNEIHGI PNSIGRLTKLEVLNLSSNFNNLMGVPDTITDLTNLRELDLSNNQIQAIPDSFYRLRKLEKLNLDQNPLEIPSQEVATQGAEVVREFMRKRWGDIMAEQQQRIG VEAERHGDENGWVYWGTSMVTNLVSGVTHTIGFGGATSDGGDKKPGDSYFYHQI
At1g12970/ sp|Q8W4Q3	PIRL3	MDHDLEIFPLLSYVLHHSDPASHAPPSLAIQQSLANRYPLLTNPYVISSLIESIPSTITQTLFVFGSLGPRPDPLAVSSARSKIREIKENDSLSPEDAAKEEQVYAA VVSLEEVHEGYEKQLRDLEEEIGRVYASAVESLSGGDEVNEEVLAVIKDAEDGGVVERIDLSDHELKLLPDALGKIVGLVSLNVSRNNLRFLPDTISGLEKLEE LDLSSNRLVFLPDSIGLLLNLRILNVTGNKLTLLPESIAQCRSLVELDASFNNLTSLPANFGYGLLNLERLSIQLNKIRFFPNSICEMRSLRYLDAHMNEIHGLPIA IGRLTNLEVMNLSSNFSDLIELPDTISDLANLRELDLSNNQIRVLPDSFFRLEKLEKLNLDQNPLEYPPQEMVNQSAEAVREFMRKRWEEMVEEEQLRSVIEAE KQQGGATGWLSWGSSIVTSLFSGGTHGGAAKKPKNSFLDEQL
At4g35470/ sp|Q9SVW8	PIRL4	MDLMQMDKRLDSTEQVVEEIMRIHRSLPARPGIDEVEAAKGLIDNVEKEDQACLEAIARQRKSSEVPGELFMVLQEMKKGYVQFRSKEQIREALKLLDLESV HSLFDDFIQRASNCIASPSSNGSVSSRPPLPPATTTAARSDSQSSLNFSERAPVRPKDMVSRDDSFVTKSKPSSLYSDGFAAPPRRPQILDSTLTTGNDGEKLSLI KLASLIEVSAKKATQEINLQNKLTEQLEWLPDSLGKLSSLTSLDLSENHIVVLPNTIGGLSSLTKLDLHSNRIGQLPESIGELLNLVYLNLGSNQLSSLPSAFSRL VRLEELDLSCNNLPILPESIGSLVSLKKLDVETNDIEEIPYSIGGCSSLIELRADYNKLKALPEAIGKITTLEILSVRYNNIRQLPTTMSSLASLKELDVSFNELESV PESLCFATTLVKLNIGNNFADMVSLPRSIGNLEMLEELDISNNQIRVLPDSFKMLTKLRVFRAQENPLHIPPRDIAEKGPQAVVQYMNDLVETRNAKSLMVKP KKSWVQMCFFSKSNKRKQSSMEIV
At2g17440/ sp|Q5G5E0	PIRL5	MDSKEMVVEEIMRIHRSLPLRPEIDDVETATSLIQNVEKEDRNRLEAIDKLVKTSSSEVPLELFNVFKEMKKSLVRFQSTEQTREATKILDLESVHVVFDELIQR ASFCIASPNSTTALPRSVPVPAPVVSSDEIPFKSKEIISRDDTFVKKAKSSFYSDGLLAPSKPQVLDSTLHQAKNVAGNDGEKLSLIKLASLIEVSAKKATQELNL QHRLMDQLEWLPDSLGKLSSLVRLDLSENCIMVLPATIGGLISLTRLDLHSNRIGQLPESIGDLLNLVNLNLSGNQLSSLPSSFNRLIHLEELDLSSNSLSILPESI GSLVSLKKLDVETNNIEEIPHSISGCSSMEELRADYNRLKALPEAVGKLSTLEILTVRYNNIRQLPTTMSSMANLKELDVSFNELESVPESLCYAKTLVKLNIGN NFANLRSLPGLIGNLEKLEELDMSNNQIRFLPYSFKTLSNLRVLQTEQNPLEELPRDITEKGAQAVVQYMNDLVEARNTKSQRTKPKKSWVNSICFFCKSSTN
At2g19330/ sp|O64566	PIRL6	MICEEAYHQQPQIQKEQMMTMDQRNNHQRKRSPLSSPSSPSSPSSPSSPKSPSFNNNEEERLEVVNLSGMALESLPNPSLNLAQICKLDLSNNHLQTIPESLTAR LLNLIALDVHSNQIKALPNSIGCLSKLKTLNVSGNFLVSFPKSIQHCRSLEELNANFNKLIRLPDSIGFELTNLRKLSINSNKLISLPISITHLTSLRVLDARLNCLM ILPDDLENLINLEILNVSQNFQYLSALPSSIGLLMNLIELDVSYNKITVLPESIGCMRRLRKLSVEGNPLVSPPIEVMEQNLQVVREYLTQKMNGGSPRSPSKKKS WGFGKLVKYGTFNGGSRSWNREEREGFIMPEYRSIDSLASPRYSGMFSPRRLFSPRTYFSR
At4g29880/ sp|Q5G5D8	PIRL7	MICEDAYQYQQLHGQKDHMMTMMMMDLSTSPPSSPLSPSLSPKSPSYNNNEEERLEVVNLSGMALQSLPNPSLNLANICKLDLSNNHIKKIPESLTARLLNLI ALDIHSNQIKALPNSIGCLSKLKILNVSGNFLVSLPQTIQNCRSLEELNANFNELIRLPDNIGLELTNLKKLCVNSNKLISLPATITCLTSLRVLDARLNCLMILPE DLENLINLEILNVSQNFQYLSALPSSIGLLLNLLELDISYNKITVLPESIGCMRRLRKLSAEGNPLVSPPIEVVEQSLHAVREYLSQKMNGKLVNTAAKKKTWGF RKLVKYGTFNGRSRVWTREEREGLIMPEYRPIDILTSTKFPVTCSPRRLFSPRTYFSR

Table 3-1: Continued

At4g26050/ sp|Q8RWE5	PIRL8	MMGYEQMNQMTMTTTAMMKNYNKKGLINTPQKKMTRRSVSAIDGGAAATAKEGDRRQNIKTLDLSGMSLASLSASSINLASISKLDLSNNNIQKIPESLVA RMLNLWALDLQSNQLKTLPNSIGCLSKLKFLNVSGNYLQSLPKTIEDCRSLEELNANFNELTRLPDAIGFELTNLTKLSVNSNKLVLLPNSVSYLTSLRVLDAR LNRLSSLPEDLENLVNLQVLNVSQNFQHLTTLPYSVGLLISLVELDVSYNGITVLPDSLGCLRRIQKLSVEGNPLISPPFEVVEQGLEALKQYMSEKMTESYKK TPTKKKSWGIGKLVKYGLSSSPGRSTGREDGKEGFINVSDYRQIDGIASPRHVSLFNPRRLLSPLSAYFSPPRY
At3g11330/ sp|Q8VYG9	PIRL9	MAAEPNPKNFPVLSYVLARLPSFTAKSPSSSVPPFDIEQPPPSSSSSSIEIVTQMPHLTQPDVLASMTSAISDVAETRSILRTLGPRPDHESVDKARAKLSEIESFLS ESFEDIALTDAAAKDEKRRQEMDQEKTWCESILKLDEVHASYEKLLKEAEERLVRIYESAEKNAAEDEENVAAVEVNEEVVGILQHASANPVDRVDLSGRK LRLLPEAFGRIQGLLVLNLSNNKLESIPDSIAGLHSLVELDVSTNSLETLPDSIGLLSKLKILNVSTNKLTSLPDSICRCGSLVILDVSFNRLTYLPTNIGPELVNLE KLLVQYNKIRSFPTSIGEMRSLKHLDAHFNELNGLPDSFVLLTNLEYLNLSSNFSDLKDLPFSFGELISLQELDLSNNQIHALPDTFGTLDSLTKLNVDQNPLVV PPEEVVKEGVEAVKTYMGQRRISMLEEEEKKKMEEEMEQANAGWLTRTTSKLKTYVADVSEYLGSNSPRDPYLERQL
XP_009122185.1	BrPIRL1	MATELNPNNFPVLSYVLDRLPSFTAKSSSDGDKPPSKSDPSSSSSHSIEIVTQMPHLAHPDVLASMTSAIADVSQTRSVLRTLGPRPDHETVDKARARLAEIDAS LSESFEEIALSANDVDVAEKEQKRREAVDQEKTWYNSILKLNELHESYEKLLKEGEERLVRIYESAEKNAAAVAEEEAKEVEVSEEVVSILQQAEEKPLDRVD LSGRKLKLLPEAFGRIQGLLVLNLYNNQLEAIPDSIAGLHSLLELDLSTNFLETLPDSIGLLSKLKILNVSCNKLTTLPDSICKCGSLVVLDASYNNLTYLPTNIGF ELVHLEKLLIHLNKIRSLPTSVGEMRSLRYLDAHFNELNGLPESFGMLTNLEYLNLSSNFSDLQDLPASFGDLISLQELDLSNNQIHSLPDAFGTLVNLTKLNLD QNPLVVPPEEVVKQGVDAVKMYMGKRWVSMLEEEEKMANMKEEMEQANADWLARTTSKLKTYVTEVSEYLGSNSPKDPFLDQQL
XP_009129502.1	BrPIRL2	MEHDLDKFPLLSYVLHQYDSKHHAPPSMAVQQTLAPSFPLLSDPQIMYSLTQSIPTTITQTLTVLASLGPRPDPSAVSSARSMIAEILQMDSLSPEEAAKEAEIY AGAVRLEEVYDSYEKELSDLEEKLSRVYATEAESLLRSREEMNEEVVKVLKAAESGKVLERVDLSGQELKLLPEAICKIVGLVSLNISGNNLTFIPDAISKLKK LQELDVSSNSLESLPDSIGMLLNLRILNVSANNLTSLPESIAHCRSLVELDASYNNLTSLPTNIGYGLQNLERLLIHLNKLRYFPGSISEMISLKYLDAHMNEIHG LPSSMGRLKKLEVLNLSSNFNNLMRVPDAITDLINLRELDLSNNQIQAIPDSFYMLKKLEKLNLDHNPLEIPSQEVAKQGAEAVREFMRKRWDMIMGEEQQRI GVEAERHGDGTGWVSWGTSMVTNLVSGVSQTVGFGGGPGDGGDKKPGESHFYYQI
XP_009118040.1	BrPIRL3	MDHDLEIFPLLSYALHHSDPASHAPPSLSVQHSLANRYPLLTNPHVISTLIESIPSTITQTLHVFASLGPRPDPSSVSSARAKIAQIRETDPSSLSPEDAAKEEQIYV TVVKLEEVHEGYEKQLRGLEEKLSEVYASAVESLDGGDEVNEEVLEILDGGGVERIDLSDRRLKLLPEALGNNVSLVSLNLSRNDLKLLPDTISGLEKLEELD VSSNLLESLPDSFGLLLNLRVLNVSGNKLTYLPESITQCRSLVELDASFNNLASLPANIGYGLLNLERLSIHLNKLRYFPNSICEMRSLRYLDAHMNEIHGLPIAI GRLTSLEVLNLSSNFSDLTELPDTISDLANLKELDVSNNQIRVLPDSFFRLEKLEKLNLDQNPLEFPPQEMVNQGAEGVREYMRKRWEEMAEEEQLRSVIEAE KQQGGVTGWLSWGSSIVSNLLSGGTQSGGANKPKEDSYMDQLL
XP_009138361.2	BrPIRL4	MDSMQLDKRLDSTEQVVEEIMRLHRSLPPRPGLDDVEAARSLILNVEQEDQAWLEAIANQRKPSDVPGDLFTVLQEMKKGLVLFRSKEQRREATKLLDLET VHSSFDEFIQRASHCIASPSSNGSAPSRPPRVPKPPASLYLSEKAPVRPKEMVSRDDSFVTTKAKPSSLYGDALVAHRSPQLLDSTLTTGKFAGNDGDNLSLIKL ASLIEVSSKKATKVLNLQNKLTEQVEWLPDSIGKLSSLTSLDLSENHIVVLPNTIGKLSSLTKLNLHSNRITHLPESIGELLNLVYLNLSSNQLSSLPSSFSKLSQL EELDLSCNNLPILPESIGSLANLKKLDVETNEIEEFPYSIGGCSSLKEVRADYNKLKALPEAIGKITTLEILSVRYNNIRQLPTTMSSLASLKEVDVSFNELESVPE SLCFATTLVKLNVGNNFADMVSLPRSIGNLELLEELDISNNQIRVLPESFRMLTKLRVFRAHENPLQVPPRDVAEKGPQAVIQYMNDLVEMRNEKSLVVKPK KSWVQMCFFPKSNKRKHNSMEIV
XP_009112430.1	BrPIRL5	MMNQVVEEIMSIHRSLPPRPDIDDVEAATSLIQNVENDDQSRLDAVDREIKSSGVPQELFDVLQEMRRGLVRFQSKEQKREAAKVLDLESAHVVFDELIQRA YANLSRPPLAPVVSPASLYCSDEAHVKSKDMFTRDDTFVNKVKSSLYSDGFLAPRKPQVLDSTTLQAKNLTGHDGEKLSLIKLATLIEVSAKKATQELNLQH KLMDNLEWLPDSLGKLSSLVRLDLSENCIMALPATIGGLLSLTRLDLQSNRIGQLPESIGDLMNLVNLNLSGNQLTSLPSSLSRLVNLEELDLSSNSLSVLPETI GSIVSLEKLDVETNNIEEIPHSISGCSSLKELRADYNRLKALPEAVGKITTLEILSVRYNNIRQLPTTMSSMANLKELDVSFNELESVPESLCYATTLVKLNIGNN FANLRSLPGLIGNLEKLEELDMSNNQIRYLPYSFKALSQLRVLHTQQNPLEELPRDIIKKGAQAVVQYMNDLVEARNTKCQRTKQNKSWVVRICFLCKSTN

Table 3-1: Continued

XP_009102178.1	BrPIRL6	MICEETYHQQPQAPIKEHMMTMMMMDQHQSRKSPLSSSPSSPSSSPRSPSSPRSPSFNINNEEERLEVVNMSGMALESLPNPSINLAQICKLDLSNNYLQTIPES LTARLLNLIALDVHSNQLKALPNSIGCLSKLKTLNVSGNFLVSLPKSIQHCRSLEELNANFNKLIRLPDSIGYELTNLRKLSVNSNKLISLPISITHLTSLRALDAR LNCLMILPDDLENLINLEILNVSQNFQYLTALPSSIGLLMNLIELDVSYNKITVLPESIGCMRRLRKLSVEGNPLVSPPAEVMEQNLQVVREYLTQKINGTAPKS PSKKKSWGFGKLVKYGTFNGGSRSWNREEREGFIMPEYRSIDSLASPRYSGMFSPRRLFSPRSYFSR
XP_009137871.1	BrPIRL7	MICEEAYQYQQLHAQNDHMMTMMMMDLSQSPLSSPILSKNTDNNEEERLEDVNLSCMALQSLPNPSLNLGIICKLDLSNNHIKKIPESLTARLLNLVALDIHS NQIKALPNSIGCLSKLKILNVSGNFLVYLPKTIQNCRSLEELNANFNELIRLPDSIGLELTNLRKLCVNSNKLITLPTSITYLTSLRVLDARLNCLMILPEDLENLIN LEILNVSQNFQYLTTLPSSIGLLMNLLELDISYNKITVLPESIGCMRRLKKLSAEGNPIVSPPIEVVEQSLQAVREYLSQKMNGRLVNASPKKKSWGFRKLVKY GTFNGRSRAWTREEREGLIMPEYRPIDILASNRFPGISPRRIFSPRTYFSR
XP_009137574.1	BrPIRL8	MMGYEQMNQMTMTTTAMMKNFNKMGPINTPHKKITTKRSVSAIDGGAAVMAGEGDRRRNLKTLDLSGMSLASLSASSINLASISKLDLSNNNIQQIPESLV ARMLNLWALDLHSNQLKTLPNSIGCLSKLKVLNVSGNNLQHLPKTIEDCRSLEELNANFNELTMLPDTIGFELTNLTKLSVNSNKLVVLPSSLSHLTSLRVLD ARLNRLGSLPDDLENLVNLQVLNVSQNFQHLKELPYSVGLLISLVELDVSYNGITVLPDSIGCLRRIQKLSLEGNPLVSPPFEVVEQGLEAVKLYMSEKMTESY KETPMKKKLWGIGKMVKYKTFNGLSSSPGRSPGRRTGGDHHGNERGGFINVSDYRQIDGIASPRHVSLFNPRRLLSPFSAYFSPPRY
XP_009146736.1	BrPIRL9	MAADPNPNKFPVLSYVLSRLPSFTATKSSSPSSSSSSAPAFDVEQPIEIVTQMPHLAHPSVLASMTKAISDVAQTRSILRTLGPRPDHESVDKARAKLSEIEGILS ESLNDIAINEGKDEDEDEKKREEMGKDKTVCESILKLDEVHDSYEKLLKEAEERLVRMYESAAVAADEEGVAAVEVNEEVVGILQQALDNRVERVDLSGRK LRLLPEAFGRIQGLLVLDLSNNQLQAIPDSIAGLHDLVELNVSGNILETLPDSIGLLSKLKILNVSTNKLTVLPDSICRCGSLVILDVSFNRLTYLPTNIGSELVNL EKLMIQYNKIRSFPSSIGEMISLTYLDAHFNELQGLPDSFCLLANLEYLNLSSNFSDLIELPISFGDLINLQELDLSNNQIHALPDTFGSLESLTKLNVSQNPLVVP PEEVVKEGAEVVKMYMGKRRISMFEEEEKRKMEEEMEQANAGWLTRTTSKLKTYVTDVSEYLGSGSPRDSYLEQKL
XP_006287428.2	CrPIRL1	MATELNPKNFPVLSYVLDRLPSFSAKSSSDVDRSSSSSKSDPSSSSSSSSHSIEIVTQMPHLAHPDVLASMTNAIADVAQTRSVLRTLGPRPDHETVDKARARLV EIDASLSESFEEIALSPNDIDVAEKEQKRREAVEQEKTWYNSILKLNELHQSYEKLLKEAEERLVRIYESAEKNAAAVAEEEAAEVEVNEEVVSILQQASENPL DLVDLSGRKLKILPEAFGKIQGLLVLNLYNNQLEAIPDSIAGLQNLLELDVSTNFLQILPDSIGLLSKLKILNVSCNKLTTLPDSICHCGSLVVLDASYNNLTYLP TNIGFELVKLEKLLIHLNKIRSLPTSVGEMRSLRYLDAHFNELNGLPNSFGMLINLEYLNLSSNFSDLQDLPASFGDLISLQELDLSNNQIHSLPDAFGTLVNLTK LNLDQNPLVIPPQEVVTQGVDAVKMYMGKRWVSMLEEEEKMANLKDEMDQTNTDWLTRTTSKLKTYVTEVSDYLGSNSPKDPYLDQQL
XP_006292787.2	CrPIRL2	MTCSTIDMVPLLKTSINLQLALTNNHKTMDLDRFPLLSYVLHQLDSNLHAPPSMAAQQTLLPSFPLLSDPQIMSSLTQSIPKTITQTLFVFNSLGSRPNQSAVSS ARSKIAQIMDSLSPEEAAKETEIYAGVVRLDEVHDSYEKKLKDLEEDLSRVYVTEVESMLKSSQEVNEEVVAVLKAAESGGIIERIDLSGQELKLIPEAFGKIV GLVYLNLSSNDLTFIPDAISKLKNLEELNVSSNSLESLPDSIGMLLNLRILNVNANNLTALPESIAHCRSLVELDGSYNNLTSLPTNIGYGLQNLERLSIQLNKLR YFPGSISEMYNLKYLDAHMNEIHGIPNSVGRLTKLEVLNLSSNFNNLMSVPDTITDLTNLRELDLSNNQIQTIPDSFYLLRKLEKLNLDQNPLEIPSQEVANQGA EAVREFMRKRWDRIMAEQQQRIGVEAERHGDETGWVYWGTSMVTNLVSGVTQTIGFGGGSGDGGDKKLGDSHYYHQL
XP_006307445.1	CrPIRL3	MDHDLEIFPLLSYVIHHSDPASHAPPSLTIQQSLANRYPLLTNPHVISSLIESIPSTITQTLFVFGSLGPRPDPSAVSSARAKIVAIRENDSLSPEDAAKEEQFYAAV VKLEEVHEGYERQLRDLEEELSRVYASAVESLDGGDEVNVEVLSVIKEAEDGGVVERIDLSDRGLKLLPDALGKIVGLVSLDLSRNDLKFLPDTISGLEKLEE LDLSSNYLRSLPDSIGLLLNLRILNVTGNKLTSLPESIAQCRSLVELDASFNNLTSLPANIGYGLLNLERLSIQLNKIRFFPNSICEMRSLRYLDAHMNEIHGLPIAI GRLTSLEVMNLSSNFGDLTELPDTISDLANLRELDLSNNQIRVLPDSFFRLEKLEKLNLDQNPLELPPQEIVNQSAESVRDFMRKRWEEMVEKEQVKSVIEAEQ QQGGAAGWLSWGNSIVTGLFSGGTHGGAAKKDSYLDQQL
XP_006283467.1	CrPIRL4	MDLMQMDKRLDSTEQVVEEIMRIHRSLPPRPGIDEVEAAKGLVDNVDKEDQSCFEAIAKQRKGSEVPAELFMVLQDMKRGFLHFRSKEQKREALKLLDLEA THAFFDDLIQRASNCIASPSSSNGSVPSRPPPAPTPAPAPRTPSPSSLYFSEKPPVRPKEMVSRDDSFVSKTKPSLYTDAFAAPRKPQIMDSTLTAGKFAGNDGD KLSLIKLASLIEVSAKKATQELNLQNKLTDQVEWLPDSIGKLSSLISLDLSENHIVVLPNTIGGLSSLTKLDLHSNRIGQLPESIGELLNLVYLNLGSNQLSSLPSA FSRLLRLEELDLSCNNLPILPESVGSLVSLKKLDVETNDIEEIPHSIGGCSSLKELRADYNKLKALPEAIGKITTLEVLSVRYNNIRQLPTTMSSLANLKELDASFN ELESVPESLCFATTLVKLNIGNNFADMISLPRSIGNLEMLEELDISNNQIRVLPDSFKMLTKLRVFRAQENPLQVPPRDIAEKGPQAVVQYMNDLVETRNVKSQ MVKPKKSWVQRCFFSKSNKRKQSSMEIV

Table 3-1: Continued

XP_006297403.1	CrPIRL5	MEKRFDSKDKVVEEIMKIHRSLPSRPEIEDVETATSLVQNVEEEDRIRLEDIDDEHKMIQNSGVPKELFNVLKEMRRSLVHFQSKEQRREANKILDLESVHVVF DELIQRASNCIASPNGMTTTTISVPRSVPVPVPASVVSSDQGLVKSKEMLTRDDMFVKKERSSFYNDGLLAPRKPQVLDSTLMAKRVIGHEGEKLSLIKLASLI EVSAKKATQELNLQHKLMDQLEWLPDSIGKLLSLVRLDLSENCIMVLPETIGGLLSLTKLDLHSNRIGQLPESIGDLVYLVNLNLSGNQLSSLPPAFSRLIHLEE LDLSSNSLSTLPESIGSLVSLKKLDVETNNIEEIPHNISGCSSLKELRADYNRLKALPEAVGKLSTLEILTVRYNNIRQLPTTMSSMANLKELDVSFNELESVPES LCHAKTLVKLNIGNNFANLRSLPGLIGNLEMLEELDMSNNQIRFLPYSFKTLSQLRILHTQQNPLEELPRDITEKGAQAVVQFMNDLVEARNTKSQRSKPKKS WVNSICFLCKSTK
XP_023642045.1	CrPIRL6	MDRILKAARTSGSLNLSNRSLLDVPTEVYQCLETTGEGENWWEAVDLQKLILAHNDIEVLREDLKNLACLVVLNVSHNKLSELPAAIGELTAMKSLDVSFNS ISELPEQIGSAISLVKLDCSSNRLKELPESLGRCLDLSDLKASNNQISSLPEDMVNCSKLSKLDMEGNKLTVLSEKHIASWTMLTELNASKNILGCLPQNIGSLS RLIRLDLHQNKISSVPPSIGGCSSLVEFYLGINLLSTLPAEIGDLSRLGTLDLRSNQLKEYPVGACKLKLSYLDLSNNSLTGLYPELGNMITLRKLVLVGNPLRTL RSTLVNGPTAALLKYLRSRLSDSEETSASTPTKENVIASAARMSISSKELSLEGLNLSAVPAEVWESGEITKVNLSKNSIEELPAQLSSSVSLQTLILSRNKIKDW PGAILKSLPNLVCLKLDNNPLKQIPLDGFQAVSGLQILDLSGNAVFREHPKFCHLPQLQELYLSRIQLSEVPEDILNLSSLLILDLNQNSLQSIPKGIKSMTSLKHL DISNNNISSLPPELGLLEPTLEVLRLDGNPLRSIRRPILERGTKAVLNYLKDRLPDQ
XP_006294454.1	CrPIRL7	MICEDAYQYQQLHGQKDHMMTMMMMDLSTSSTISPSSSPKSPSHNNDEEERLEVVNLSGMALQSLPNPSLNLANICKLDLSNNHIKKIPESLTARLLNLIALD IHSNQIKALPNSIGCLSKLKILNVSGNFLVSLPKTIQNCRSLEELNANFNELTRLPDNIGLELTNLRKLCVNSNKLISLPNSITYLTSLRVLDARLNCLMILPEDLE NLINLEILNVSQNFQYLSVLPSSIGLLLNLLELDISYNKITVLPESIGCMRRLRKLSAEGNPLVSPPVEVVEQSLQAVREYLSQKMNGKLVNIAAKKKTWGFRK LVKYGTFNGRSRAWTREEREGLIMPEYRPIDILASTKFPVMCSPRRLFSPRTYFSR
XP_006283906.1	CrPIRL8	MMGYEQMNQMTMTTTSMMKNFNKRGLNNITPHKKITRRSVSAIDGGAAAAATDGEGDRRQILKTLDLSGMSLASLSASSINLASISKLDLSNNNIQKIPESL VARMLNLSALDLHSNQLKTLPNSIGCLSKLKFLNVSGNYIQFLPKTIEDCRSLEELNANFNELTRLPDAIGFELTNLTKLSVNSNKIVQLPQSVSHLTSLRVLDA RLNRLGSLPEDLENLVNLQVLNVSQNFQHLTTLPYSVGLLISLVELDVSYNGITVLPDSLGCLRRIQKLSVQGNPLISPPFEVVEQGLEALKQYMSEKMTESYK KTPTKKKSWGIGKLVKYGLSSSPGRRASRGGEREGFINVSDYRQIDGIASPRHVSLFNPRRLLSPLSAYFSPPRY
XP_006296704.1	CrPIRL9	MAAEPNPKNFPVLSYVLARLPSFTTKSPSSSAVPPFNIEQSPSSSHSIEIVTQMPHLTQPDVLASMTSAISDVAETRSILRTLGPRPDHESVDKARVKLSEIESSLS ESFEDIALTDAAAKDEKRRLEMDQDKTWCESILKLDEVHASYEKLLKEAEERLVRIYESAEKNAAEDEDNVAAVEVNEEVVGILQHASANPVDRIDLSGRKL RLLPEAFGRIQGLLVLNLSNNKLEAIPDSIAGLHSLVELDVSTNSLETLPDSIGLLSKLKVLNVSTNKLSALPDSICRCGSLVVLDVSFNRLTYLPTNIGFELVNL EKLLIQYNKIRSFPTSIGEMRSLKHIDAHFNELHGLPDSFVLLTNLEYLNLSSNFSDLKELPFSFGDLVSLEELDLSNNQIHALPDTFGTLHSLTKLNVEQNPLMV PPKEVVKEGVEAVKTYMGQRRITILEEEEKMRMEKEMEQANAGWLTRTTSKLKTYVTDVSEYLGSPSSRDHYLDQQL
Os04g51560/ sp|Q7XNY1.2	OsIRL1	MREMGEKRRRGHLNPAGFAGGLHDHEEKKNEEHKLDMSGMSMDALPHLTMSLGQVTILDLSNNNLESIPESIIARLLNVVVLDVRSNQLKSLPNSIGCLSKL KVLNVSGNLLESLPNTIEECRALEELHANFNELTKLPDTLGFELHSLRKLSVNSNKLAQLPSSTSHMTALRALDARLNCLRALPDGLENLANLEALNVSQNFQ FLRELPYAVGLLASLRELDVSYNSIAALPDSMGCLTKLARFSAVGNPLVSPPMDVVEQGLDAMRAYLTARMNGGDGKRKKKAWLPKLVKYSTFTARMTPG RTRVHENTEGLLMSDYRSLNGIASPRFLTMLSPRRLFSPRRNSPKHC
Os02g38040/ sp|Q6ZH85.1	OsIRL2	MDPTPQSHPILAYVLSRLPSLLPVSPSLSTPRARDIEQPSPRAPSGAAEFDLVSRMPGLRHPSVLSAMTRAVADVSSARDALRLLGPRPDHELVDSARAFLRSH AAEEAEEEEEDEKVAKSREVVRLDEAHESYGGLLREAEERLDRVYRTAMRGRDMQVVAAAHGGGGEEEAGVVDDEVVRVLRDAEEGKAVERLLLADRQ LRHLPEQLGRIRGLLVLDVSRNQLKNVPDAIGGLEHLEELRLASNALVSLPDSIGLLTSLKILDVSGNKLRSLPDSISKCRSLVELDVSYNVLSYLPTGIGQEMA RLEKLWVHLNKLRSLPSSVCEMRSLRLLDAHFNQLRGLPAGIGRLAALESLNLSSNFSDMRDLPASFGDLLGLRELDLSNNQIHALPDCFGRLQRLERLRLDQ NPLAVPPKEVVAGGVGAVKEYMARRWRDARAEEERRGSAVAESPRVSTPKEWLVRSVSSLGSWVSDVTRYGAGQDKAAAEEEEDAYLQQNL

Table 3-1: Continued

Os04g40080/ sp|Q7XK44. 3	OsIRL3	MPGLRHPSVLRAMTRAVADVSAARSALQVLGPRPDHELVDSSRAIVAATDAEAGGSRRVPEGDLEACRAVVRLEETHDAYEALLQEAEGRLEAVYRSAME GKDLEEPDGRDESAAAAAGDDAAVQEEVIAVLRQAEEGKPVESVRLVDRQLRHLPEAFGRIQGLRVLDVSRNQLEVIPDAIGGLDHLEELRLASNALISLPDS IGLLLNLRILNVGSNRLRSLPDSISKCRSLIELDASYNGLAYLPTNIGYELVNLRKLWVHMNKLRSLPSSICEMRSLYLLDAHFNELCGLPSAIGKLSSLEILNLS SNFSDLKDLPASFGDLLNLRELDLSNNQIHALPDNFGRLDKLEKLNLEQNPLSMPPMEIVNKGVDAVKEYMLQRWLDILLEEERKSIAAAESPQAPTTPSAWL ARSVSWVSDVSGSLVGYLSGENKTEKDAYLDQQY
Os08g40090/ sp|Q6Z8P4.1	OsIRL4	MGAVGVEAGVFDTVDGLVGEVMRLHRSLPARPAVEEVEAAEALAAAADREERARADAVARLRRSPAVPDELLCVAQEMHRALAGFQCREQKRDAARLLE LEALHTLFDDLIQRASQCLPSTSTRAAPRIAAPAAATTTTSTAAAGSSSSSAVGNAERHASSGTNGFTASRVAGTSTSTGRVSMDDSYVRKAKAAMWDGGAA ATNSHLPRGPVEANSVAVRADGNYGDDNEKLSLIKLASMIEVSAKKGARDLNLQGKLMAQIEWLPDSIGKLTGLVTLDISENRLLALPDAIGKLFSLAKLDIH ANRISQLPESIGDLRSLIYLNMRGNQLSSLPSSIGRLLNLEELDVGSNGLSSLPDSIGSLTRLKKLIVETNDLDELPYTIGHCVSLVELQAGYNHLKALPEAVGKL EPLEILSVRYNNLRSLPTTMASLTKLKEVDVSFNELESIPENFCFATSLIKLNVGNNFADLQYLPRSIGNLEMLEELDMSNNQIRVLPDSFGNLKHLRVLRAEEN PLQVPPRDIALKGAQAVVQYMSDASKRTTKSEPMKPKKTWVHFCFFSRPNKRKHDRIDNAT
Os10g42190/ sp|Q8S7M7.1	OsIRL5	MASAAEAVEELTRLYRELPPRPAVEEVEAAEAVLASADAEEAARLDEVAREEASASASSSAAAPGRADGELLAVLREARRNAVRLRALQQRKEAAYVVELE RRFKVFDDLIQRASRVVSSSSDAAEAGGGTTGDGYVGVGADSVDLEMELRKKEAAVAAAAAVAEMERGSKGLAALGLESKPISSLRRDVSAGTDMEKLSLI QVASLIESSAKKGITELSLRGKLVDQIEWLPVSLGKLQDVTELDLSENRIMALPSTIGSLRYLTKLDLHSNQLINLPDAFGELSNLIDLDLHANQLKSLPSSFGNL TSLANLDLSSNMLKALPDCLGKLANLRRLIVETNELEELPYTIGSCTSLVELRLDFNQLKALPEAIGKLEKLEILTLHYNRIKGLPTTVGSLSRLRELDVSFNEV EVIPENICFATSLVKLNLSRNFADLRALPKSIGNLEMLEELDISSNQIRVLPDSFRCLSRLRVFHADETPLEFPPREVVKLGAQAVVKYMNDLNAARGTNQKKT DRGSFWTWLFSLFGCCKKNQEVGLPV
Os02g58030/ sp|Q6K7R2.1	OsIRL6	MERVLKSARESGSLNLSNRSLREVPKEVYNNLDTGAQDEKWWEGVDLQKLILAHNNLEVLREDLRNLSSLVVLNISHNNISSLPAAIGDLPLLKSLDVSSNQI NAFPEEIGFATALVKVDCSNNCLTDLPVSLARCLELSELNASNNTISVLPDELAGCSKLFRLNLEGNKLVTLSDKMFMSWTMLTEMNAAKNLLTAIPDGIGAL SKLIRLDLHQNKITLIPPSIKDCSSLAEFYMGNNLLTSIPEDIGMLSNLGILDLHSNQLKEYPVGACRLKLSFLDLSNNSLSGLPAELGTMTTLRKLLLTGNPMRT LRSSLVSGPTTALLKYLRSRLSSDEGASGSGSTPTKDDQIAAARRLSLSSKELDLSGLGVTSVPPAAWETNDVMKLDLSKNSIEDLPNELSLCSSLQSLILSNNK IKRWPGTVFSSLASLSLLKLDNNPLAEILATDLEALSKLEVLDLSGSASSLPEPSAVSKLPHLKELYLRRMKLHGFPDSLLGLKLLRILDLSQNYLTSVPEGIKD LTSLIELDLSDNNITTLPPELGLLEPNLQVLKLDGNPLRSIRRTLLERGTKAILKYLKEKLPAE
Os03g11360/ sp|B9F655.1	OsIRL7	MGCCSSRSADSPASRVTRWRSTGIVALRDARLKVVPNEVLQVGNSLRILDLTNNKIAEIPQEVGTLVNMQRLVLAGNLVESIPANIGYLRNLKILTLDRNKISV LPEELGSLSNLQQLSISQNSLSRLPKSVGDLRNMLLLNVSDNKLIALPESIGGCSSLEELQANGNSIEDVPSSICNLVCLKSLSLNGNKIRQLPQNLLKDCKALQN ISLHDNPISMDQFQQMDGFTEFEARRRKKFDKQIDSNVMMSSTALDEGIDLN
Os10g31790/ sp|Q7XDQ7.1	OsIRL8	MESSPPPPPPTITVQVKFGGRTIPVEVPAAATAADLKRLLQPLTNVLPRGQRLICKGKVLADAASLSSMQVVNGSKVMLMASQGLHQGDGPITKNSSVPAPST RRASNVKEAQIQKSDTNVSKIRPERWKATGIIALSDSSLKAVPEEVWGCGSSIRVLDVSNNCIEAIPQEIAALRSLQKLILTANDIADGNISWEGLTCVQTLTVL SLSQNRLVTLPSSLGSITHLRELRIANNRLENLPVEIGLLKHLEILIANNNRITSLPSSIGGCESLNEVDLSSNLLAELPEAFGNLQHLKALSVRNNGLTSLPSAFFI KCSQLITLDLHGTEITNDVLRQVDGWEEFDERRRKKHQKQLDFRVGSSVVFDEGADDDYRRL
KAE8703459.1	HsPIRL1	MDSHLKNSPLLSYVLSRLPSISSSKPHYDPLVDIEQPPPTDASSSATLPPIVDEMPNLSHPKVLAAMTHAILDVAQTRSVLQTLGPRPDHESVDMARSKLAEIES GVSKSLGELVLSPRPAEVHQAEWRANLAEKEQQIRQEAEKEKSMYKSILQLDEMHEAYGKLVKQAEDRLVKIYEKAGEAEENLEQIEDINPEVVGILEEAQG KGLERVDLCGRKLRFLPEAFGKISGLLSLNLSGNQLEVIPDSLAGLQKLEELNVSSNLLQSLPDSIGLLPNLKILDVSGNKLNALPDSICQCRSLIELDVSFNSLL YLPTNLGNELGNLQRLSVYLNKLRSLPTSICKMRSLRFLDAHFNELRGLPDEIGRLTNLEVLNVRCNFADMTELPESLGELVNLKELDISNNQINALPDSFGLL DKLTKLNLDQNPLVVPPKEIVNQGVDAVKIFMANRWADKLAEEERKIMMEVNEVQETGWLTRSASFLKSYASIVGGTVSGYIGPAAPRDPFLDEER

Table 3-1: Continued

KAE8721983.1	HsPIRL2	MIPGLHNIIAHVIYGDIPSQQPIFSRQSTKNGYPIHNTMLRNMTRKPNLPVPRNLKSLWPGFLPNPLSSEATAKTTGSILPKPKLPYPVNERRRQAPNERERGPSN NRAGCEQRKPLNQVKQYSTRRGKQHLAFTTARHGAHQQRLLMDPTLSKFPILSYICSQQDPYNYPSLPRDISIDLFTRFPRLYDPAILSSLSQSIPSTVTQTHSLL RSLGPRPDPSAVSAARSKIIQIQETQSSSQEAEIFKSVIRLEALHEDYERQLTELEENLGRLYRSAVEQMRGEIEVNEEVVRILEEAETGVVERVELSGRGLRLLP EAFGKLHGLVHLNLSSNQIEVIPDSIGGLKKLEELDASSNQLQYLPDSIGLLLNLRILNVSGNKLNALPESIARCRCITSDEDIANLVEEYDRVASPPSSLKIRAFL SPLKPARKSICSPPKPPRKSISSPPSSSTSSSSSPRYSCIRQIPRTPVAFPLCSNKSAGKMIPCYGYHGQPSHIYLVHSGNYRQ
KAE8665008.1	HsPIRL3	MDPTLSKFPILSYICSQQDPYNYPSLPRDISIDLFTRFPRLSDPAILSSLSQSIPSTVTQSHSLLRSLGPRPDPSAVSAARSKIIQIQETQSSSQEAEIFKSVIRLEALHE DYERQLTELEENLGRLYRSAVEQMRGEIEVNEEVVRILEEAETGVVERVELSGRGLRLLPEAFGKLHGLVHLNLSSNQIEVIPDSIGGLKKLEELDASSNQLQY LPDSIGLLLNLRILNVSGNKLNALPESIARCSSLRELDASFNNLSFLPTNIGYGLLNLEKLSIHLNKIRFLPSSICEMRSLRYLDAHFNELHGLPQAIGRLTKLEVL NLSSNFNDFTEVPDTITDLTDLRELDLSNNQIRVLPYTFGRLGKLVKLNLDQNPLIVPPAEIANKGAEAVKEFMSKKWIEIITEEQRRINLEASNQQGQTGWLT WGSSLVSNIASGVGGYLSGPKAPSDPYLDQQL
KAE8664234.1	HsPIRL4	MVESCAVRSTDEAVEEIMRIHRSLPPRPALDEVQAAKELIRNVEKEDQARLDAIARKIKSPNVPQELFLILLEMQNKCVYFQSKEQKREAYKLLDLEAVHDLF DEFIQRASDCLSSSPSSSKFHDKSTHSNELPSAAAPPPSSNNSFAAATTSSFTTREPASGRVLFSRDDSYVKKAKSSFYGNATDRGLGISVSSTPHILDSSLKSDA ATASVQDGEKLSLIKLASIIEVSAKKGSRDLNLQAKLMDKIDWLPDSVGKLSSLITLDLSDNRIVALPDTIGGLSSLKKLDLHSNKIAQLPDSIGDLLSLVFLDLS ANQLSSLPATFGRLALLEDLDLSSNHLPSLPDTIGSLINLKKLNVETNDIEEIPHTIGHCSSLKELRADYNRLKALPEAVGKIETLEVLSVRYNNIKQLPTTMSSL VNLRELDVSFNELESLPESLCFVTTLVKMNIGNNFADLRSLPRSIGNLEMLQELDISNNQIRVLPDSFRMLTSLKVLRVEENPLEVPPRHIVEQGAQAVVWYM ADVVEKRDVKLPPMKQKKSWAQICFFSKSNKRKRNGMDYVKA
KAE8678495.1	HsPIRL5	MAMMSKQDPSPSFLQTLQEIMRLYRSLPPRPSIADVEASKSVLKTLENEEKVKLEEISKEKPPEDVPGELFSILQQVRKTMVLFQSHEQKKDALHLVEADKLFE TFDGLIQRASLLVSGDTQDEKVTTFGEHVSKFDTETIITDDSLVKQEEDGELDKDDAKGENSSEKLNLMKTAALIENTARTGGVVLDLRGKLMDQIEWLPVSI GKLNDVTELDISGNRIMALPPSIGGLQALTKLDFHSNQLINLPDSVGELVNLIELDLHANRLKSLPASFGNLTNLMNLDLSSNEFTHLPEAIGNLSSLKRLIVET NELEELPYTIGNCSSLSELKLDFNQIKALPEAIGKLQCLEILTAHYNRLKGLPTTIGNLSNLKELDVSFNEIEFIPENLCFAVSLRKLNVGKNFADLRALPRSIGNL EKLEELDISDNQIKVLPDSFGSLSKLRVLGAEETPLEVPPREVIKLGSQAAVEFMANLVAKRDTTISARAKKKSFFSRICFICWPF
KAE8705959.1	HsPIRL6	MEMSRIKGDDHHHHHHGSRPRRSSGDQEEKVRIGTVDLSGMSLDSLPISSLNLSFVSKLDLSNNNLQSIPESLTARLLNVVAMDVHSNQLKSLPNSIGCLSKLK FLNVSGNLLRALPKTIGNCKSLEELNANFNQLTMLPETIGFELTCLKKLSVNSNKLILLPQSITHLTSLRVLDARLNCLRSLPGDMENLINLEVLNVSQNFQYLE TLPYSIGLLMSLVELDVSYNKIKYLPDSIGCLRKLQKLSVEGNPLVSPPVDVLEQSLQVVKEYLCEKMKAGQNPQKKRSWVGKLVKYASFNGKMTMTGGG GRRSWEKEGSIMAEYRSIDGLAAPRCVGISSPGRLFSTHNTGMLSPRRLFPSRTYK
KAE8658303.1	HsPIRL7	MGCFQSRGADSKANRIARWRSTGIVALRDAKLKARQFSFLGSSFFLFVYIIHNSSVFEIPMDISNLVNMQRLILATNLIERLPINLGKLQALKVMILDGNQITSLP DELGQLVRLEKLSISGNMLMSLPETIGSLRNLSLLNVSNNKLKYLPESVGSCFSLEELQANDNLIEELPASVCNLVHLKSLCLNNNKISQIPPNLLKDCKALQNI SLHDNPISMDQFQQMEGFQEFEARRKKKFDKQIDSNVMIGSKGLDEVLIYNSAAFTVLIGQWLHIFNNIRYQGTWIG
KAE8710516.1	HsPIRL8	MMTEQQQLMRMGDGSRSGKRFMEEEERLDIVDLSGLSMDSLPKSSLNLTTICKLNLSNNNLQNIPESLTARLLNLVAFDVHSNQLKCLPNSIGCLSKLKTLNV SGNLLRSLPKTIKNCRSLEELNANFNILTKLPESMGFDLIHMKKLSVNSNKLVCLPQSITHLTNLRVLDARLNCLRTIPEDMENLINLQVLNVSQNFQYLQNLP YSIGLLVSLVELDVSYNKIATLPDSIGCMKRLQKLSVEGNPLMSPPAEVFEQGLHAVKEYLGEKMNAGHRSPQKKKSWVGKLVKCGTFNGSSEREGREGEG REGFIISEYRSIDGLASPRYMGMFSPRRLFSSGRYFSR
KAE8693161.1	HsPIRL9	MDPHLKSYPLLSYVLSRLPSMSSSKPHYDPPSDLEQPPPASSSSANHPSIVDEMPNLSHPKVLASMTHAIFDVAQTRSVLQTLGPRPDHESVDMARSKLAEINS GLSKSLEELVLSPRPADVDQAEWRAHLAEKEQRIRQEAEKEMSMYKSILQLDEMHEAYEKLVKQAEERLIKIYEKAGEVEESLEQIEETDPEVVGILEEAQGK GLERVDLCGRKLRFLPEAFGKISGLLSFNLSGNQLEVIPDSLAGLQKLEELNVSSNLLESLPDSIGLLQNLKILLSVYLNKLRSLPTSICKMRSLHFLDAHFNELR GLPDEIGRLTNLEVLNVRCNFSDLTELPESLGELTNLKELDISNNQINALPDSFGRLDKLTKLNVDQNPLVVPPKEIVDQGVDAIKMFMAERWVDKLAEEERE SMMEVNEVEETGWLTRSASMLKSYASVVGETVSTYLGSAGPRDPVLDEAR

Table 3-1: Continued

PWZ40074.1	ZmPIRL1	MIVASSSSSFSISFQEWDRDDMRDMGEKRRHGHGHGHLVGFGAGGVVGHATEHEEKRMEQKKLDMSSMSMDTLPHLTTPLGNITTLDLSNNNLQSIPESIIA RLLNVVVLDVRSNQLKSLPNSIGCLSKLKVLNVSGNLLQELPATIEECRALEELNANFNQLTRLPDTLGFELHGLRRLSVNSNKLAYLPSSTSHMTALRSLDA RLNCLRALPDGLENLGGLEALNVSQNFQYLRELPYGIGLLVSLRELDVSYNSIAALPDSMGCLTKLARFSAAGNPLVCPPMDVVEQSLDAMRAYLSARMNG TAKAKKKSWVPKLVKYSTFSAGMMTPGRTKVHGNNTDGLHMSDYRSLDGGGVASSAFLSMLSPRRLFSPRRNSAKH
PWZ20945.1	ZmPIRL2	MDPTPQSHPILAYVLSRLPSLPAVRTPRSPRERDLEQPSPRTPSGAAEIDLVGRMPGLRHPSVLSAMTRAVADVSSARDAIRLLGPRPDHEQVDASRELLRLAD AGKKADANAGVKTKDLDEEKLAKCREVVRLEEDHEAYGALLRDAEGKLEHVYQMAMHGRDIKKVGGGDGKGEEGSGAVDEEVVRVLKDAGEGKVVER VNLADRQMRLLPEPIGRIRGLLALDVSRNQLKFSSRANFLFGAFNSDVPCLNSQVIPDAIGGLEHLEELRLASNDLVSLPDSIGLLSNLKILDVSGNRLRVLPDTI SKCRSLVELDASYNALAYLPTGIGHELVHLQILRVHLNKLRSLPSSVCEMRSLRLLDAHFNELHGLPAAIGQLSALETLDLSSNFSDMRDLPPSFGDLGGLREL DLSNNQIRALPDCFGRLAKLERLRLDQNPLAVPPPEVVADGVVAVNEYMARRWAEAVAEEERRRANAAAVAESPRASTPREWLTRSVSSLSTWVSDVTVK VVGQEKVDDEDEFLQQQF
AQK72233.1	ZmPIRL3	MDPTPQSHPILAYVLSRLPSLPAVRTPRSPRERDLEQPSPRTPSGAAEIDLVGRMPGLRHPSVLSAMTRAVADVSSARDAIRLLGPRPDHEQVDASRELLRLAD AGKKADANADVKTKDLDEEKLAKCREVVRLEEDHEAYGALLRDAEGKLEHVYQMAMHGRDIKKVGGGDGKGEEGSGAVDEEVVRVLKDAGEGKVVER VNLADRQMRLLPEPIGRIRGLLALDVSRNQLKFSSRANSLFGAFNSDVPCLNSQVIPDAIGGLEHLEELRLASNDLVSLPDSIGLLSNLKILDVSGNRLRVLPDTI SKCRSLVELDASYNALAYLPTGIGHELVDLQILRVHLNKLRSLPSSVCEMRSLRLLDAHFNELHGLPAAIGQLSALETLDLSSNFSDMRDLPPSFGDLAGLREL DLSNNQIRALPDCFGRLAKLERLRLDQNPLAVPPPEVVADGVVAVNEYMARRWAEAVAEEERRRANAAAVAESPRASTPREWLTRSVSSLSTWVSDVTVK VVGQEKVDDEDEFLQQQF
XP_008669104.1	ZmPIRL4	MGTALDAAAFGSVDGVVGEIMRLHRALPARPAPEEAEAAEALVRAADREERARLDAAARLRRPPAVPDELFGVALEMHRALAAFHCREQKRDAARLLELD ALHGLFDDLIQRASQCVPSSSGSSSTRAAPRVAAATTAAASSSFAAASSSAVAADSGAHRYSSMEPNGFSAPRMVTGMGRVSMDDSYVKKAKAAVWDDRV VASSSHMPRGAVSANSVATPVDGGYGDDNQKLTLIKLASMIEVAAKKGARDLNLQGKLMNQIEWLPDSIGKLTGLVTLDISENRILALPEAIGMLSSLAKLD LHANRIAQLPESIGDLSNLIYLDLRGNQLASLPASLGRLVKLEELDVSANHLTSLPDSIGSLTRLKKLIAETNDLDELPYTIGNCVSLVELRVGYNHLKALPEAV GKLESLEVLSVRYNTIRGLPTTMASLTKLKEVDASFNELESIPENFCFVTSLIKLNVGNNFADLQSLPRSIGNLEMLEELDISNNQIRVLPDSFGNLQRLRVLRAE ENPLQVPPRDVALKGAQAAVQYMAEYVAKKATRSQPMKTKKTWAQFCFFSRPNKRKHDRIDTAS
PWZ05808.1	ZmPIRL5	MAAAGPTTSPATAGAVEELTRLYRELPPRPAVEEVEAAAAVLASAAAEEEARLAEIAREEALARARARGGAPPELLDVLWEARRSSVRLRALQQRKEAAHV LELERRFRLFDDLIQRASRLLSPGGGAGARIGTGGAAVDHDEVVEVEATRDTELDAAPAEIGRGSKGGLGLEPKSVSSLRRAASAGTDTEKLGLIQVASLIESS AKKGTTELNLRGKLVDQVEWLPVSLGKLQDVTELDLSENRIMALPSTIGSLRYLTKLDLHSNQLINLPDTFGELSSLIDLDLRANQLKSLPTSFGNLTSLANLD LSSNLLKVLPDCLGKLKNLRRLIAETNELEELPYTIGSCTSLVELRLDFNQLKALPEAIGKLENLEILTLHYNRIKGLPTTIGHLTRLRELDVSFNEVETIPENICF AASLVKLNVSRNFADLRALPKSIGELEMLEELDISSNQIRVLPDSFGHLSKLRVFHADETPLEVPPKEVVKLGAQELVNYMKNMVAAREVSQNQTDKRSFWT WLRSLFGCYKKNQGLGPVPA
PWZ57041.1	ZmPIRL7	MGCCSSRSSDSPASRVTRWRSTGIVALRDARLKEVPNEVLQVGNSLRTLDLTNNKLVEIPQEIGTLANMQRLVLAGNLIEIIPANIGYLQNLKILTLDRNRISILP EELGSLSNLQQLSVPQNFLLCLPKSIGDLRNMSVLNVSDNKLKELPESIGGCSSLEEFQANASPTSGTDLEAKYSGNAIEDVPASICNLVCLKSLSLNGNKIRQL PQNLLKDCTALQSLSLHDNPITMDQFQQMDGFGEFEARRRKKFDKQIDSGVMMGSTALDEGVDFH
AQK76376.1	ZmPIRL9	MSFNQINTLPEEIGLATALVKVDFSNNCLTELPPNLATCPDLSELKASNNNISRVPDVLAGCSKLSKLDLEGNKLVALSENMFVSWTMLTELNLAKNLLTAIP GSIGALPKLIRLDMHQNKITSIPPSIKGCSSLAELYMGNNLLSSIPADIGTLSKLGILDLHSNQLKEYPVGACNLKLSFLDLSNNSLSGLPAELGKMTTLRKLLLT GNPMRTLRSSLVSGPTTTLLKYLRSRLSSDEEGSRSTPTKDDQIAAARRLSLSSKELDLSGLGVTSVPAAAWETSDVVKLDLSKNSIEDLPNELSLCSSLQSLVL SNNKIKRWPHTVVSSLPCLSSLKLDNNPLVEISSTDLVPLSKLEVLDLSGNASALPEPSAVSALPQLQELYLRRMKLHEFPNGLLGLKLLRILDLSQNHLTTVPE GIKNFTALIELDLSDNNITALPAELGLLEANLQVLKLDGNPLRSIRRTLLERGTKAVLKYLKEKLPSE

Table 3-1: Continued

XP_002530026.1	RcPIRL3	MDQEFPILSYLLSQLDPNSHPPLPQVIYQNLITQFPQLNNPKVISSLTQSIPSTIIQSLFLLKALGPRPDPDAVSTARIKIQELGETGKEVEIYKAVVRMEEMHNEY ERQLREVEERLSGVYKNVVGEFEDVKVNEEVVSILKQVESGSVVERVDLSGRQLKLLPEAFGKLHGLVLLNLSRNQLEVLPDSIAGLQKLEELDVSSNLLLSL PDSIGLLRTLKVLNVSGNKLNYLPESIALCSSLVELDASFNNLVSLPTNIGYGLTNLERLSIQLNKIHILPPSICEMKSLRYLDVHFNELHGLPYAIGRLTNLEVL DLSSNFSDLTELPETVGDLANLRELNLSNNQIRALPDTFGRLENLANLILDENPLVIPPKEIVNKGVQAVREFMQKRWLDMIAEEQQRRMLEVNQQQSQTGW LAWGNSLLNNFVSGVSQSVSGYIGGTKPPQDPYLDQQL
XP_002532476.1	RcPIRL4	MEATAATTSFRKIRSIDEAVEEIMRIHRSLPERPGIEEVEAAKALIQNVDKEDQGRIEAISRQTKSPDVPGELFVILLEMQKNLVYFQGKEQKRDALKLLDLENV HSLFDDFIQRASKCLPLSSSSSSSSSSTTTAAAAASALSSSFTYANGSASTVSTSKPPASTSTNKSSSNLNYSEQNSSRTELFTRDDSYVKKVRSSFYSDGIGAAV SSMPRIVDSTLKTATTTSGQDGDKLSLIKLASLIEVSKKKGTKDLNLQNKLMDQIEWLPDSIGKLSNLVSLDLSENRIVALPATIGGLSSLTKLDLHSNKIAELP ESIGDLLSLVFLDLRANHISSLPATFSRLVRLQELDLSSNHLSSLPESIGSLISLKILNVETNDIEEIPHSIGRCSSLKELHADYNRLKALPEAVGKIETLEVLSVRY NNIKQLPTTMSSLLNLKELNVSFNELESVPESLCFATSLVKINIGNNFADLQYLPRSIGNLENLEELDISNNQIRALPDSFRMLTKLRVLRVEQNPLEVPPRHIAE KGAQAVVQYMAELFEKKDVKTPIKQKKSWAQICFFSKSNKRKRSGMDYVKA
XP_002519837.1	RcPIRL5	MAAKSSSNDQHPSPAFLETVEEIMKLYRSLPAARPSIEEAEAAMSVIKSVNCEEQQKLEEISKQECPRNVPDELFYVLKELRRNMVLFQSHEQRKEALHLIEVD KMFQTFDGLIQRASILVSGDTHKDKMIGFSDPLEKVETESTVKEESLINRREDGNLAKYGFQGFVKSSSTKPSLFSGEGEPEKFSLMKVAAIIENSAKTEDVVL DLKGKLMDQIEWLPLSIGKLSFITELDLSENRIMALPTTITSLKVLTKLDIHSNQLINLPDSFGELMNLTDLDVRANRLKSLPSSFGNLKNLLNLDLSSNQFTHLP EALGDLTSLKILNVEINELEEIPYTIENCSSLVELRLDFNRLRALPEAIGKLGCLEILTLHYNRIRKLPTTMGDLSYLRELDVSFNELESIPENLCFAASLKKLKVG ENFADLTDLPRSIGNLEMLEELDISDDQIRVLPDSFRFLSKLRVFRADGTPLEVPPRQVAKLGAQASVQFMADLVAKRDVKIRPTKKKKGFWHRACLIFWPFR RNSQ
XP_002518243.1	RcPIRL6	MLYEQQQQQQHQMMVRVDMGKKADNRESIEEQKLEIVDLSGMSLDTLPSPSLNLATICKLDLSNNNLQSIPESLTARLLNIVILDVHSNQLKSLPNSIGCLSKL KVLNVAGNLLACLPKTIENCRSLEELNANFNKLSVLPNTIGFELVNLKKLSVNSNKLVFLPHSITHLTSLKTLDARLNNLRSLPEDLENLINLKVLNVSQNFQY LETLPYSIGLLFSLIELDISYNRITSLPNSIGCLRKLQKLSVEGNPLVSPPMEVVEQGLHTVKEYLSEKMNAGHKSPQKKKSWVGKLVKYGTFNGSTRNQINST NNEERKAFIMSEYRSIDGLASPSYMGMFSPRRLFSPKNIFH
XP_015572103.1	RcPIRL7	MGCCASQNADSKANMIARWRSTGIVAMRDAKLKTFPDEVLDLERCVRTLDFTHNKLVNIPIEISRLVNMQRLLLSDNLIERLPMNLGKLQSLKVMILDGNCIS SLPDELGQLVRLEQLSISGNMLMSLPETIGSLRNLALLNVSNNKLKTLPESIGSCFSLEELQANDNSIEDLPASICNLVHLKSLSLNNNNVSKIPTNLLKECKALQ KISLHDNPISMDQFQQLEGFQEFEERRKRKFDKQIDSNVMISSKGLDEGIDL
XP_015579324.1	RcPIRL8	MEGEDSNSNTINITVKFSGRSIPISVSLNSTVRDLKCLLQPLTNVLPRGQKLICKGRVLTDTMTLMQSELTNGVKIMLVASQGLHQGVIPDEVWACGILTRVLD VSNNCIQDIPTKISSLSSMQKLILNGNGMSDESIQWEGFTFLKHLTILSLNRNHLSILPSELGALSSLRQLHVSNNKLNCLPVEIGLLTQLEILRANNNRICSLPASI GNCKSLVEVDLSSNLLIDLPESFGNLHNLKAVQLGNNGLKSLPSTLFKMCLQLSTLDLHNTEITTDMLRQFEGWEAFDDRRRLKHQKQLDFRVVGSAEFDEG ADKN
XP_002511324.1	RcPIRL9	MEPNPKSFPILSYVMARLPSFGPKSSSSETSFDIEQPPPPRAPSDPSASQTPITSQLPHLTDPKLLASMTRAISDVSQTRSVLQTLGPRPDHETVDNARIKLAEIESD LSKQLEEIVLSPRPAEVERLEWRSHLADKEQECRKSAEKEKNLCKMVLQLDEMHAEYDRMLKDAEKRLVQIYERAERGEDEDNHKDNEEVNEEVVGIMKE ASGRVLERVDLSNRRLRFLPEAFCRISGLKVLDLSNNQLEVIPDSIAGLENLDELNLASNLLEALPDFIGLLVNLKVLNVSSNKLESLPDSISHCRSLLELDVSFN RLTYLPTNIGYELVNVKRLSIQLNKIRSLPTSIGEMRSLQHLDAHFNELQGLPLSFGRLINLEILKLSSNFSDLKELPDTLGDLTNLKELDLSNNQIETLPDSFGRL DNLTKLNLDQNPLILPPPEVVKEGVEAVKIFMAKRWLDILVEEERKSMVEVQEQAQSGWLTRSTSWLKSYAANVTENVSEYLSPRSRSPRDSYLNQQL

Table 3-2. Oligonucleotides used in this study

Oligonucleotide Name*	Sequence**
ProPIRL1-F (-966)	AAAAAGCAGGCTCCGACACTTCACACGCAGACCATTTCTC
ProPIRL1-R (+3)	AGAAAGCTGGGTAGACACTCATTGTTGGGAGCTTGATGG
ProPIRL2-F (-2020)	AAAAAGCAGGCTCCGACACTGAATCCGTGTTATGGTTGTTAT
ProPIRL2-R (+3)	AGAAAGCTGGGTAGACACTCATGGTTTTTGTGATTATTAGTC
ProPIRL3-F (-921)	AAAAAGCAGGCTCCGACACTATTCTCCGGCAAGAAACCTT
ProPIRL3-R (+3)	AGAAAGCTGGGTAGACACTCATTCTCAATGAGATTGAAGATGAGAGC
ProPIRL4-F (-1080)	AAAAAGCAGGCTCCGACACTCACATGGCGTTTTCCTCTCT
ProPIRL4-R (+3)	AGAAAGCTGGGTAGACACTCATTACAAAATTTGGAAGAAACGAAAAG
ProPIRL5-F (-2198)	AAAAAGCAGGCTCCGACACTGCTCTTTGGTTACAGGGATG
ProPIRL5-R (+3)	AGAAAGCTGGGTAGACACTCATTTTCTACAAAATCAAAATTCAC
ProPIRL6-F (-2105)	AAAAAGCAGGCTCCGACACTACAGAACACCTGACATTAACTA
ProPIRL6-R (+3)	AGAAAGCTGGGTAGACACTCATCTTTCACACTATCTATATATA
ProPIRL7-F (-1999)	AAAAAGCAGGCTCCGACACTCCTATTTATCATGAAATTTGGGT
ProPIRL7-R (+3)	AGAAAGCTGGGTAGACACTCATCGTTTTATGTGTGTTTGTAT
ProPIRL8-F (-2098)	AAAAAGCAGGCTCCGACACTCGTAGTACTATGTTTTTCAGCT
ProPIRL8-R (+3)	AGAAAGCTGGGTAGACACTCATATCTTCCTATGTGTATGTG
ProPIRL9-F (-2073)	AAAAAGCAGGCTCCGACACTGGGAAGAGAAAGATCACTGG
ProPIRL9-R (+3)	AGAAAGCTGGGTAGACACTCATTGTTTTCGTTAAGCTTCGG

*The A of the translational initiation codon is designated +1.

**Underlines indicate regions corresponding to partial *att*B1 and *att*B2 sequences (12 bp).

Results

Phylogenetic analysis shows a relationship between *A. thaliana* PIRLs and PIRLs found in other species

Phylogenetic analysis of amino acid sequences from *A. thaliana* (PIRL), *Brassica rapa* (BrPIRL), *Capsella rubella* (CrPIRL), *Oryza sativa* (OsPIRL), *Hibiscus syriacus* (HsPIRL), *Zea mays* (ZmPIRL), *and Ricinus communis* (RcPIRL) showed that, the PIRLs from *A. thaliana* showed some similarity to those from other plants. The phylogenetic tree revealed that the phylogenetic relationships between and among species were clustered into six groups (Fig. 3-1A). In group I, PIRL4 and PIRL5 formed a cluster with CrPIRL4 and CrPIRL5, with bootstrap values of 93 and 87, respectively. The highest number of clusters was found in group III, where PIRL6 formed a cluster with BrPIRL6, and PIRL7 and PIRL8 formed a cluster with CrPIRL7 and CrPIRL8, respectively. Group IV contained PIRL2 and PIRL3, which formed a cluster with CrPIRL2 and CrPIRL3. Finally, PIRL1 and PIRL9 formed a cluster with BrPIRL1 and CrPIRL9, and these were grouped together into Group V. Next, the author predicted the number of LRR in each *A. thaliana* PIRL (Fig. 3-1B and Table 3-3). All PIRLs were found to contain the defining LRR; PIRL4 and PIRL5 contained the highest number (11) of LRRs, while PIRL1, PIRL2, PIRL3, PIRL6, PIRL7, PIRL8, and PIRL9 all showed 10 LRRs (Fig. 3-1B and Table 3-3).

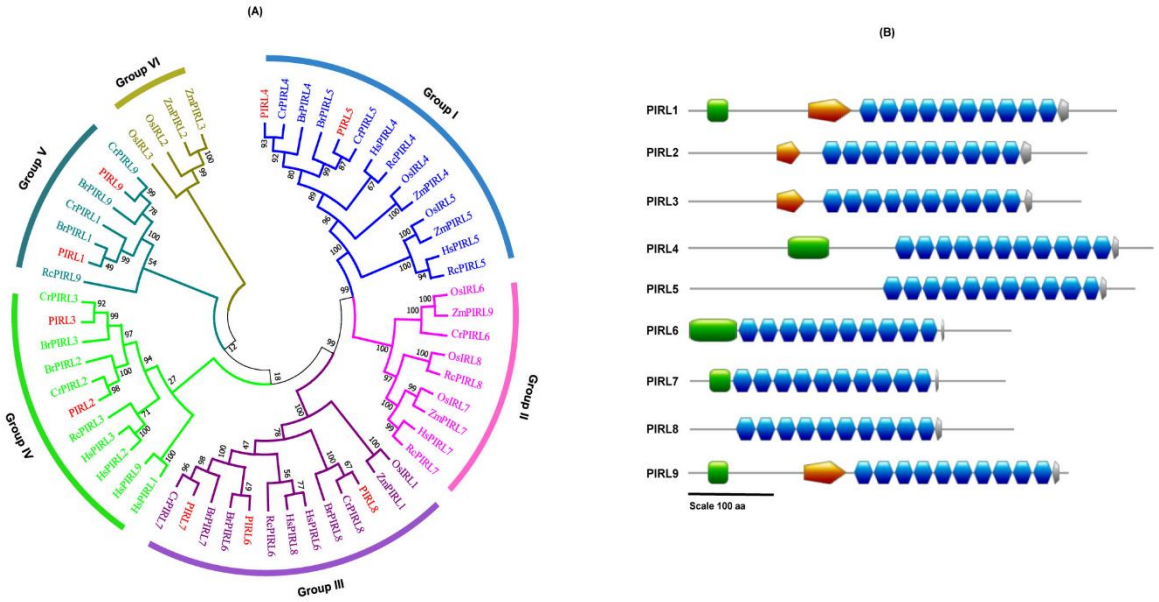

Fig. 3-1. **Phylogenetic tree of *A. thaliana* PIRLs including homologous PIRLs from other plants as well as the domain structure of the nine *A. thaliana* PIRLs**. (A) An unrooted phylogenetic tree was created using the full-length protein sequences of the nine *A. thaliana* PIRLs and their homologs found in other plants. Group I, II, III, IV, V, and VI are denoted by blue, fuchsia, purple, lime, teal, and olive, respectively, while PIRLs from *A. thaliana* are indicated in red. The prefixes Br, Cr, Os, Hs, Zm, and Rc were used to designate *Brassica rapa*, *Capsella rubella*, *Oryza sativa*, *Hibiscus syriacus*, *Zea mays*, and *Ricinus communis*, respectively. BrPIRLs, CrPIRLs, HsPIRLs, ZmPIRLs, and RcPIRLs were numbered according to their registered names in the NCBI database. (B) Domain structure of the nine *A. thaliana* PIRLs. The following scheme was used to indicate domains: green squares represent disordered regions; orange horizontal pentagons indicate coiled coil regions; blue hexagons indicate LRR; gray horizontal pentagons indicate the GVYW.

Table 3-3. Predicted domain of PIRLs in *A. thaliana*

Gene name	Protein length (aa)	Domain name	Position of domain (aa)
PIRL1	506	LRR1	203-225
		LRR2	226-249
		LRR3	251-272
		LRR4	273-295
		LRR5	297-319
		LRR6	320-342
		LRR7	344-364
		LRR8	365-389
		LRR9	390-412
		LRR10	414-436
		Region (Disordered)	24-48
		Coiled coil	143-193
		GVYW motif	437-449
PIRL2	471	LRR1	159-182
		LRR2	183-205
		LRR3	206-229
		LRR4	231-251
		LRR5	253-275
		LRR6	276-298
		LRR7	300-321
		LRR8	324-346
		LRR9	347-369
		LRR10	371-392
		Coiled coil	106-133
		GVYW motif	393-405
PIRL3	464	LRR1	160-183
		LRR2	184-206
		LRR3	207-230
		LRR4	232-252
		LRR5	254-275
		LRR6	276-299
		LRR7	301-322
		LRR8	323-347
		LRR9	348-370
		LRR10	372-393
		Coiled coil	106-138
		GVYW motif	398-406
PIRL4	549	LRR1	245-268
		LRR2	269-291
		LRR3	293-313
		LRR4	314-337
		LRR5	339-360
		LRR6	362-383
		LRR7	384-406
		LRR8	407-430
		LRR9	432-454
		LRR10	455-476
		LRR11	478-500
		Region (Disordered)	119-167
		GVYW motif	501-508
PIRL5	526	LRR1	229-252
		LRR2	253-275
		LRR3	276-297
		LRR4	298-321
		LRR5	323-344
		LRR6	346-367
		LRR7	368-390
		LRR8	391-414

Table 3-3: Continued

		LRR9	416-437
		LRR10	438-463
		LRR11	465-484
		GVYW motif	485-492
PIRL6	380	LRR1	59-82
		LRR2	83-105
		LRR3	107-129
		LRR4	130-152
		LRR5	154-176
		LRR6	177-199
		LRR7	201-222
		LRR8	223-247
		LRR9	248-271
		LRR10	273-293
		Region (Disordered)	1-57
		GVYW motif	298-301
PIRL7	373	LRR1	52-75
		LRR2	76-98
		LRR3	100-122
		LRR4	123-145
		LRR5	147-169
		LRR6	170-192
		LRR7	194-215
		LRR8	216-240
		LRR9	241-264
		LRR10	266-286
		Region (Disordered)	25-49
		GVYW motif	291-294
PIRL8	383	LRR1	56-79
		LRR2	80-102
		LRR3	104-126
		LRR4	127-149
		LRR5	151-173
		LRR6	174-197
		LRR7	199-219
		LRR8	221-244
		LRR9	245-268
		LRR10	270-290
		GVYW motif	291-298
PIRL9	449	LRR1	197-219
		LRR2	220-243
		LRR3	245-266
		LRR4	267-289
		LRR5	291-312
		LRR6	313-336
		LRR7	338-359
		LRR8	360-383
		LRR9	384-406
		LRR10	408-430
		Region (Disordered)	25-48
		Coiled coil	138-187
		GVYW motif	431-438

PIRL expression in different vegetative tissues in *A. thaliana*

The author subjected T2 or T3 plants from ProPIRL:GUS transgenic lines to histochemical GUS staining at different developmental stages. As shown in Fig. 3-2, seedlings (1-, 4-, 8-, and 16-DAG) exhibited different expression patterns in their vegetative organs. For *PIRL1*, GUS expression was observed at the junction between the root and hypocotyl at 4-DAG, at the primary root tip and in the differentiated region of the primary and secondary roots at 8-DAG, and in the shoot apex at 16-DAG (Fig. 3-2A). For *PIRL2*, the author observed unique expression in root hair, and while lower expression was observed in the vascular tissues of the primary and secondary roots from 1- to 8-DAG, the author also observed moderate expression in leaves and strong expression in stipules at 16-DAG (Fig. 3-2B). *PIRL3*, *PIRL4*, *PIRL7*, and *PIRL9* showed two similar trends: for each of these *PIRL* genes, the author observed GUS expression in root (1- to 8-DAG) but faint or no signal in aboveground organs at 16-DAG (Fig. 3-2C, Fig. 3-2D, Fig. 3-2G and Fig. 3-2I). For *PIRL5*, the author observed expression in the root tip and in the vascular tissue of the first and secondary roots at 4- and 8-DAG, but again almost no expression in aboveground organs at 16-DAG (Fig. 3-2E). *PIRL8* showed GUS expression in roots (8-DAG), the shoot apex region, and young leaves (Fig. 3-2H). The author did not observe considerable expression of *PIRL6* in any vegetative organs (Fig. 3-2F). All the results of GUS staining experiments are summarized in Table 3-4.

PIRLs are expressed in various reproductive tissues in *A. thaliana*

The author subjected the flowers of 40-DAG transgenic plants to GUS staining. For *PIRL1*, GUS was weakly expressed in petals and filaments, but was strongly expressed in anthers and pollen (Fig. 3-3A). Expression was also detected in the pollen tube (Fig. 3-3A). For *PIRL2*, expression was strong in flower buds but was lower in sepals, petals, filaments, and stigmas of open flowers (Fig. 3-3B). The author observed distinct expression of *PIRL3* in anthers and pollen, but not in the pollen tube (Fig. 3-3C). Next, for *PIRL4*, the author did not find any expression in any floral organs whatsoever (Fig. 3-3D). Similarly, *PIRL5* was detected very weakly and only in anthers (Fig. 3-3E). However, clear GUS expression was detected in both pollen and pollen tubes for both *PIRL*6 and *PIRL*7 (Fig. 3-3F and Fig. 3-3G). GUS activity was not observed in any floral organ for either *PIRL8* or *PIRL9* (Fig. 3-3H and Fig. 3-3I). All GUS staining results are summarized in Table 3-4.

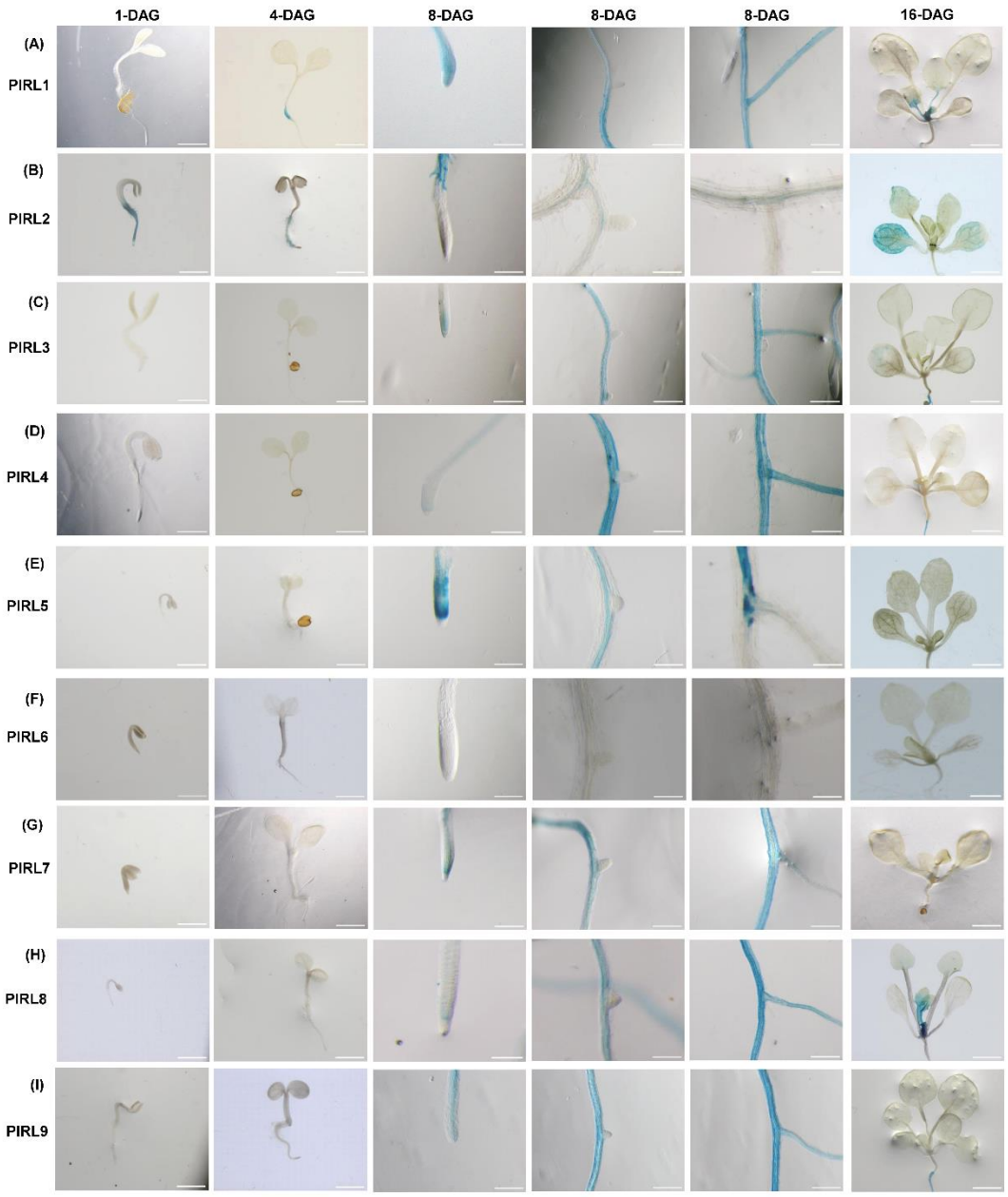

Fig. 3-2. Expression patterns of *PIRL* genes in the vegetative tissues of *A. thaliana*. (A) ProPIRL1: GUS, (B) ProPIRL2:GUS, (C) ProPIRL3:GUS, (D) ProPIRL4:GUS, (E) ProPIRL5:GUS, (F) ProPIRL6: GUS, (G) ProPIRL7:GUS, (H) ProPIRL8:GUS, (I) ProPIRL9:GUS. GUS staining is shown for 1-DAG seedlings, 4-DAG seedlings, 8-DAG primary root tips (left), 8-DAG initiated lateral roots (center), 8- DAG differentiated roots (right), and 16-DAG aboveground organs of transgenic *A. thaliana*. Scale bars = 1 mm.

Table 3-4. Summarized results of promoter:GUS assay of *PIRLs* in *A. thaliana*

	Root			Shoot				Flower							
	Primary root tip	Root hair	Differentiated root	Shoot apex	Stipule	Young leaf	Mature leaf	Sepal	Petal	Filament	Anther	Pollen	Pollen tube	Stigma	Ovule
PIRL1	++	−	++	++	−	+	−	+	+	+	++	++	++	++	−
PIRL2	−	++	+	−	++	−	++	+	+	+	++	−	−	+	−
PIRL3	+	−	++	−	−	−	−	−	−	−	++	++	−	+	−
PIRL4	++	−	++	−	−	−	−	−	−	−	−	−	−	−	−
PIRL5	++	−	+	−	−	−	−	−	−	−	+	−	−	−	−
PIRL6	−	−	−	−	−	−	−	−	−	−	+	++	++	+	+
PIRL7	+	−	++	−	−	−	−	−	−	−	+	++	++	++	−
PIRL8	+	−	++	++	−	−	−	−	−	−	−	−	−	−	−
PIRL9	+	−	++	−	−	−	−	−	−	−	−	−	−	−	−

− Not stained
\+ Weakly stained
++ Strongly stained

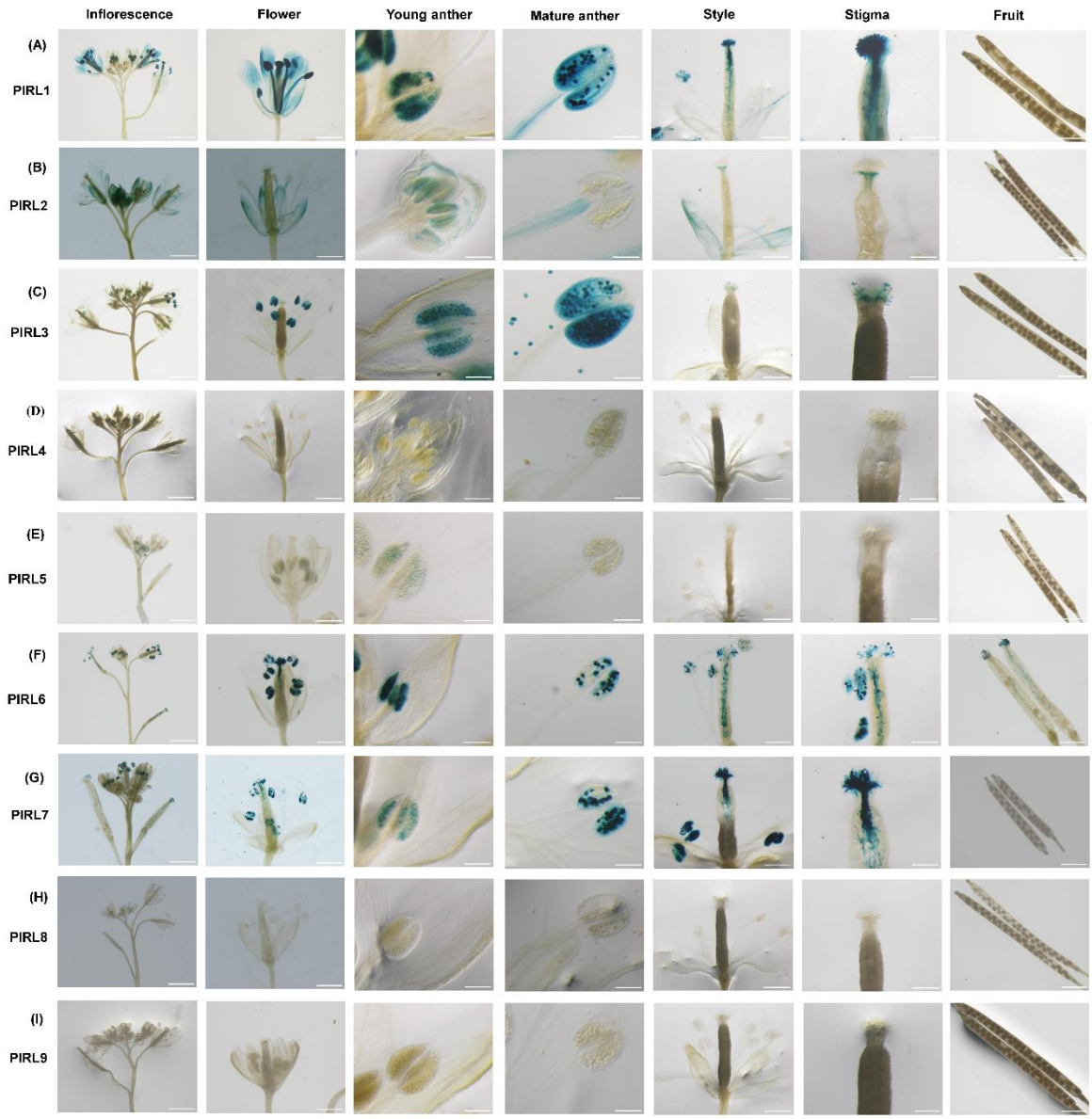

Fig. 3-3. Expression patterns of *PIRL* genes in the floral organs of *A. thaliana*. (A) ProPIRL1:GUS, (B) ProPIRL2:GUS, (C) ProPIRL3:GUS, (D) ProPIRL4:GUS, (E) ProPIRL5:GUS, (F) ProPIRL6:GUS, (G) ProPIRL7:GUS, (H) ProPIRL8:GUS, (I) ProPIRL9:GUS. GUS staining is shown for the inflorescence, flower, young anther, mature anther, style, stigma, and fruit tissue of 40-DAG transgenic *A. thaliana*. Scale bars = 1 mm.

In silico expression and co-expression analysis of *PIRLs*

The author generated a heat map that used microarray datasets of *PIRL* genes sourced from the Arabidopsis eFP browser (Fig. 3-4A). This heat map analysis showed that *PIRL6* was specifically expressed in pollen (Fig. 3-4A), that *PIRL1* and *PIRL3* were expressed strongly in pollen and moderately in vegetative organs (Fig. 3-4A), and that *PIRL5* was expressed in pollen and roots (Fig. 3-4A). This analysis also showed that both *PIRL4* and *PIRL9* were expressed in a variety of organs, although *PIRL4* was not expressed in pollen (Fig. 3-4A). Interestingly, weak expression in root tissue was observed for *PIRL8* (Fig. 3-4A). Moreover, a microarray study using visual expression of *PIRL* genes during developmental stages revealed that *PIRL1* and *PIRL3* were significantly expressed in floral organs, specifically in mature pollen rather than vegetative organs (Fig. 3-5). According to the microarray expression developmental map, *PIRL4* and *PIRL9* were expressed in a number of regions, while no expression was found for *PIRL4* in pollen (Fig. 3-5). *PIRL5* and *PIRL6* showed vigorous expression in mature pollen, whereas root-specific expression was also observed for *PIRL4* and *PIRL8,* respectively. The microarray datasets contained no expression values for *PIRL2* and *PIRL7*. Further, to identify the functional relationship between *PIRLs* and other genes, the author generated a co-expression network using the ATTED-II (ath-m.c9-0 platform) (Fig. 3-4B). Of the nine *PIRL* genes, only *PIRL1* and *PIRL3* were found to co-express with each other. Furthermore, *PIRL1* expression was correlated with the expression of VQ-motif containing protein 9 (VQ9, At1g78310), which is a class of transcription factor (Liu et al. 2020), and zinc finger nuclease 2 (ZFN2, AT2G32930) (Fig. 3-4B). The author also found that *PIRL3* co-expressed strongly with a member of the Type One Protein Phosphatase family known as TOPP8 (AT5G27840), as well as IBR5 (AT2G04550) and an F-box domain-containing protein (At3g17710) (Fig. 3-4B). Expression of *PIRL4* was found to strongly correlate with expression of TMK1 (AT1G66150) (Fig. 3-4B), while *PIRL5* was weakly co-expressed with SK32 (AT4G00720) and CYP721A1 (AT1G75130) (Fig. 3-4B). *PIRL6* was co-expressed with GLOX1 (AT1G67290) and PAB3 (AT1G22760) (Fig. 3-4B), two genes whose expressions are known to have been restricted to the anther and tapetum (Phan et al. 2011). *PIRL8* showed co-expression with IMMUNE ASSOCIATED NUCLEOTIDE BINDING 4 (IAN4, At1g33900) and a member of the Alpha Expansion gene family (EXPA17, AT4G01630) (Fig. 3-4B). The expression of *EXPA17* is root-specific and it is vital for lateral root formation (Lee and Kim 2013). Finally, *PIRL9* was found to co-express with UDP-DEPENDENT GLYCOSYLTRANSFERASE 76B1 (UGT76B1, AT3G11340) and At4g02940 (Fig. 3-4B). Co-expression data was not available for *PIRL2* and *PIRL7.*

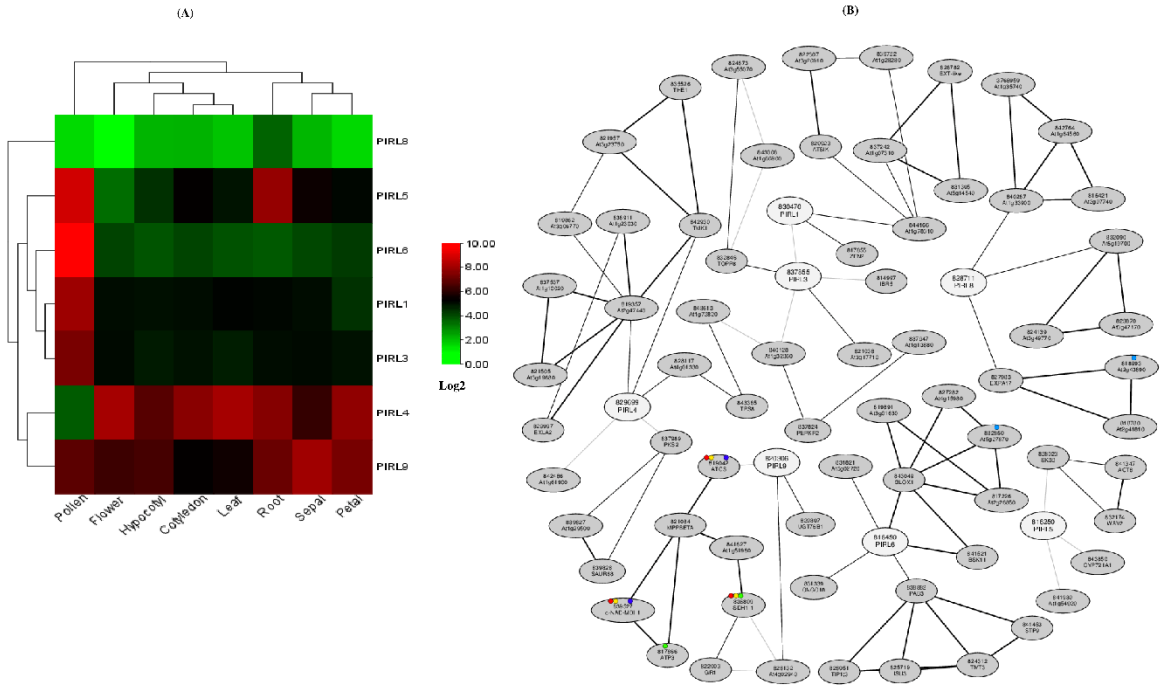

Fig. 3-4. **In silico gene expression and co-expression analyses of *PIRL* genes.** (A) Gene expression (Log2 transformed) heat map of *A. thaliana PIRL* genes at different developmental stages. *PIRLs* are shown on the right side, and tissues are indicated at the bottom. Red indicates a higher level of gene expression, while green indicates lower expression. (B) Co-expression networks were generated by the ATTED-II using *PIRL* as query genes. Red, yellow, blue, sky-blue, and green circles indicate groups of genes involved in different metabolic pathways.

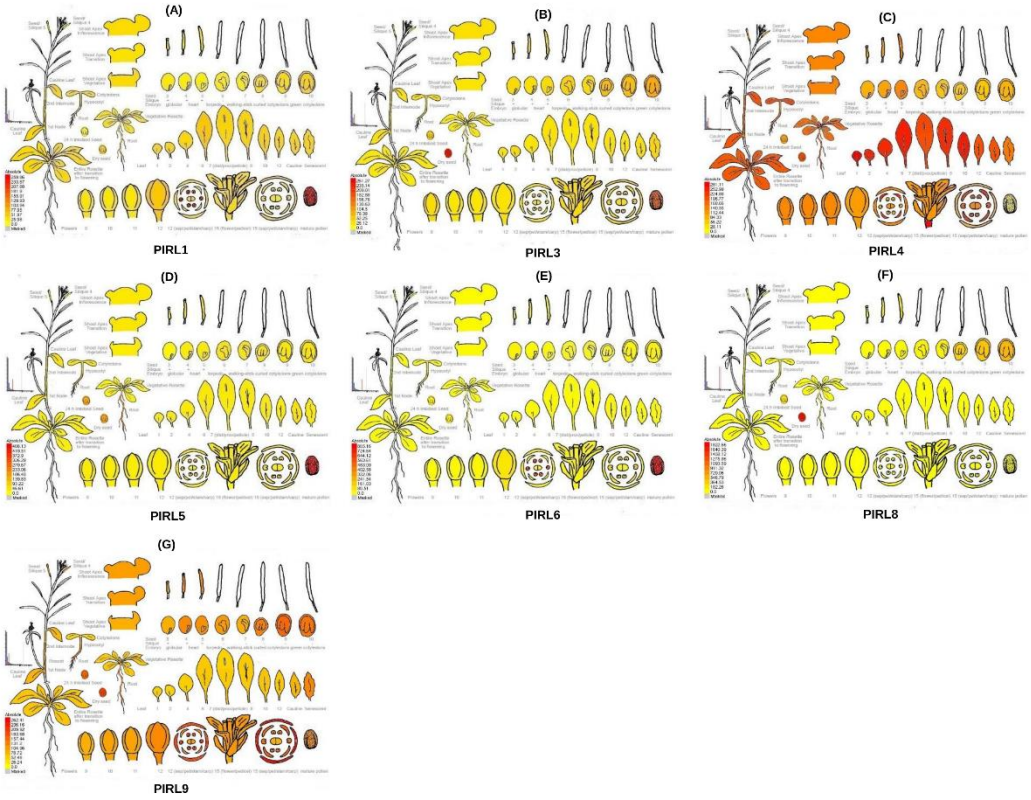

Fig. 3-5. Developmental map showing tissue specific microarray expression of *A. thaliana PIRL* genes. (A) PIRL1, (B) PIRL3, (C) PIRL4, (D) PIRL5, (E) PIRL6, (F) PIRL8, (G) PIRL9.

Discussion

LRR proteins are found in many plant species, where they perform important biological functions linked to growth and development. For instance, many proteins from the LRR-receptor-like kinases (RLKs) and related-receptor-like proteins (RLPs) families play crucial roles in plant growth and development and in defense-related pathways (Jeong et al. 1999; Lease et al. 1998; Shiu and Bleecker 2001b). In *A. thaliana*, nine *PIRLs* have been identified, some of which have been previously examined for functional roles in developmental signaling. In the present study, the author used promoter:GUS assays and in silico approaches to analyze the amino acid sequences and detailed expression patterns of nine *PIRLs* found in *A. thaliana*. Phylogenetic analysis revealed the relationships of the *A. thaliana* PIRL proteins with other plants PIRLs and resolved all sequences into six groups (Fig. 3-1A). Each *A. thaliana* PIRL was found to be close in sequence to one of the PIRLs found in *C. rubella* (CrPIRL) and others from *B. rapa* (BrPIRL). *A. thaliana* PIRL1 and PIRL9 belong to Group V, a group that also contains PIRLs from *C. rubella* and *B. rapa*. *A. thaliana* PIRL4 and PIRL5 belong to a clade that includes PIRL4 and PIRL5 from both *C. rubella* and *B. rapa*, designated here as Group I. This group also contained PIRL4 and PIRL5 from

O. sativa, *Z. mays*, *H. syriacus*, and *R. communis*. PIRL6, PIRL7, and PIRL8 from *A. thaliana*, *C. rubella* and *B. rapa* all belong to Group III, a group that also includes PIRL1 from *O. sativa* and *Z. mays*. PIRL2 and PIRL3 from *A. thaliana*, *C. rubella*, and *B. rapa* belong to the same clade, designated here as Group IV. Interestingly, Groups IV and V did not include PIRLs found in *O. sativa* and *Z. mays*. Group VI contains PIRLs only from rice corresponding to *PIRL1*, *PIRL9*, *PIRL2* and *PIRL3*, and there is no *PIRL* corresponding to *OsIRL2* and *OsIRL3*. *PIRL1* and *PIRL9* have been reported to be essential for pollen development (Forsthoefel et al. 2010). Although the function of *OsIRL2* and *OsIRL3* is not yet known, they may be redundantly involved in pollen development like *PIRL1* and *PIRL9* because they are most similar to *PIRL1* and *PIRL9* among *OsIRLs*, and their expression was shown in stamens (You et al. 2010). *OsIRL2* and *OsIRL3* may have diverged and acquired additional functions in rice. For example, expression of *OsIRL2* and *OsIRL3* is also shown in endosperm (You et al. 2010). Since the *osirl3* mutant exhibited a normal phenotype, analysis of *osirl2*;*osirl3* double mutant will be a clue to clarity their function. Analysis of the domain organizations by Uniprot showed that the number of LRRs present in *A. thaliana* PIRLs is 10 or 11 (Fig. 3-1B and Table 3-3). The number of LRRs found in PIRL1, PIRL2, PIRL3, PIRL6, PIRL7, PIRL8, and PIRL9 was one more than reported by Forsthoefel et al. (2005). This difference may be due to differences in the length of the first LRR between the previous prediction and the Uniprot prediction used in this study.

In silico analysis revealed that *PIRL1*, *PIRL3*, and *PIRL6* were preferentially expressed in pollen (Fig. 3-4A). Microarray developmental map, RNA-seq (Winter et al. 2007; Loraine et al. 2013) and promoter:GUS assays (Fig. 3-5 and Fig. 3-3) also indicated strong expression of *PIRL1*, *PIRL3*, and *PIRL6* in pollen. These results are consistent with reports that have demonstrated that *PIRL1* and *PIRL9* are vital for the differentiation of microspores into pollen (Forsthoefel et al. 2010). In addition, recent studies have also shown that *pirl2;pirl3* double mutant generated a wide range of abnormal pollen morphologies (Forsthoefel et al. 2013). Moreover, promoter:GUS assay of *PIRL6* showed expression also in the ovule (Fig. 3-3F), a finding that is consistent with a previous result that showed that *PIRL6* was essential for both male and female gametogenesis processes in *A. thaliana* (Forsthoefel et al. 2018). Forsthoefel et al. (2018) reported abundant functional transcript in flowers and a small amount of non-functional transcript by alternative splicing in leaf and root. These and our promoter:GUS results indicated transcriptional and post-transcriptional regulation of *PIRL6*.

Next, the co-expression analysis showed that the expression of *PIRL1* and *PIRL3* are correlated with each other and that *PIRL1* expression is also associated with the expression of *VQ9* and *ZFN2* (Fig. 3-4B). The essential role of VQ proteins in vegetative plant growth, differentiation, and seed development has been previously described (Liu et al. 2020). The relative expression of *VQ9* has also been reported in roots by Hu et al. (2013), a finding that is consistent with the observed

expression of *PIRL1* in roots. Taken together, these findings suggest a contribution of *PIRL1* to root development in addition to its role in pollen formation. *PIRL1* and *PIL9* are closely related gene pairs, and *pirl1;pirl9* double knockout plants (*pirl1* -/-, *pirl9* -/-) were not established due to the developmental defect of *pirl1;pirl9* microspore (*pirl1* -, *pirl9* -) into viable pollen (Forsthoefel et al. 2010). Analysis of double mutants using weaker alleles may reveal their function in the development of vegetative organs, including roots. Next, the author also identified *TOPP8* and *IBR5* as genes that were co-expressed with *PIRL3*. *TOPP8* is also known as *ATUNIS2* (*AUN2*) and plays a vital role in pollen germination and pollen tube growth (Franck et al. 2018). Pollen- and root-specific expression of *AUN2* has also been reported by Franck et al. (2018), who used a microarray analysis that showed a pattern of expression resembling that of *PIRL3*, further suggesting their functional similarity. The author also found that *PIRL6* expression was strongly correlated with the expression of genes coding for glyoxal-oxidase-related protein (GLOX1) and PAB3. *GLOX1* was reported to be important for pollen development; Phan et al. (2011) found *GLOX1* promoter-driven GUS expression within anthers of floral buds as well as strong GUS activity in mature and released pollen grains. Belostotsky (2003) also described tapetum and pollen-specific expression of *PAB3* after performing promoter:GUS assays in *A. thaliana.* These results support the possibility that the function of *PIRL6* in pollen development is related to *GLOX1* and *PAB3*. Although no expression values were available in the database for *PIRL7*, the promoter:GUS assay revealed clear expression of *PIRL7* both in pollen and in the pollen tube (Fig. 3-3G), suggesting that *PIRL7* plays a role in pollen development. The promoter:GUS assay of *PIRL2* showed unambiguous staining of filaments (Fig. 3-3B). Therefore, the requirement of *PIRL2* for pollen development (Forsthoefel et al. 2013) may be exerted in the filament. The author obtained root-specific promoter:GUS expression for *PIRL4* (Fig. 3-2D). As shown in Fig. 3-4, co-expression analysis revealed that *PIRL4* was co-expressed with LRR-RLK TMK1 (Chang et al. 1992), which has been found to be expressed in roots by RT-PCR and promoter:GUS assays (Dai et al. 2013). Dai et al. (2013) also reported that the root lengths of *tmk1; tmk4* double mutants were approximately one-third of that of the wild type. The biological functions of *PIRL4* remain unknown; however, co-expression of *PIRL4* and *TMK1* in roots suggests that *PIRL4* may be involved in the growth and development of roots. Furthermore, the author also observed promoter:GUS expression of *PIRL5*, *PIRL8*, and *PIRL9* in the root apical region, as well as in the primary and secondary roots (Fig. 3-2E, Fig. 3-2H, and Fig. 3-2I). According to the heat map and microarray developmental map, *PIRL5*, *PIRL8*, and *PIRL9* are also known to be expressed in roots (Fig. 3-4A and Fig. 3-5). In addition, the author found that *PIRL8* showed co-expression with *EXPA17*; a previous study by Lee and Kim (2013), who used the promoter:GUS of *EXPA17* and recorded its expression in lateral root and lateral root primordia. Therefore, they suggested that *EXPA17* may be required to promote lateral root formation during auxin response. Together, these findings signify that *PIRL8* may have root-specific functions.

In this study, the author investigated the detailed expression patterns of nine *A. thaliana PIRL* genes at different developmental stages. Promoter:GUS assay showed that most *PIRLs* were expressed in roots and in the vasculature of the primary and lateral roots. In addition, the author observed that some *PIRLs* were strongly expressed in floral organs, suggesting their possible biological function to regulate the growth and development of these organs. Moreover, co-expression network analysis indicated that functionally similar *PIRLs* are expressed simultaneously. Therefore, these results will be helpful for future tissue-specific expression analyses of other LRR proteins and may provide useful information to improve our understanding of their biological function.

Chapter 4

Proposed conclusions

A. thaliana is a model organism used to investigate the roles of various essential plant genes. The author revealed in the **Chapter 2** of this thesis that *bgl23-D*, a novel dominant mutation of *ATCSLD5*, affects the cytokinesis of guard mother cells and exine formation in *A. thaliana.* This study also suggested the essential role of plant intracellular Ras-group-related leucine-rich repeat (LRR) proteins (PIRLs) in the vegetative and reproductive organs of *A. thaliana* in the **Chapter 3** using the promoter:GUS assay. The author proposes the conclusions of this thesis as follows:

(i) *bgl23-D* is a novel dominant mutation allele of *ATCSLD5.*

bgl23-D mutant (dominant mutant) was isolated from ethylmethanesulfonate (EMS) mutagenized seeds of *A. thaliana* L*er* by obtaining bagel-shaped stomata using bright-field microscope. Whole genome sequencing and Mitsucal computer system revealed a C to T substitution at the position of 3,220 bp in the AT1G02730 encoding *A. thaliana cellulose synthase-like D5* (*ATCSLD5*). Transgenic plants established by inserting a construct of own promoter-driven *ATCSLD5* cDNA containing C3220T (C2989T in the cDNA) substitution (*ProBGL23:bgl23-D* construct) into WT-Col showed similar bagel-shaped stomata as seen in the *bgl23-D* mutant. It was concluded that *bgl23-D* was a novel dominant negative allele of *ATCSLD5*.

(ii) *bgl23-D* affects the cytokinesis of guard mother cells.

By ectopic expression of *bgl23-D* cDNA with promoter of stomata-lineage genes, a variety of defects were observed in the cytokinesis of guard mother cells. The severity of these defects was more prominent when *bgl23-D* cDNA was expressed by the promoter of FAMA gene.

(iii) *bgl23-D* disrupts pollen shape and exine structure.

Expression of *bgl23-D* with the promoters of tapetum- or anther-specific genes gave rise to slightly shrunken to severely shrunken pollen grains. The characteristic reticulate shape of exine was also lost partially in transgenic *A. thaliana. bgl23-D* disrupted the shape of microspores during the onset of pollen mitosis I (PMI) and exhibited severely shrunken microspores after pollen mitosis I (PMI) at the bicelluar stage.

(iv) Leaf growth was enhanced due to *bgl23-D* mutation.

Enhanced leaf growth in the transgenic *A. thaliana* was observed in the *bgl23-D* mutant. Transgenic plant expressing *bgl23-D* with the promoters of stomata-lineage genes showed larger epidermal cells. The *bgl23-D* mutant will be a useful genetic tool to modify the plant growth**.**

(v) Plant intracellular Ras-group-related leucine-rich repeat (LRR) proteins (PIRLs) are important for vegetative and reproductive organs growth.

The promoter:GUS assay revealed that *PIRL2*, *PIRL4*, *PIRL8*, and *PIRL9* are expressed in the root region, while *PIRL1*, *PIRL3, PIRL6*, and *PIRL7* are highly expressed in the reproductive organs of *A. thaliana*. *PIRL2* showed unique expression in root hair and stipule, while *PIRL4*, *PIRL8*, and *PIRL9* are expressed in primary and secondary roots. *PIRL1* and *PIRL3* exhibited distinct expression in anthers and pollen, while *PIRL6* and *PIRL7* showed expression in pollen and pollen tubes. Expression analysis will be useful in understanding the function of the genes in specific region of plant.

References

Aboulela M, Nakagawa T, Oshima A, et al (2018) The Arabidopsis COPII components, AtSEC23A and AtSEC23D, are essential for pollen wall development and exine patterning. J Exp Bot 69:1615–1633

Aboulela M, Tanaka Y, Nishimura K, et al (2017) Development of an R4 dual-site (R4DS) gateway cloning system enabling the efficient simultaneous cloning of two desired sets of promoters and open reading frames in a binary vector for plant research. PLoS One 12:e0177889

Aklilu E (2021) Review on forward and reverse genetics in plant breeding. All Life 14:127–135

Al-Shehbaz IA, O'Kane SLJ (2002) Taxonomy and phylogeny of Arabidopsis (brassicaceae). Arab B 1:e0001

Ali Khan A, Raess M, de Angelis MH (2021) Moving forward with forward genetics: A summary of the INFRAFRONTIER Forward Genetics Panel Discussion [version 1; peer review: 1 approved, 2 approved with reservations]. F1000Research 10

Alonso-Blanco C, Koornneef M (2000) Naturally occurring variation in Arabidopsis: an underexploited resource for plant genetics. Trends Plant Sci 5:22–29

Ariizumi T, Toriyama K (2011) Genetic regulation of sporopollenin synthesis and pollen exine development. Annu Rev Plant Biol 62:437–460

Baker NR (2008) Chlorophyll Fluorescence: A Probe of Photosynthesis In Vivo. Annu Rev Plant Biol 59:89–113

Baumberger N, Ringli C, Keller B (2001) The chimeric leucine-rich repeat/extensin cell wall protein LRX1 is required for root hair morphogenesis in *Arabidopsis thaliana*. Genes Dev 15:1128–1139

Belostotsky DA (2003) Unexpected complexity of poly (A)-binding protein gene families in flowering plants: three conserved lineages that are at least 200 million years old and possible auto-and cross-regulation. Genetics 163:311–319

Bennett MD, Leitch IJ, Price HJ, Johnston JS (2003) Comparisons with Caenorhabditis (approximately 100 Mb) and Drosophila (approximately 175 Mb) using flow cytometry show genome size in Arabidopsis to be approximately 157 Mb and thus approximately 25% larger than the Arabidopsis genome initiative estimate. Ann Bot 91:547–557

Berger D, Altmann T (2000) A subtilisin-like serine protease involved in the regulation of stomatal density and distribution in *Arabidopsis thaliana*. Genes Dev 14:1119–1131

Bernal AJ, Jensen JK, Harholt J, et al (2007) Disruption of *ATCSLD5* results in reduced growth, reduced xylan and homogalacturonan synthase activity and altered xylan occurrence in Arabidopsis. Plant J 52:791–802

Bernal AJ, Yoo C-M, Mutwil M, et al (2008) Functional analysis of the cellulose synthase-like genes *CSLD1*, *CSLD2*, and *CSLD4* in tip-growing Arabidopsis cells. Plant Physiol 148:1238–1253

Billah M, Sajib SA, Roy NC, et al (2020) Effects of DBD air plasma treatment on the enhancement of black gram (*Vigna mungo* L.) seed germination and growth. Arch Biochem Biophys 681:108253

Blackmore S, Wortley AH, Skvarla JJ, Rowley JR (2007) Pollen wall development in flowering plants. New Phytol 174:483–498

Busso D, Delagoutte-Busso B, Moras D (2005) Construction of a set Gateway-based destination vectors for high-throughput cloning and expression screening in *Escherichia coli.* Anal Biochem 343:313–321

Chang C, Schaller GE, Patterson SE, et al (1992) The TMK1 gene from Arabidopsis codes for a protein with structural and biochemical characteristics of a receptor protein kinase. Plant Cell 4:1263–1271

Chen C, Chen H, Zhang Y, et al (2020) TBtools: an integrative toolkit developed for interactive analyses of big biological data. Mol Plant 13:1194–1202

Chowdhury MR, Ahamed MS, Mas-ud MA, et al (2021) Stomatal development and genetic expression in *Arabidopsis thaliana* L. Heliyon 7:e07889

Claudianos C, Campbell HD (1995) The novel flightless-I gene brings together two gene families, actin-binding proteins related to gelsolin and leucine-rich-repeat proteins involved in Ras signal transduction. Mol Biol Evol 12:405–414

Condon AG, Richards RA, Farquhar GD (1987) Carbon isotope discrimination is positively correlated with grain yield and dry matter production in field-grown wheat 1. Crop Sci 27:996–1001

Cosgrove DJ (2005) Growth of the plant cell wall. Nat Rev Mol cell Biol 6:850–861

Curtis MD, Grossniklaus U (2003) A gateway cloning vector set for high-throughput functional analysis of genes in planta. Plant Physiol 133:462–469

Dai N, Wang W, Patterson SE, Bleecker AB (2013) The TMK subfamily of receptor-like kinases in Arabidopsis display an essential role in growth and a reduced sensitivity to auxin. PLoS One 8:e60990

Doblin MS, Kurek I, Jacob-Wilk D, Delmer DP (2002) Cellulose biosynthesis in plants: from genes to rosettes. Plant cell Physiol 43:1407–1420

Dong J, MacAlister CA, Bergmann DC (2009) BASL controls asymmetric cell division in *Arabidopsis*. Cell 137:1320–1330

Favery B, Ryan E, Foreman J, et al (2001) *KOJAK* encodes a cellulose synthase-like protein required for root hair cell morphogenesis in *Arabidopsis*. Genes Dev 15:79–89

Forsthoefel NR, Cutler K, Port MD, et al (2005) PIRLs: a novel class of plant intracellular leucine-rich repeat proteins. Plant cell Physiol 46:913–922

Forsthoefel NR, Dao TP, Vernon DM (2010) *PIRL1* and *PIRL9*, encoding members of a novel plant-specific family of leucine-rich repeat proteins, are essential for differentiation of microspores into pollen. Planta 232:1101–1114

Forsthoefel NR, Klag KA, McNichol SR, et al (2018) Arabidopsis PIRL6 is essential for male and female gametogenesis and is regulated by alternative splicing. Plant Physiol 178:1154–1169

Forsthoefel NR, Klag KA, Simeles BP, et al (2013) The *Arabidopsis* plant intracellular Ras-group LRR (*PIRL*) family and the value of reverse genetic analysis for identifying genes that function in gametophyte development. Plants 2:507–520

Franck CM, Westermann J, Bürssner S, et al (2018) The protein phosphatases ATUNIS1 and ATUNIS2 regulate cell wall integrity in tip-growing cells. Plant Cell 30:1906–1923

Gay NJ, Packman LC, Weldon MA, Barna JC (1991) A leucine-rich repeat peptide derived from the Drosophila Toll receptor forms extended filaments with a beta-sheet structure. FEBS Lett 291:87–91

Geisler M, Nadeau J, Sack FD (2000) Oriented asymmetric divisions that generate the stomatal spacing pattern in Arabidopsis are disrupted by the *too many mouths* mutation. Plant Cell 12:2075–2086

Gómez JF, Talle B, Wilson ZA (2015) Anther and pollen development: a conserved developmental pathway. J Integr Plant Biol 57:876–891

Gu F, Bringmann M, Combs JR, et al (2016) Arabidopsis CSLD5 functions in cell plate formation in a cell cycle-dependent manner. Plant Cell 28:1722–1737

Gu J, Zhu J, Yu Y, et al (2014) DYT 1 directly regulates the expression of *TDF1* for tapetum development and pollen wall formation in A rabidopsis. Plant J 80:1005–1013

Hara K, Kajita R, Torii KU, et al (2007) The secretory peptide gene *EPF1* enforces the stomatal one-cell-spacing rule. Genes Dev 21:1720–1725

Harholt J, Suttangkakul A, Vibe Scheller H (2010) Biosynthesis of pectin. Plant Physiol 153:384–395

Hartley JL, Temple GF, Brasch MA (2000) DNA cloning using in vitro site-specific recombination. Genome Res 10:1788–1795

Hasegawa J, Sakamoto Y, Nakagami S, et al (2016) Three-dimensional imaging of plant organs using a simple and rapid transparency technique. Plant Cell Physiol 57:462–472

Hedberg O (1957) Afroalpine vascular plants: a taxonomic revision

Hoffmann MH (2002) Biogeography of *Arabidopsis thaliana* (L.) Heynh.(Brassicaceae). J Biogeogr 29:125–134

Honys D, Reňák D, Twell D (2006) Male gametophyte development and function. Plant Biotechnol 1:209–224

Hu J, Zhu L, Zeng D, et al (2010) Identification and characterization of *NARROW ANDROLLED LEAF 1*, a novel gene regulating leaf morphology and plant architecture in rice. Plant Mol Biol 73:283–292

Hu Y, Chen L, Wang H, et al (2013) A rabidopsis transcription factor WRKY 8 functions antagonistically with its interacting partner VQ 9 to modulate salinity stress tolerance. Plant J 74:730–745

Hunt L, Gray JE (2009) The signaling peptide EPF2 controls asymmetric cell divisions during stomatal development. Curr Biol 19:864–869

Hunter CT, Kirienko DH, Sylvester AW, et al (2012) *Cellulose Synthase-Like D1* is integral to normal cell division, expansion, and leaf development in maize. Plant Physiol 158:708–724

Ishiguro S, Nishimori Y, Yamada M, et al (2010) The Arabidopsis *FLAKY POLLEN1* gene encodes a 3-hydroxy-3-methylglutaryl-coenzyme A synthase required for development of tapetum-specific organelles and fertility of pollen grains. Plant cell Physiol 51:896–911

Jeong KW, Lee Y-H, Stallcup MR (2009) Recruitment of the SWI/SNF chromatin remodeling complex to steroid hormone-regulated promoters by nuclear receptor coactivator flightless-I. J Biol Chem 284:29298–29309

Jeong S, Trotochaud AE, Clark SE (1999) The Arabidopsis *CLAVATA2* gene encodes a receptor-like protein required for the stability of the CLAVATA1 receptor-like kinase. Plant Cell 11:1925–1933

Kajava A V (1998) Structural diversity of leucine-rich repeat proteins

Katzen F (2007) Gateway® recombinational cloning: a biological operating system. Expert Opin Drug Discov 2:571–589

Kim CM, Park SH, Je B Il, et al (2007) *OsCSLD1*, a cellulose synthase-like D1 gene, is required for root hair morphogenesis in rice. Plant Physiol 143:1220–1230

Kim Y, Schumaker KS, Zhu J-K (2006) EMS Mutagenesis of *Arabidopsis* BT - Arabidopsis Protocols. In: Salinas J, Sanchez-Serrano JJ (eds). Humana Press, Totowa, NJ, pp 101–103

Kobe B, Deisenhofer J (1994) The leucine-rich repeat: a versatile binding motif. Trends Biochem Sci 19:415–421

Kobe B, Kajava A V (2001) The leucine-rich repeat as a protein recognition motif. Curr Opin Struct Biol 11:725–732

Kumar S, Stecher G, Tamura K (2016) MEGA7: molecular evolutionary genetics analysis version 7.0 for bigger datasets. Mol Biol Evol 33:1870–1874

Kusumi K (2013) Measuring stomatal density in rice. Bio-protocol 3:e753–e753

Lease K, Ingham E, Walker JC (1998) Challenges in understanding RLK function. Curr Opin Plant Biol 1:388–392

Lee HW, Kim J (2013) *EXPANSINA17* up-regulated by LBD18/ASL20 promotes lateral root formation during the auxin response. Plant Cell Physiol 54:1600–1611

Lee Y-H, Campbell HD, Stallcup MR (2004) Developmentally essential protein flightless I is a nuclear receptor coactivator with actin binding activity. Mol Cell Biol 24:2103–2117

Li M, Xiong G, Li R, et al (2009) Rice cellulose synthase-like D4 is essential for normal cell-wall biosynthesis and plant growth. Plant J 60:1055–1069

Li W, Han M, Guan K-L (2000) The leucine-rich repeat protein SUR-8 enhances MAP kinase activation and forms a complex with Ras and Raf. Genes Dev 14:895–900

Liepman AH, Wightman R, Geshi N, et al (2010) Arabidopsis–a powerful model system for plant cell wall research. Plant J 61:1107–1121

Liu C, Liu H, Zhou C, Timko MP (2020) Genome-wide identification of the VQ protein gene family of tobacco (*Nicotiana tabacum* L.) and analysis of its expression in response to phytohormones and abiotic and biotic stresses. Genes (Basel) 11:284

López-García CM, Ruíz-Herrera LF, López-Bucio JS, et al (2020) ALTERED MERISTEM PROGRAM 1 promotes growth and biomass accumulation influencing guard cell aperture and photosynthetic efficiency in Arabidopsis. Protoplasma 257:573–582

Loraine AE, McCormick S, Estrada A, et al (2013) RNA-seq of Arabidopsis pollen uncovers novel transcription and alternative splicing. Plant Physiol 162:1092–1109

Maple J, Møller SG (2007) Mutagenesis in Arabidopsis. Methods Mol Biol 362:197–206.

McHale L, Tan X, Koehl P, Michelmore RW (2006) Plant NBS-LRR proteins: adaptable guards. Genome Biol 7:1–11

Meinke DW, Cherry JM, Dean C, et al (1998) *Arabidopsis thaliana*: a model plant for genome analysis. Science 282:662,679-682

Mizuno Y, Okamoto S, Hara M, Mizoguchi T (2014) EMS mutagenesis and characterization of *Brassica rapa* mutants. Plant Biotechnol advpub

Moresco EMY, Li X, Beutler B (2013) Going forward with genetics: recent technological advances and forward genetics in mice. Am J Pathol 182:1462–1473

Morris ER, Walker JC (2003) Receptor-like protein kinases: the keys to response. Curr Opin Plant Biol 6:339–342

Motohashi K (2017) Evaluation of the efficiency and utility of recombinant enzyme-free seamless DNA cloning methods. Biochem Biophys reports 9:310–315

Nakagawa T, Ishiguro S, Kimura T (2009) Gateway vectors for plant transformation. Plant Biotechnol 26:275–284

Nakagawa T, Kurose T, Hino T, et al (2007a) Development of series of gateway binary vectors, pGWBs, for realizing efficient construction of fusion genes for plant transformation. J Biosci Bioeng 104:34–41

Nakagawa T, Nakamura S, Tanaka K, et al (2008) Development of R4 gateway binary vectors (R4pGWB) enabling high-throughput promoter swapping for plant research. Biosci Biotechnol Biochem 72:624–629

Nakagawa T, Suzuki T, Murata S, et al (2007b) Improved Gateway binary vectors: high-performance vectors for creation of fusion constructs in transgenic analysis of plants. Biosci Biotechnol Biochem 71:2095–2100

Nakamura S, Suzuki T, Kawamukai M, Nakagawa T (2012) Expression analysis of *Arabidopsis thaliana* small secreted protein genes. Biosci Biotechnol Biochem 76:436–446

Narusaka M, Shiraishi T, Iwabuchi M, Narusaka Y (2010) The floral inoculating protocol: a simplified *Arabidopsis thaliana* transformation method modified from floral dipping. Plant Biotechnol 27:349–351

Obayashi T, Aoki Y, Tadaka S, et al (2018) ATTED-II in 2018: a plant coexpression database based on investigation of the statistical property of the mutual rank index. Plant Cell Physiol 59:e3–e3

Ohashi-Ito K, Bergmann DC (2006) *Arabidopsis* FAMA controls the final proliferation/differentiation switch during stomatal development. Plant Cell 18:2493–2505

Owen HA, Makaroff CA (1995) Ultrastructure of microsporogenesis and microgametogenesis in *Arabidopsis thaliana* (L.) Heynh. ecotype Wassilewskija (Brassicaceae). Protoplasma 185:7–21

Pacini E, Franchi GG, Hesse M (1985) The tapetum: Its form, function, and possible phylogeny in *Embryophyta*. Plant Syst Evol 149:155–185

Padole DA, Ingle KP (2017) Arabidopsis-A Model Plant. Trends Biosci 10:557–559

Phan HA, Iacuone S, Li SF, Parish RW (2011) The MYB80 transcription factor is required for pollen development and the regulation of tapetal programmed cell death in *Arabidopsis thaliana*. Plant Cell 23:2209–2224

Pillitteri LJ, Bogenschutz NL, Torii KU (2008) The bHLH protein, MUTE, controls differentiation of stomata and the hydathode pore in Arabidopsis. Plant cell Physiol 49:934–943

Pillitteri LJ, Dong J (2013) Stomatal development in Arabidopsis. Arab book/American Soc Plant Biol 11

Pillitteri LJ, Sloan DB, Bogenschutz NL, Torii KU (2007) Termination of asymmetric cell division and differentiation of stomata. Nature 445:501–505

Pillitteri LJ, Torii KU (2012) Mechanisms of stomatal development. Annu Rev Plant Biol 63:591–614

Qian Q, Yang Y, Zhang W, et al (2021) A novel *Arabidopsis* gene *RGAT1* is required for GA-mediated tapetum and pollen development. New Phytol 231:137–151

Reece-Hoyes JS, Walhout AJM (2018) Gateway recombinational cloning. Cold Spring Harb Protoc 2018:pdb.top094912

Richmond TA, Somerville CR (2000) The cellulose synthase superfamily. Plant Physiol 124:495–498

Richmond TA, Somerville CR (2001) Integrative approaches to determining Csl function. In: Plant cell walls. Springer, pp 131–143

Risso-Pascotto C, Pagliarini MS, Valle CB, Jank L (2005) Symmetric pollen mitosis I and suppression of pollen mitosis II prevent pollen development in Brachiaria jubata (Gramineae). Brazilian J Med Biol Res = Rev Bras Pesqui medicas e Biol 38:1603–1608

Rose A, Meier I (2001) A domain unique to plant RanGAP is responsible for its targeting to the plant nuclear rim. Proc Natl Acad Sci 98:15377–15382

Saeidfirozeh H, Shafiekhani A, Cifra M, Masoudi AA (2018) Endogenous chemiluminescence from germinating Arabidopsis thaliana Seeds. Sci Rep 8:16231

Sai N, Bockman JP, Chen H, et al (2022) SAI: Fast and automated quantification of stomatal parameters on microscope images. bioRxiv 2002–2022

Saitou N, Nei M (1987) The neighbor-joining method: a new method for reconstructing phylogenetic trees. Mol Biol Evol 4:406–425

Sanders PM, Bui AQ, Weterings K, et al (1999) Anther developmental defects in *Arabidopsis thaliana* male-sterile mutants. Sex Plant Reprod 11:297–322

Sandhu APS, Randhawa GS, Dhugga KS (2009) Plant cell wall matrix polysaccharide biosynthesis. Mol Plant 2:840–850

Sarojam R, Sappl PG, Goldshmidt A, et al (2010) Differentiating Arabidopsis shoots from leaves by combined YABBY activities. Plant Cell 22:2113–2130

Schroeder JI, Allen GJ, Hugouvieux V, et al (2001) Guard cell signal transduction. Annu Rev Plant Physiol Plant Mol Biol 52:627–658

Shiba H, Takayama S, Iwano M, et al (2001) A pollen coat protein, SP11/SCR, determines the pollen S-specificity in the self-incompatibility of *Brassica species*. Plant Physiol 125:2095–2103

Shirakawa M, Ueda H, Nagano AJ, et al (2014) FAMA is an essential component for the differentiation of two distinct cell types, myrosin cells and guard cells, in *Arabidopsis*. Plant Cell 26:4039–4052

Shiu S-H, Bleecker AB (2001a) Receptor-like kinases from *Arabidopsis* form a monophyletic gene family related to animal receptor kinases. Proc Natl Acad Sci 98:10763–10768

Shiu S-H, Bleecker AB (2001b) Plant receptor-like kinase gene family: diversity, function, and signaling. Sci STKE 2001:re22–re22

Sieburth DS, Sun Q, Han M (1998) SUR-8, a conserved Ras-binding protein with leucine-rich repeats, positively regulates Ras-mediated signaling in *C. elegans*. Cell 94:119–130

Siegfried KR, Eshed Y, Baum SF, et al (1999) Members of the *YABBY* gene family specify abaxial cell fate in *Arabidopsis*. Development 126:4117–4128

Somerville C (2006) Cellulose synthesis in higher plants. Annu Rev Cell Dev Biol 22:53–78

Stratford S, Barnes W, Hohorst DL, et al (2001) A leucine-rich repeat region is conserved in pollen extensin-like (Pex) proteins in monocots and dicots. Plant Mol Biol 46:43–56

Sultana MM, Hachiya T, Dutta AK, et al (2020) Expression analysis of genes encoding malectin-like domain (MLD)-and leucine-rich repeat (LRR)-containing proteins in *Arabidopsis thaliana.* Biosci Biotechnol Biochem 84:154–158

Suzuki T, Kawai T, Takemura S, et al (2018) Development of the mitsucal computer system to identify causal mutation with a high-throughput sequencer. Plant Reprod 31:117–128

Suzuki T, Masaoka K, Nishi M, et al (2008) Identification of *kaonashi* mutants showing abnormal pollen exine structure in *Arabidopsis thaliana*. Plant Cell Physiol 49:1465–1477

Suzuki T, Tsunekawa S, Koizuka C, et al (2013) Development and disintegration of tapetum-specific lipid-accumulating organelles, elaioplasts and tapetosomes, in *Arabidopsis thaliana*

and *Brassica napus*. Plant Sci 207:25–36

Svozil J, Gruissem W, Baerenfaller K (2016) Meselect–A rapid and effective method for the separation of the main leaf tissue types. Front Plant Sci 7:1701

Takayama S, Shiba H, Iwano M, et al (2000) The pollen determinant of self-incompatibility in *Brassica campestris*. Proc Natl Acad Sci 97:1920–1925

Tanaka Y, Nishimura K, Kawamukai M, et al (2013) Redundant function of two Arabidopsis COPII components, AtSec24B and AtSec24C, is essential for male and female gametogenesis. Planta 238:561–575

Till BJ, Reynolds SH, Weil C, et al (2004) Discovery of induced point mutations in maize genes by tilling. BMC Plant Biol 4:12

Twell D, Park SK, Lalanne E (1998) Asymmetric division and cell-fate determination in developing pollen. Trends Plant Sci 3:305–310

Uemura T, Kim H, Saito C, et al (2012) Qa-SNAREs localized to the *trans*-Golgi network regulate multiple transport pathways and extracellular disease resistance in plants. Proc Natl Acad Sci 109:1784–1789

Vernon DM (2002) Leucine-rich repeat proteins in plants: diverse roles in signaling and development. Res Signpost Recent Res Dev Plant Biol 2:201–214

Von Groll U, Berger D, Altmann T (2002) The subtilisin-like serine protease SDD1 mediates cell-to-cell signaling during Arabidopsis stomatal development. Plant Cell 14:1527–1539

Wang W, Wang L, Chen C, et al (2011) Arabidopsis *CSLD1* and *CSLD4* are required for cellulose deposition and normal growth of pollen tubes. J Exp Bot 62:5161–5177

Wang X, Cnops G, Vanderhaeghen R, et al (2001) *AtCSLD3*, a cellulose synthase-like gene important for root hair growth in Arabidopsis. Plant Physiol 126:575–586

Wang Y, Noguchi K, Ono N, et al (2014) Overexpression of plasma membrane H+-ATPase in guard cells promotes light-induced stomatal opening and enhances plant growth. Proc Natl Acad Sci 111:533–538

Weigel D, Glazebrook J (2002) Arabidopsis: a laboratory manual. CSHL Press

Wilson ZA, Zhang D-B (2009) From *Arabidopsis* to rice: pathways in pollen development. J Exp Bot 60:1479–1492

Winter D, Vinegar B, Nahal H, et al (2007) An “electronic fluorescent pictograph” browser for exploring and analyzing large-scale biological data sets. PLoS One 2:e718

Wu C, Fu Y, Hu G, et al (2010) Isolation and characterization of a rice mutant with narrow and rolled leaves. Planta 232:313–324

Xie X, Zhang Z, Zhao Z, et al (2020) The mitochondrial aldehyde dehydrogenase OsALDH2b negatively regulates tapetum degeneration in rice. J Exp Bot 71:2551–2560

Xu J, Ding Z, Vizcay-Barrena G, et al (2014) *ABORTED MICROSPORES* acts as a master regulator of pollen wall formation in *Arabidopsis*. Plant Cell 26:1544–1556

Yamamoto Y, Nishimura M, Hara-Nishimura I, Noguchi T (2003) Behavior of vacuoles during microspore and pollen development in *Arabidopsis thaliana*. Plant Cell Physiol 44:1192–1201

Yang J, Bak G, Burgin T, et al (2020) Biochemical and genetic analysis identify CSLD3 as a beta-1, 4-glucan synthase that functions during plant cell wall synthesis. Plant Cell 32:1749–1767

Yin L, Verhertbruggen Y, Oikawa A, et al (2011) The cooperative activities of CSLD2, CSLD3, and CSLD5 are required for normal *Arabidopsis* development. Mol Plant 4:1024–1037

You C, Dai X, Li X, et al (2010) Molecular characterization, expression pattern, and functional analysis of the *OsIRL* gene family encoding intracellular Ras-group-related LRR proteins in rice. Plant Mol Biol 74:617–629

Zhao L, Li Y, Xie Q, Wu Y (2017) Loss of *CDKC*;*2* increases both cell division and drought tolerance in *Arabidopsis thaliana*. Plant J 91:816–828

Zhao L, Sack FD (1999) Ultrastructure of stomatal development in *Arabidopsis* (Brassicaceae) leaves. Am J Bot 86:929–939

Zhu J, Lee B, Dellinger M, et al (2010) A cellulose synthase-like protein is required for osmotic stress tolerance in *Arabidopsis*. Plant J 63:128–140

List of publications

Chapter 2

Hossain, M. F., Dutta, A. K., Suzuki, T., Higashiyama, T., Miyamoto, C., Ishiguro, S., Maruta, T., Muto, Y., Nishimura, K., Ishida, H., Aboulela, M., Hachiya, T. and Nakagawa, T. Targeted expression of *bgl23-D*, a dominant-negative allele of *ATCSLD5*, affects cytokinesis of guard mother cells and exine formation of pollen in *Arabidopsis thaliana.* Planta (Accepted; 12 February 2023)

Chapter 3

Hossain, M. F., Sultana, M. M., Tanaka, A., Dutta, A. K., Hachiya, T. and Nakawaga, T. Expression analysis of plant intracellular Ras-group related leucine-rich repeat proteins (PIRLs) in *Arabidopsis thaliana.* Biochemistry and Biophysics Reports, 30:101241

Acknowledgements

At first, I would like to express my deep feelings of gratitude and appreciation to my major supervisor, **Prof. Dr. Tsuyoshi NAKAGAWA,** Director, Interdisciplinary Center for Science Research, Department of Molecular and Functional Genomics, Shimane University, Matsue, Japan, for his scholastic and invaluable suggestions at different stages of the preparation of this research work. Throughout my doctoral studies, he guided me and taught me a lot about molecular biology, functional genomics, and plant biology methodologies. Without his guidance and help, this research work would not have been completed.

I wish to express my sincere thanks to **Prof. Dr. Makoto KAWAMUKAI**, **Associate Prof. Dr. Tomohiro KAINO, and Associate Prof. Dr. Yasuhiro Matsuo** (Shimane University) for giving me constructive and helpful comments about my research during different seminars and meetings.

I am grateful to **Assistant Prof. Takushi HACHIYA** for his valuable suggestions and for helping me during my research work, especially by teaching me confocal microscopy.

I would also like to give my heartfelt thanks to **Prof. Dr. Kinya AKASHI** (Tottori University), who is one of my co-supervisors, for his intellectual comments and suggestions on my research during the regular progress meetings.

I would like to give thanks to **Prof. Takanori MARUTA, Associate Prof. Hideki ISHIDA, and Associate Prof. Kohji NISHIMURA (**Shimane University) for their technical support regarding different experiments during my research work**.**

I would like to express my gratitude to **Associate Prof. Dr Sumie ISHIGURO** (Nagoya University) for his insightful comments on my manuscript.

I wish to express my deepest thanks to **MOSTAFA ABOULELA** for his help and guidance during semi-thin sectioning of anthers.

I would like to express my thanks to present and past colleagues Kota MONDEN, Yuki MUTO and Amit Kumar DUTTA for their help and cooperation during my research work.

My special thanks go to the Ministry of Education, Culture, Sports, Science, and Technology of Japan (MEXT) for giving me this opportunity to study for my Ph.D. degree at the United Graduate School of Agricultural Sciences, Tottori University.

Finally, I express my profound gratitude to my beloved parents and family members for their understanding and continuous inspiration during the entire period of this work. My special thanks to my beloved wife Dalia for her enormous support, encouragement, and patience.

Summary

A. thaliana has been the most used plant model system for decades. The current significance of *Arabidopsis* research reflects scientists growing recognition that this simple angiosperm may serve as a useful model for addressing fundamental concerns of biological structure and function common to all eukaryotes as well as plant biology. *A. thaliana* is helpful to researchers for genetic mapping and sequencing because of its small genome size. Apart from these, its short life cycle, self-pollinating nature and ability to produce many seeds make *A. thaliana* a valued genetic model plant to the scientific community.

The research described in this thesis aimed to improve our understanding of the use of novel dominant-negative mutations as a genetic tool to suppress the function of a specific gene in the target tissue. The development of a compatible genetic tool to modify the target tissue or organ is highly required to understand the role of specific genes. However, tissue-specific expression analysis is also required to understand the physiological functions of specific genes.

In the Chapter 1, the author provides a general introduction to this work. The **Chapter 2** presents the identification of a new dominant-negative mutation, *bgl23-D,* in the *A. thaliana cellulose synthase-like D5* (*ATCSLD5*) gene that was reported to function in the division of guard mother cells. In plant cells, cellulose is an important component of cell wall and is synthesized by the cellulose synthases known as CESA proteins. The *CSLD* gene family is highly related to *CESA* because of sequence similarity. *ATCSLD5* was a direct target of SPEECHLESS and was involved in cell plate formation, including stomata lineage cells. A novel dominant-negative mutation showing bagel-shaped stomata has been successfully identified in *ATCSLD5* from ethylmethanesulfonate (EMS) mutagenized seeds of *A. thaliana* L*er* by next-generation sequencing and Mitsucal computer system using genomic DNA of bulk populations. The construct of own promoter-driven *ATCSLD5* cDNA containing C3220T (C2989T in the cDNA) substitution was introduced into WT-Col and found that the transgenic plants showed bagel-shaped stomata phenotype similar to the *bgl23-D* mutant, revealing that *ATCSLD5* is the responsible gene for the *bgl23-D* mutant. To assess the efficacy of the *bgl23-D* mutant in suppressing ATCSLD5 functions in target tissues or cells, two types of targets were chosen: (1) stomata: the region showing phenotype in the *bgl23-D* mutant, and (2) pollen and root: regions not showing phenotype in the *bgl23-D* mutant. The binary construct was prepared to express *bgl23-D* cDNA with the promoter of stomata-lineage specific genes. *ProSDD1:bgl23-D*, *ProMUTE:bgl23-D*, and *ProFAMA:bgl23-D* showed incompletely divided GCs that observed in the *bgl23-D,* as expected due to its dominant nature. The *ProFAMA:bgl23-D* plants showed highest percentage of abnormal bagel-shaped stomata. In addition, The *ProFAMA:bgl23-D* plants exhibited a wide range of severe cytokinesis defects, ranging from donut-shaped SGC having a single pore at the middle of the cell

to the most severely affected spherical SGC without a pore. Moreover, bagel-shaped stomata were found on the abaxial and adaxial surfaces of the leaves of *ProFIL:bgl23-D* plants with different frequencies. Tapetum plays an important role in the proper development of pollen and exine patterning by providing nutrients to the developing pollen grains. Expression of *bgl23-D* cDNA produced new phenotypes with promoter of tapetum- or anther-specific genes. The study revealed that *ProSP11:bgl23-D* showed slightly shrunken pollen grains, while *ProATSP146:bgl23-D* exhibited a combination of slightly shrunken and severely shrunken pollen grains. The normal reticulate structure of exine was lost in *ProSP11:bgl23-D* and *ProATSP146:bgl23-D*, respectively. However, microspores with no cellular content in *ProATSP146:bgl23-D* after pollen mitosis I (PMI) at the bicellular stage suggested that *bgl23-D* was expressed in microspores and disturbed cell division to some extent. Since the promoter activity of *ATSP146* was found in both the anther and the QC, root and QC phenotypes of *ProATSP146:bgl23-D* were analyzed. *ProATSP146:bgl23-D* exhibited a normal QC pattern and well-organized cell layer in the root apical region, as observed in WT. Additionally, *bgl23-D*, *ProSDD1:bgl23-D*, *ProMUTE:bgl23-D*, and *ProFAMA:bgl23-D* showed increased rosette size and larger epidermal cells, which indicate that *bgl23-D* has an effect on plant growth and development. Thus, this work suggests that *bgl23-D* could efficiently alter pollen shape and exine patterning as well as enhance plant growth, which makes it suitable to use as a genetic tool to modify the target tissue or cell.

To understand the physiological roles of specific genes, it is essential to know their expression patterns. After gaining insightful knowledge about the effect of *bgl23-D* on pollen shape and exine structure, it is essential to know the expression analysis of genes that have a role in reproductive organ development. For these reasons, expression analysis of plant intracellular Ras-group related leucine-rich repeat (LRR) proteins (PIRLs) was studied and presented in the **Chapter 3.** Plants contain a tiny group of proteins that are structurally similar to Ras-group LRRs named plant intracellular Ras-group LRR proteins (PIRLs). These PIRLs are involved in the growth and development of male and female reproductive organs in plants. Promoter:GUS assay revealed that *PIRLs* are expressed throughout the vegetative and reproductive organs. Concerning *PIRL1*, GUS expression was observed in the junction between the root and hypocotyl, the primary root tip, while *PIRL2* showed unique expression in root hairs and strong expression in the stipule, which indicate their specific functions in this region. *PIRL3*, *PIRL4*, *PIRL7*, and *PIRL9* showed expression in root but not in the aboveground organs. Concerning reproductive tissues, for *PIRL1*, GUS was slightly expressed in petals and filaments but was strongly expressed in anthers and pollen. Pollen tube-specific expression was observed for *PIRL1*, *PIRL6*, and *PIRL7.* Distinct expression of *PIRL3* was found in anthers and pollen but not in pollen tube. *PIRL5* was detected very weakly and only in anthers. Heat map analysis using microarray datasets of *PIRL* genes sourced from the Arabidopsis eFP browser revealed that *PIRL6* was specifically expressed in

pollen, while *PIRL1* and *PIRL3* were expressed strongly in pollen and moderately in vegetative organs, and that *PIRL5* was expressed in pollen and roots. Moreover, a microarray study using visual expression of *PIRL* genes during developmental stages revealed that *PIRL1* and *PIRL3* were significantly expressed in floral organs, specifically in mature pollen rather than vegetative organs.

In the Chapter 4, the author provides proposed conclusions and remarks and highlights the key findings presented in this study.

In a nutshell, next-generation sequencing and Mitsucal computer system could successfully identify the novel dominant-negative mutation, *bgl23-D,* in *ATCSLD5.* The expression of *bgl23-D* cDNA with cell- or tissue-specific promoters inhibited ATCSLD5 functions in target tissues while stimulating plant growth. A detailed expression patterns of nine *PIRLs* were analyzed by promoter:GUS assay. These findings will open the way to use *bgl23-D* as a tool for functional analysis of ATCSLDs and other genes in specific tissues and organs and manipulate plant growth.

摘要

シロイヌナズナは有用なモデル植物として使用されている。ゲノムサイズが小さく、ライフサイクルが短い。自殖により多数の種子が得られることから分子遺伝学に有用な植物である。

本論文では、標的組織で特異的遺伝子抑制を行うことを目的とした新規ドミナントネガティブ変異の利用について述べた。遺伝子の役割を深く理解するためには、標的組織を修飾するための遺伝的ツール開発が必要とされる。また、遺伝子の生理機能を理解するためには組織特異的発現の解析も必要とされる。

第 1 章では、本論文の概要を述べた。第 2 章では、孔辺母細胞の細胞質分裂に機能することが報告されているシロイヌナズナセルロース合成酵素様タンパク質 D5（*ATCSLD5*）遺伝子の新規ドミナントネガティブ変異である *bgl23-D* の同定について述べた。植物細胞において、セルロースは細胞壁の重要な要素であり、CESA タンパク質であるセルロース合成酵素によって合成される。*CSLD* は *CESA* に配列が類似した遺伝子ファミリーであり、その一つ *ATCSLD5* 遺伝子は転写因子 SPEECHLESS の直接のターゲットで、気孔系譜を含めて細胞板形成に働いている。シロイヌナズナ EMS 変異種子からベーグル状の気孔形態を示すドミナント変異体が単離され、次世代 DNA シークエンスと Mitsucal システムによる F2 集団バルク DNA の解析により *ATCSLD5* 遺伝子に変異が見出された。自身のプロモーターで *ATCSLD5* C3220T（cDNA では C2989T)を発現するコンストラクトをシロイヌナズナ野生株に導入したところ、*bgl23-D* 変異体と類似の表現型が観察され、*ATCSLD5* の C3220T が新規のドミナントネガティブ変異である *bgl23-D* 変異の原因であると結論付けた。*bgl23-D* を利用し、以下の 2 種類の細胞・組織で ATCSLD5 機能の抑制を試みた。(1)気孔：*bgl23-D* 変異体で表現型が観察される標的、(2)花粉と根：*bgl23-D* 変異体で表現型が観察されない標的である。(1)のため、*bgl23-D* cDNA を気孔系譜プロモーターで発現させるバイナリコンストラクトが作製された。*bgl23-D* がドミナント変異であることから予想されるように、これら *ProSDD1:bgl23-D*, *ProMUTE:bgl23-D*, and *ProFAMA:bgl23-D* コンストラクトでは、*bgl23-D* 変異体で観察されたような不完全に分裂した孔辺細胞が生じた。これらのうち、*ProFAMA:bgl23-D* は最も高い割合でベーグル状の気孔形態を示した。さらに *ProFAMA:bgl23-D* では、中央部に孔があいたドーナツ状の単一孔辺細胞や孔がない球状の孔辺細胞など、様々な程度に細胞質分裂が重篤阻害された表現型が生じた。FIL プロモーターで *bgl23-D* を発現させる *ProFIL:bgl23-D* コンストラクトでは、葉の背軸側と向軸側において、異なる頻度でベーグル状の気孔が観察された。タペート細胞は発達中の花粉粒に物質を供給する細胞で、花粉の発達やエキシンパターン形成に重要な役割を果たしている。タペート細胞特異的遺伝子あるいは葯特異的遺

伝子のプロモーターで *bgl23-D* cDNA を発現させると、新たな表現型が生じた。*ProSP11:bgl23-D* ではわずかに収縮した花粉粒が形成され、*ProATSP146:bgl23-D* ではわずかに収縮した花粉と過度に収縮した花粉が生じた。いずれの場合も、正常な網状のエキシンパターンは失われていた。*ProATSP146:bgl23-D* では、PMI 後の 2 核期に細胞内容物が失われた花粉（小胞子）ができ、*bgl23-D* が小胞子でも発現し細胞分裂を阻害していることが示された。*ATSP146* 発現が QC でも認められるため、*ProATSP146:bgl23-D* の根の表現型が解析されたが、野生株との差はなかった。さらに、*bgl23-D* 変異体, *ProSDD1:bgl23-D*, *ProMUTE:bgl23-D*, および *ProFAMA:bgl23-D* ではロゼット径が増加し、表皮細胞も大きくなった。この結果は *bgl23-D* が植物の増殖と発達に影響を及ぼすことを示している。これらの研究は、*bgl23-D* が植物の増殖を促進する機能に加え、花粉の形態やエキシンパターンを高い効率で変化させる能力を持つことを示した。

遺伝子の生理的役割を理解する上で、その発現パターンを知ることが必須である。*bgl23-D* が花粉の形とエキシンパターンに影響を及ぼすことがわかったため、生殖器官の発達に関わる遺伝子の発現解析を進めることが重要である。そのため 3 章では、シロイヌナズナで 9 遺伝子からなるファミリーを形成している Plant Intracellular Ras-Group LRR protein (PIRL)の発現解析を行った。*PIRL* は雄性、雌性生殖器官の発達に関与している。Promoter:GUS の解析により、*PIRL* が栄養成長、生殖成長を通じて発現していることが示された。*PIRL1* では根と胚軸の境界および根端、*PIRL2* では根毛と托葉で発現し、同領域で機能していることが考えられた。*PIRL3*, *4*, *7* および *9* は根で発現し、地上部での発現は見られなかった。生殖器官に関しては、*PIRL1* が花弁と花糸で弱く、葯と花粉で強く発現していた。*PIRL1*, *6*, 7 では花粉管で発現が観察された。*PIRL3* は葯では発現し、花粉では発現していなかった。*PIRL5* は葯でのみ弱く発現していた。マイクロアレイデータベースを利用したヒートマップにより、PIRL 転写パターンを示した。

第 4 章では結論と本研究の主要な発見を記載した。

次世代シークエンスと Mitsucal システムにより、*ATCSLD5* の新たなドミナントネガティブ変異 *bgl23-D* の同定に成功した。細胞あるいは組織特異的プロモーターによる *bgl23-D* cDNA 発現は標的組織における *ATCSLD5* 機能を阻害した一方で、植物の成長は促進した。Promoter:GUS により *PIRL* 遺伝子群の発現パターンが詳細に解析された。これらの発見は特定の組織や器官における *ATCSLD* 遺伝子群および他の遺伝子群機能解析における *bgl23-D* 利用と植物増殖操作の道を開くものである。